



**University of  
Nottingham**

UK | CHINA | MALAYSIA

Department of Civil Engineering

***The Performance of Structural Foamed Concrete with  
Textile Reinforcement (TRFC)***

By

Abdalla Ragrag, BSc Eng., MSc Eng

Thesis submitted to the University of  
Nottingham for the degree of  
Doctor of Philosophy

March 2024



## **Abstract**

Foamed concrete (FC) has gained substantial interest in the construction sector owing to its lightweight nature, workability, thermal and sound insulation properties, and ease of fabrication. However, FC's high permeability exacerbates corrosion in conventional steel reinforcements. Textile Reinforced Concrete (TRC) presents an innovative alternative, replacing conventional steel with textile reinforcement. Utilizing TRC as reinforcement in foamed concrete offers potential reductions in size, weight, and cost.

This study explores the interaction between foamed concrete's benefits and its compatibility with textile reinforcement, capitalizing on the FC's lack of coarse aggregate and high workability. The novelty lies in producing and experimentally analysing AR glass textile reinforced foamed concrete (TRFC) beams and assessing various failure scenarios through theoretical calculations. The primary aim is to identify optimal configurations for structural applications among TRFC cases and evaluate their environmental and cost implications.

The research encompasses several stages. Firstly, formulating FC mixes with a density of 1800 kg/m<sup>3</sup>, compressive strength ranging from 21 to 35 MPa, and workability exceeding 300 mm. Theoretical analyses predict the flexural behaviour of simply supported TRFC beams under tension and compression. Subsequently, beams are experimentally examined across multiple failure modes, utilizing Digital Image Correlation (DIC) to facilitate displacement measurement and crack tracking. Finally, environmental and cost impacts are evaluated through a life cycle assessment (LCA) of TRFC one-way slabs.

Key findings reveal significant agreement between experimental and theoretical results, with variations for TRFC samples ranging between 6.25% and 12.78%. Moreover, short fibres enhance the elastic limit of the TRFC samples, requiring 40% more load to initiate cracking compared to TRC samples. Furthermore, the TRFC under compression failure sample exhibits the highest energy absorption capacity with 165 kN·mm.

The TRFC slab demonstrates a higher embodied CO<sub>2</sub> of 2490 kgCO<sub>2</sub> compared to the TRC slab's 1884 kgCO<sub>2</sub>, primarily due to its increased cement content. However, both TRFC and

CRC slabs display similar results in the embodied energy analysis, each having an embodied energy of 15700 MJ.

Given the structural performance of TRFCS-Com, further large-scale experiments involving beams and slabs are recommended to compare performance with conventional reinforced concrete. Moreover, additional research and data collection is necessary to interpret the environmental impacts and sustainability considerations of textile reinforced foamed concrete.

## **Acknowledgement**

First and foremost, I express gratitude to ALLAH for bestowing upon me health, patience, strength, countless blessings, the opportunity, and knowledge to successfully complete this PhD journey. My heartfelt appreciation goes to my parents, whose unwavering support and inspiration have been invaluable throughout this endeavor. To my dear mother, thank you for your patience during my absence. To my beloved father, though you could not be with us physically, your memory has been a guiding light every step of the way. May Allah bless your soul.

I am also deeply thankful to my wife for her continuous support and understanding, and to my brothers, sisters, and all my friends who have been pillars of strength during this journey.

I extend my sincere thanks and gratitude to my supervisors, Dr. Nick Thom, Dr. Luis Neves, and Dr. Bahman Ghiassi, for their guidance, encouragement, and invaluable insights throughout this research.

**Declaration**

The work described in this thesis was conducted at the Department of Civil Engineering, University of Nottingham between October 2019 and March 2024. I declare that, unless otherwise cited in the text, the work is my own and has not been submitted for a degree at another university.

**Abdalla Ragrag**

March 2024

## Abbreviations and notations

<b>ACI</b>	American Concrete Institute
<b>ASTM</b>	The American Society for Testing and Materials
<b>BS</b>	British Standard
<b>EC</b>	European Standard
<b>IStruct</b>	Institution of Structural Engineers
<b>SCOSS</b>	Standing Committee on Structural Safety.
<b>LWC</b>	Lightweight Concrete
<b>AAC</b>	Autoclaved Aerated Concrete
<b>RAAC</b>	REINFORCED AUTOCLAVED AERATED CONCRETE
<b>FC</b>	Foamed Concrete
<b>FCS</b>	Foamed Concrete with Short Fibre
<b>FCFA</b>	Foamed Concrete with Fly Ash
<b>C</b>	Fine-grained Concrete
<b>CS</b>	Fine-grained Concrete with Sort Fibre
<b>CC</b>	Conventional concrete
<b>TRFC-Ten<sub>1</sub></b>	Textile Reinforced Foamed Concrete Failing in Tension with Low Reinforcement
<b>TRFC-Ten<sub>2</sub></b>	Textile Reinforced Foamed Concrete Failing in Tension with High Reinforcement
<b>TRFC-Com</b>	Textile Reinforced Foamed Concrete Failing in Compression
<b>TRFCS-Ten<sub>1</sub></b>	Textile Reinforced Foamed Concrete with Short Fibre Failing in Tension with Reinforcement
<b>TRFCS-Ten<sub>2</sub></b>	Textile Reinforced Foamed Concrete with Short Fibre Failing in Tension with High Reinforcement
<b>TRFCS-Com</b>	Textile Reinforced Foamed Concrete with Short Fibre Failing in Compression
<b>TRC-Ten<sub>1</sub></b>	Textile Reinforced Concrete Failing in Tension with Low Reinforcement
<b>TRC-Ten<sub>2</sub></b>	Textile Reinforced Concrete Failing in Tension with High Reinforcement
<b>TRC-Com</b>	Textile Reinforced Concrete Failing in Compression
<b>TRCS-Ten<sub>1</sub></b>	Textile Reinforced Concrete with Short Fibre Failing in Tension with Low Reinforcement
<b>TRCS-Ten<sub>2</sub></b>	Textile Reinforced Concrete with Short Fibre Failing in Tension with High Reinforcement
<b>TRCS-Com</b>	Textile Reinforced Concrete with Short Fibre Failing in Compression
<b>CRC</b>	Conventional Reinforced Concrete
<b>w/c</b>	Water-Cement Ratio
<b>w/b</b>	Water-Binder Ratio
<b>C:S</b>	Cement to Sand Ratio
<b><math>f_{ct}</math></b>	Flexural Strength
<b><math>F</math></b>	Applied Load
<b><math>l</math></b>	Span Length
<b><math>d</math></b>	Specimen Depth
<b><math>b</math></b>	Specimen Width
<b><math>E</math></b>	Modulus of elasticity
<b><math>\sigma_a</math></b>	Upper Loading Stress
<b><math>\sigma_b</math></b>	Base Stress
<b><math>\epsilon_a</math></b>	Strain Under ( $\sigma_a$ )
<b><math>\epsilon_b</math></b>	Strain Under ( $\sigma_b$ )
<b><math>\rho</math></b>	Hardened Concrete Density
<b><math>M_a</math></b>	Weight of the Specimen in Air
<b><math>M_w</math></b>	Weight of the Specimen in Water
<b><math>\rho_t</math></b>	Target Plastic Density
<b><math>M_2</math></b>	Combined Mass of Container and Samples
<b><math>M_1</math></b>	The Mass of Empty Container
<b><math>V</math></b>	The Volume of the Container
<b><math>\sigma_f</math></b>	Flexural Stress in the Fibres at The Midpoint
<b><math>P</math></b>	Load at a Given Point on the Load-Deflection Curve
<b><math>L</math></b>	Supported Span

## Abbreviations and Notations

---

$\epsilon_f$	Strain at Failure
$D$	Maximum Deflection of The Centre of The Beam
$M_u$	Ultimate Bending Capacity
$F_{t,i}$	Internal Tensile Forces
$Z_i$	Lever Arms Between the Forces.
$h$	Height
$\epsilon_c$	Concrete Ultimate Strain
$\epsilon_{t,0}$ and $\epsilon_{t,l}$	Lowest and Highest Textile Strain Layer Respectively
$X$	Neutral Axis Depth
$\sigma_c$	Concrete Stress
$\sigma_{t,0}$ and $\sigma_{t,l}$	Textile Stresses
$F_c$	Compressive Force
$\epsilon_{cu}$	Ultimate Concrete Strain
$\sigma_c$	Ultimate Concrete Stress
$\epsilon_{tu}$	Ultimate Textile Strain
$E_{tex}$	Textile Young's Modulus of Elasticity
$k_{0\alpha}$	Load-Bearing Capacities Between Sloped Textile Reinforcements and the Textile Aligned in the Load Direction ( $0^\circ$ )
<b>tex</b>	Grams of Textile per Kilometre Length of Textile
<b>AR-fibre glass</b>	Alkali-Resistant Fibre Glass
$F_{uTex}$	Textile Ultimate Tensile Stress
$E_{Tex}$	Textile Tensile Modulus of Elasticity
$\epsilon_{uTex}$	Textile ultimate strain
$A_Y$	Yarn Area
$n_Y$	Number of Textile Layer
$\epsilon_{FC}$	Foamed Concrete Strain
$\epsilon_{Tex1}$ and $\epsilon_{Tex2}$	Textile Strain at the 1 <sup>st</sup> Layer and at the 2 <sup>nd</sup> Layer Respectively
$C_{AN}$	Neutral Axis Depth
$A$	Compressive Foamed Concrete Depth
$\sigma_{FC}$	Foamed Concrete Stress
$\sigma_{Tex}$	Textile Stress
$T_{Tex}$	Textile Tension Force
$F_{FC}$	Foamed Concrete Compressive Force
$V_c$	Shear Capacity
$\lambda$	Coefficient of Lightweight Concrete
<b>DIC</b>	Digital Image Correlation
<b>LCA</b>	Life cycle assessment
<b>LCI</b>	Life Cycle Inventory Analysis
<b>LCIA</b>	Life Cycle Impact Assessment
<b>CH4</b>	Methane
<b>N2O</b>	Nitrous Oxide
<b>CO2</b>	Carbon Dioxide
<b>Cl</b>	Chloride Ion
<b>SO3</b>	Sulfur Trioxide
<b>CaO</b>	Calcium oxide
<b>Al2O3</b>	Aluminum Oxide (Alumina)
<b>Fe2O3</b>	Iron (III) Oxide (Ferric Oxide)
<b>Na2O</b>	Sodium Oxide
<b>MgO</b>	Magnesium Oxide
<b>PO4<sup>3-</sup></b>	Phosphate Ion
<b>K2O</b>	Potassium Oxide
<b>SiO2</b>	Silicon Dioxide (Silica)
<b>Si</b>	Silicon
<b>CaCO3</b>	Calcium Carbonate



<b>ABSTRACT</b>	<b>II</b>
<b>ACKNOWLEDGEMENT</b>	<b>IV</b>
<b>DECLARATION</b>	<b>V</b>
<b>ABBREVIATIONS AND NOTATIONS</b>	<b>VI</b>
<b>CHAPTER 1 INTRODUCTION</b>	<b>1</b>
<b>1.1. Background</b>	<b>1</b>
<b>1.2. Foamed Concrete Advantages</b>	<b>4</b>
<b>1.3. Why Use Textiles as Reinforcement?</b>	<b>5</b>
<b>1.4. Problem Statement</b>	<b>5</b>
<b>1.5. Scientific Novelty</b>	<b>6</b>
<b>1.6. Scope of Research</b>	<b>6</b>
<b>1.7. Aim, Objectives, and Methodology</b>	<b>7</b>
1.7.1. Aim	7
1.7.2. Objectives	7
1.7.3. Methodology	8
<b>1.8. Outline of Thesis</b>	<b>11</b>
<b>CHAPTER 2 LITERATURE REVIEW</b>	<b>13</b>
<b>2.1. Introduction</b>	<b>13</b>
<b>2.2. Lightweight Concrete (LWC) Background</b>	<b>13</b>
2.2.1. Aerated Concrete	14
2.2.2. Foamed Concrete (FC)	15

<b>2.3. Foamed Concrete Specifications</b>	<b>17</b>
<b>2.4. Production of Foamed Concrete</b>	<b>17</b>
2.4.1. Constituent Materials	17
2.4.1.1. Cement	18
2.4.1.2. Additive	18
2.4.1.3. Water	20
2.4.1.4. Fine Aggregate	21
2.4.1.5. Foaming Agents	21
2.4.1.6. Foam	22
2.4.2. Preparation of Foamed Concrete	24
<b>2.5. Properties of Foamed Concrete</b>	<b>25</b>
2.5.1. Fresh Properties	26
2.5.1.1. Workability	26
2.5.1.2. Fresh Density	27
2.5.2. Physical Properties	28
2.5.2.1. Drying Shrinkage	28
2.5.2.2. Hardened Density	28
2.5.2.3. Air-Void Systems	29
2.5.3. Mechanical Properties	30
2.5.3.1. Compressive Strength	30
2.5.3.2. Flexural and Tensile Strength	32
2.5.3.3. Modulus of Elasticity	33

## Table of Contents

---

2.5.4. Functional Properties	33
2.5.4.1. Thermal Conductivity	33
2.5.4.2. Acoustic Insulation Resistance	34
2.5.4.3. Fire Resistance	35
<b>2.6. Textile Reinforced Concrete (TRC)</b>	<b>36</b>
2.6.1. Introduction	36
2.6.2. Textile Reinforced Concrete Material	36
2.6.2.1. Fine Grained Concrete	36
2.6.2.2. Textile	37
2.6.3. Filament Material and Properties	40
2.6.3.1. Alkali-Resistant (AR)-Glass Filament Yarns	40
2.6.3.2. Carbon Filament Yarns	41
2.6.3.3. Aramid Filaments	41
2.6.4. Textile Reinforced Concrete Bearing Capacity	42
2.6.4.1. Impregnation Influence	42
2.6.4.2. Filament, Yarn (Roving) Influence	44
2.6.4.3. Transverse Loading Influence	45
2.6.5. Textile Bond	46
2.6.6. Pull-out Test	48
2.6.7. Stress-Strain Diagram of Textile Reinforced Concrete	48
2.6.8. Textile Form Flexibility	50
2.6.9. Textile Reinforced Concrete (TRC) Design	51

## Table of Contents

---

2.6.10. TRC Ultimate Flexural Strength and Flexural Strain Review	54
2.6.11. Textile Reinforced Concrete (TRC) Durability	56
2.6.12. Textile Reinforced Concrete (TRC) Manufacturing Methods	58
2.6.12.1. Hand Lay-up Method	58
2.6.12.2. Pultrusion Method	59
2.6.13. Textile Reinforced Concrete (TRC) Applications	60
2.6.13.1. Exterior Cladding and Façade Panels	61
2.6.13.2. Sandwich elements	62
2.6.13.3. Decentralised Wastewater Treatment Plants	64
2.6.13.4. Barrel Shells	64
2.6.13.5. Cycle-Path and Footbridge	65
<b>2.7. Review the Reinforcement Foamed Concrete</b>	<b>66</b>
<b>2.8. Summary</b>	<b>69</b>
<b>CHAPTER 3 FOAMED CONCRETE: MATERIALS, MIX DESIGN, AND TESTING FOR STRENGTH AND PROPERTIES</b>	<b>71</b>
<b>3.1. Introduction</b>	<b>71</b>
<b>3.2. Materials Used</b>	<b>71</b>
3.2.1. Cement	71
3.2.2. Sand	72
3.2.3. Water	72
3.2.4. Foaming Agent	73
3.2.5. Waste Toner	74

<b>3.3. Mix Design, Production, and Tests</b>	<b>75</b>
3.3.1. Mix Design Calculation	76
3.3.2. Foam Production	77
3.3.3. Foamed Concrete Production	77
3.3.4. Sampling and Curing	79
3.3.5. Workability Test	81
3.3.6. Hardened Density Test	82
3.3.7. Compressive Strength	82
3.3.8. Static Modulus of Elasticity ( $E$ ):	83
3.3.9. Four-point flexural test	85
<b>3.4. Experimental Program for Foamed Concrete (FC) Development</b>	<b>86</b>
3.4.1. Impact of Water-to-Cement Ratio and Cement-to-Sand Ratio	87
3.4.2. Effect of Waste Toner	91
3.4.3. Effect of Density	94
3.4.4. Validating Experimental Results with the Literature	97
<b>3.5. Research Programme</b>	<b>100</b>
<b>3.6. Summary</b>	<b>101</b>
<b>CHAPTER 4 THEORETICAL PREDICTION OF TEXTILE REINFORCEMENT FOAMED CONCRETE (TRFC):</b>	<b>103</b>
<b>4.1. Introduction</b>	<b>103</b>
<b>4.2. Reviewing Design Factors of Textile Reinforced Concrete (TRC)</b>	<b>103</b>
<b>4.3. Material Mechanical Properties</b>	<b>105</b>

## Table of Contents

---

4.3.1. AR-Glass Textile Reinforcement	105
4.3.2. Foamed Concrete	106
<b>4.4. Design Assumption</b>	<b>106</b>
<b>4.5. TRFC Beam Failure in Tension with Low Reinforcement (TRFC-Ten<sub>1</sub>)</b>	<b>108</b>
4.5.1. Moment Capacity Calculation	108
4.5.2. Shear and Moment Diagram	111
<b>4.6. TRFC Beam Failure in Tension with High Reinforcement (TRFC-Ten<sub>2</sub>)</b>	<b>112</b>
4.6.1. Moment Capacity Calculation	112
4.6.2. Shear and Moment Diagram	113
<b>4.7. TRFC Beam Failure in Compression (TRFC-Com)</b>	<b>113</b>
4.7.1. Moment Capacity Calculation	113
4.7.2. Shear and Moment Diagram	115
<b>4.8. Summary</b>	<b>116</b>
<b>CHAPTER 5 FLEXURAL AND PULL-OUT TESTS BEHAVIOUR OF TEXTILE REINFORCEMENT FOAMED CONCRETE</b>	<b>117</b>
5.1. Introduction	117
<b>5.2. Materials Used</b>	<b>117</b>
5.2.1. Short Fibre	117
5.2.2. Fly Ash	118
5.2.3. Silica Fume	118
5.2.4. Superplasticiser	118
5.2.5. Limestone	119

<b>5.3. Flexural Test</b>	<b>120</b>
5.3.1. Mixes Components and Their Properties	120
5.3.2. Test Specimens and Preparations	124
5.3.3. Measurement Tool	127
5.3.3.1. Digital Image Correlation (DIC)	127
5.3.3.2. Video Gauge	128
5.3.4. Results and Analysis	129
5.3.4.1. Failure Case Comparison	129
5.3.4.2. Concrete Mixes Comparison	131
5.3.4.3. Ultimate Flexural Strength and Flexural Strain	135
5.3.4.4. Crack Propagation and Failure Modes	136
5.3.4.5. Comparison of Experimental and Theoretical Data for TRFC Beams	139
<b>5.4. Pull-out Test</b>	<b>141</b>
5.4.1. Test Specimens and Preparations	142
5.4.2. Result and Analysis	145
<b>5.5. Summary</b>	<b>147</b>
<b>CHAPTER 6 TRFC LIFE-CYCLE ASSESSMENT (LCA)</b>	<b>149</b>
<b>6.1. Introduction</b>	<b>149</b>
<b>6.2. What is LCA?</b>	<b>150</b>
<b>6.3. The Purpose and Significance of Implementing LCA</b>	<b>150</b>
<b>6.4. Implementing LCA: Methodology and Process</b>	<b>151</b>
6.4.1. Goal and Scope	151

## Table of Contents

---

6.4.2. Life Cycle Inventory Analysis Phase (LCI)	152
6.4.3. Life Cycle Impact Assessment Phase (LCIA)	152
6.4.4. Life Cycle Interpretation	153
<b>6.5. Comparative Life Cycle Assessment (LCA) Analysis for Different Concrete Mixes</b>	<b>153</b>
6.5.1. Goal and Scope, System Boundary and Functional	153
6.5.2. Life Cycle Inventory Analysis (LCI)	154
6.5.3. Life Cycle Impact Assessment (LCIA)	154
6.5.4. Interpretation of Results	156
<b>6.6. Comparative Life Cycle Assessment (LCA) of One-Way (CRC) Slab and One-Way TRFCS Slab</b>	<b>158</b>
6.6.1. Goal and Scope, System Boundary and Functional Units	159
6.6.2. Life Cycle Inventory Analysis (LCI)	160
6.6.3. Life Cycle Impact Assessment (LCIA)	160
6.6.4. Interpretation of Results	161
<b>6.7. Cost Assessment</b>	<b>163</b>
<b>6.8. Summary</b>	<b>165</b>
<b>CHAPTER 7 CONCLUSION AND RECOMMENDATIONS</b>	<b>166</b>
<b>7.1. Conclusions</b>	<b>166</b>
<b>7.2. Recommendations</b>	<b>168</b>
<b>7.3. Limitation</b>	<b>169</b>



**List of Figures**

Figure 1.1: Curtain wall panels used as sun protection (Curbach et al., 2006)	2
Figure 1.2: Multilayer cladding panel (Bamonte et al., 2017)	2
Figure 1.3: LWC structural application in USA, (a) North Pier Apartment Tower, (b) Bank of America	2
Figure: 1.4 Research methodology	10
Figure 2.1: Lightweight concrete forms (Newman and Owens, 2003)	14
Figure 2.2: Methods to produce cellular concrete (Neville, 2010)	15
Figure 2.3 Materials for foam concrete (Raj et al., 2019).	18
Figure 2.4: Foamed concrete production using the mixed foam method.	22
Figure 2.5: Foamed concrete production using the preformed method.	23
Figure 2.6: Produce preformed foam from water, foaming agents and compressed air (World Pumps, 2017)	24
Figure 2.7: Yarn construction: a) filament yarn, b) twisted yarn (Gries et al., 2006)	38
Figure 2.8: Different types of textile materials (Gries et al., 2006)	38
Figure 2.9: Warp & weft directions in bi-axial textile (Peled et al., 2008)	39
Figure 2.10: Warp & weft directions in multi-axial textile (Gries et al., 2006)	39
Figure 2.11: Three-dimensional textile (Gries et al., 2006)	40
Figure 2.12: Cross-section of Roving Without Impregnation (Left) and With Impregnation (Right) (Gries et al., 2016)	43
Figure 2.13: Comparison of the tensile strength between coated and uncoated textile in TRC element (Hegger et al., 2006)	43

## List of Figures

---

Figure 2.14: Comparison of the tensile strength of a filament, roving, textile with composite section (Hegger et al., 2006)	45
Figure 2.15: Effect of orientated 0°, 22.5°, 45°, 67.5°, 90° carbon and AR glass textile reinforced concrete in tensile tests (Hegger & Voss, 2004)	46
Figure 2.16: Roving with inner bond & outer bond (Reinhardt et al., 2006)	47
Figure 2.17: Stress-strain diagram of TRC under uniaxial loading (Hegger et al., 2006)	49
Figure 2.18: Examples of lightweight TRC structures (ventilated facade panels) (Hegger & Will, 2016)	50
Figure 2.19: AR-glass textile impregnated with epoxy-resin (Hegger & Will, 2016)	51
Figure 2.20: Large-sized TRC facade panels (Hegger & Will, 2016)	52
Figure 2.21: Backside of one TRC panel with supporting lines (Hegger & Will, 2016)	52
Figure 2.22: Experimentally determine the material characteristics (a) the concrete compression and (b) the impregnated yarn tension (Hegger & Will, 2016)	53
Figure 2.23: Cross-sectional model for the TRC beam element diagram	54
Figure 2.24: Comparison of the ultimate flexural strength and flexural strain at failure of the selected literature.	56
Figure 2.25: Pultrusion machine (Mobasher et al., 2009)	59
Figure 2.26: New extension of the testing hall of the Structural Concrete Institute Aachen University (Curbach et al., 2006)	62
Figure 2.27: Office building, Dortmund, Germany (Curbach et al., 2006)	62
Figure 2.28: Sandwich elements made of TRC: a) profiled spacer fabric, b) completed sandwich element (Curbach et al., 2006)	63
Figure 2.29: Decentralised wastewater treatment plants made of textile reinforced concrete (Curbach et al., 2006)	64
Figure 2.30: Barrel shell is made of textile reinforced concrete (Hegger and Voss, 2008)	65

## List of Figures

---

Figure 2.31: Textile reinforced concrete bridge (Curbach et al., 2006)	65
Figure 3.1: Used materials: (a). Water (b). cement (c). sand (d). toner (e). foam.	73
Figure 3.2: Foam producing: (a). Foaming agent (b). Foam machine (c). Foam	74
Figure 3.3: Waste toner cartridges	75
Figure 3.4: Production of dry foam and foamed concrete	78
Figure 3.5: Foamed concrete production	79
Figure 3.6: Prepare and apply release oil on the specimen, then position the foamed concrete mix.	80
Figure 3.7: Specimens curing in water	81
Figure 3.8: Spread ability of the foamed concrete mix	82
Figure 3.9: Compressive test for cubes	83
Figure 3.10: Static modulus of elasticity test	84
Figure 3.11: Four-point flexural test for plain FC prism	85
Figure 3.12: Experimental program: impact of water-to-cement ratios (w/c) and cement-to-sand ratio (C:S) on a density of 1800 kg/m <sup>3</sup> .	87
Figure 3.13: Excluded non-integrated mix (FC-7 mix)	89
Figure 3.14: FC compressive strength with a targeted density of 1800 kg/m <sup>3</sup> and different (w/c) and cement: sand (C:S) ratios	91
Figure 3.15: Experimental program: impact of three toner percentages on a density of 1800 kg/m <sup>3</sup>	92
Figure 3.16: Compressive Strength of FC-5, FC-10, FC-11, and FC-12 samples at 28 days	94
Figure 3.17: Experimental program: impact of different densities with (w/c) of 0.4, (C:S= 1:1.5), and toner percentage of 10%	94

## List of Figures

---

Figure 3.18: Effect of toner on different foamed concrete density	96
Figure 3.19: FC compressive strength with different targeted densities at 28 days	97
Figure 3.20: Strength to density ratios for different foamed concrete mixes	98
Figure 4.1: Experimental results for AR-glass textile reinforcement	105
Figure 4.2: Parabolic-rectangular design stress block for the ultimate limit state (EC2)	107
Figure 4.3: Parabolic-rectangular design stress block for the TRFC-Ten1 cross section.	109
Figure 4.4: Shear (V) and moment (M) diagram for TRFC-Ten <sub>1</sub> beam.	111
Figure 4.5: Parabolic-rectangular design stress block for the TRFC-Ten2 cross section.	112
Figure 4.6: Parabolic-rectangular design stress block for the TRFC-Com cross section.	114
Figure 5.1: Used materials: (a). fly ash (b). silica fume (c). superplasticizer (d). limestone	119
Figure 5.2: Ready mix (Planitop HDM Maxi) - Component A and Component B	121
Figure 5.3: Preparing and determining the sample's properties.	123
Figure 5.4: The load direction of the AR-glass textile	123
Figure 5.5: Three-point bending tests (dimensions in mm)	124
Figure 5.6: Textile layers insertion in the Plywood forms sides	125
Figure 5.7: Samples casting and curing.	126
Figure 5.8: Image frames taken before and after deformation (Wang et al., 2009)	128
Figure 5.9: Region of Interest (ROI) located at midspan for DIC monitoring.	128
Figure 5.10: Three-point bending test using a Video Gauge	129
Figure 5.11: Comparison of failure cases in flexural load-deflection curves for (a) TRFC, (b) TRFCS, (c) TRCS, and (d) TRC of samples	130

## List of Figures

---

Figure 5.12: Comparison of energy absorption among TRFC, TRFCS, TRCS, and TRC samples under three failure cases: Com, Ten <sub>2</sub> , and Ten <sub>1</sub>	130
Figure 5.13: Comparison of concrete mixes in flexural load-deflection curves for (a) Ten <sub>1</sub> , (b) Ten <sub>2</sub> , and (c) Com	134
Figure 5.14: Comparison of the ultimate flexural strength and flexural strain at failure between the research samples and selected literature (literature references are in Table 5.3)	136
Figure 5.15: a comparison between compression failure and tension failure.	137
Figure 5.16: Comparison between max moment theoretical and experimental results for TRFC beam.	140
Figure 5.17: Schematic view of specimen geometry and setup used in yarn pullout tests (Barhum & Mechtcherine, 2013)	142
Figure 5.18: Pull-out test setup.	143
Figure 5.19: Samples preparation, casting, and curing for pull-out test	143
Figure 5.20: Steel plates securely anchored and reinforced with additional textile layers at the other end of the samples	144
Figure 5.21: Epoxy (Sikadure 52)	144
Figure 5.22: Pull-out – Displacement results for TRFCS and TRCS specimens	146
Figure 6.1: Stages of LCA implementation (ISO 14040: 2006)	151
Figure 6.2: Embodied carbon for 1 m <sup>3</sup> concrete mixes	157
Figure 6.3: Embodied energy for 1 m <sup>3</sup> concrete mixes	158
Figure 6.4: Embodied carbon for the TRFCS slab and the CRC slab	162
Figure 6.5: Embodied energy for the TRFCS slab and the CRC slab	162
Figure 6.6: Cost of 1 m <sup>3</sup> concrete mixes, FCS mix, C mix, FCFA mix, and CC mix.	163
Figure 6.7: Cost of 4.05 m <sup>3</sup> TRFCS slab and 4.32 m <sup>3</sup> CRC slab	164

**List of Tables**

Table 2.1: Main published guidelines for lightweight concrete used in this research	17
Table 2.2: Literature details and references	55
Table 3.1: Chemical composition of cement (Alma'aitah & Ghiassi, 2022).	72
Table 3.2: Absolute volume method for mix design	76
Table 3.3: FC mixes with a targeted density of 1800 kg/m <sup>3</sup> and three different (w/c) and (C:S) ratios	88
Table 3.4: Properties of FC mixes with a targeted density of 1800 kg/m <sup>3</sup> and different (w/c) and (C:S) ratios	88
Table 3.5: FC mixes with a targeted density of 1800 kg/m <sup>3</sup> and three different toner percentages	92
Table 3.6: Effect of three percentages of toner on FC mean compressive strength and density.	93
Table 3.7: FC mixes with different densities with (w/c) of 0.4, (C: S= 1:1.5), and a toner percentage of 10%	95
Table 3.8: FC mean compressive strength and density of different targeted densities.	95
Table 3.9: Current study mixes that will be compared with the literature mixes.	98
Table 3.10: FC-5 foamed concrete mix hardened properties.	99
Table 4.1: Comparison between impregnated and non-impregnated textiles (Hegger & Will, 2016)	105
Table 4.2: The properties of AR-glass textile reinforcement	106
Table 4.3: Foamed concrete mix hardened properties.	106
Table 4.4: Input design details used in Solver for TRFC-Ten <sub>1</sub>	109

## List of Tables

---

Table 4.5: TRFC-Ten <sub>1</sub> Solver results	110
Table 4.6: TRFC-Ten <sub>1</sub> beam details.	111
Table 4.7: Shear & Moment results for TRFC-Ten <sub>1</sub>	111
Table 4.8: TRFC-Ten <sub>2</sub> Solver results	113
Table 4.9: Shear & Moment results for TRFC-Ten <sub>2</sub>	113
Table 4.10: The input design details in the Solver for TRFC-Com	114
Table 4.11: TRFC-Com Solver results	114
Table 4.12: Shear & Moment results for TRFC-com	115
Table 4.13: Calculated predictions for the four types of failures in TRFC beams	116
Table 5.1: Chemical composition of fly ash, silica fume, and limestone (Alma'aitah & Ghiassi, 2022)	120
Table 5.2: Components for FC and FCS mixes	121
Table 5.3: Components for C mix (Alma'aitah & Ghiassi, 2022)	122
Table 5.4: Compressive strength, densities, and workability of the mixes	122
Table 5.5: AR-glass textile experimental results	124
Table 5.6: Sample details	127
Table 5.7: Stiffness of TRFCS, TRCS, TRFC, and TRC samples	131
Table 5.8: Ductility factor of TRFCS, TRCS, TRFC, and TRC samples	133
Table 5.9: Literature review references of the Ultimate flexural strength of the TRC	135
Table 5.10: DIC images depict load at crack initiation, ultimate load, and failure.	138
Table 5.11: Comparison between max experimental and theoretical moment for the TRFC	139

## List of Tables

---

Table 6.1: Main components of concrete mixes with same compressive strength	154
Table 6.2: Materials required to produce one cubic meter of concrete mix.	154
Table 6.3: Embodied carbon factors for the materials utilized in concrete mixes.	155
Table 6.4: Embodied energy consumption factor	155
Table 6.5: Materials required to produce 4.05 m <sup>3</sup> of the TRFCS slab.	160
Table 6.6: Materials required to produce 4.32 m <sup>3</sup> of the CRC slab.	160
Table 6.7: Embodied carbon and energy factors for the concrete slabs	161



## Chapter 1 Introduction

### 1.1. Background

Concrete is a fundamental material in the construction industry, renowned for its excellent properties like strength, workability, and abundant availability of its constituents. Comprising two main components, paste and aggregates, concrete's paste primarily consists of water and cement, while aggregates are further categorized into fine and coarse aggregates. Cementitious additives are often incorporated into concrete mixtures to enhance their properties (Kosmatka et al., 2002).

In terms of weight, concrete can be broadly classified into two types: lightweight concrete (LWC) and heavyweight concrete. LWC can be achieved through various methods, including introducing air voids in the cement paste, excluding coarse aggregates (cellular concrete), omitting fine aggregates (no-fines concrete), or utilizing lightweight aggregates (Newman and Owens, 2003).

The applications of lightweight concrete vary depending on its structural role. It can be categorized into three groups. Firstly, non-structural applications, such as curtain wall panels used for sun protection, as depicted in Figure 1.1 (Curbach et al., 2006). Secondly, semi-structural applications are suitable for non-structural and semi-structural purposes like cladding panels, as illustrated in Figure 1.2 (Bamonte et al., 2017). Lastly, structural applications, such as LWC floor slabs employed in projects like the North Pier Apartment Tower and the Bank of America, are showcased in Figure 1.3, where compressive strengths exceeding 44 MPa are required (Lu, 2023).



Figure 1.1: Curtain wall panels used as sun protection (Curbach et al., 2006)



Figure 1.2: Multilayer cladding panel (Bamonte et al., 2017)



Figure 1.3: LWC structural application in USA, (a) North Pier Apartment Tower, (b) Bank of America

The compressive strength of structural lightweight concrete (LWC) is determined based on the specific design criteria of the structure in question. Typically, specified strengths range from 21 to 35 MPa, with occasional instances where they may exceed 48 MPa, although this is less common (ASTM C330, 2009; ACI 213R-03, 2003).

According to the American Concrete Institute (ACI 523), lightweight cellular concrete typically consists of a cementitious binder, sand or slag, and fine siliceous materials like fly ash, mixed with water to create a homogeneous void mixture. The void structure of cellular concrete is generated through a chemical reaction or mechanical incorporation of air. Compared to conventional concrete, cellular concrete offers several advantages, including reduced weight, superior noise and thermal insulation properties, ease of pumping and application, high fire resistance, and self-compacting characteristics (Chica & Alzate, 2019).

Foamed concrete, a prevalent type of cellular lightweight concrete in construction, incorporates air bubbles into the concrete paste through either direct mixing with the foaming agent (mix-foam method) or by creating stable foam separately and then adding it to the mixture (pre-formed foam method) (Ramamurthy & Nambiar, 2009; Nambiar and Ramamurthy, 2007). Known for its self-compacting nature, high flowability, fire resistance, lightweight properties, and excellent thermal and sound insulation capabilities (Pan et al., 2007), foamed concrete holds potential for environmentally friendly, cost-effective, and sustainable construction practices. However, its adoption in structural applications remains limited due to uncertainties and insufficient awareness regarding its engineering properties (Raj et al., 2019).

This study focuses specifically on examining foamed concrete produced via the pre-formed foam method, reinforced with AR (Alkali-Resistant) fibre textiles to create textile reinforced foamed concrete (TRFC). The TRFC specimens are intentionally designed to fail under various scenarios, aiming to identify the most viable case for structural applications.

## 1.2. Foamed Concrete Advantages

In the fresh phase, the key advantage of the foamed concrete is its self-compacting property. The fresh foamed concrete does not require compaction machines thus reducing noise and power usage. Furthermore, foamed concrete is characterised as a high workability concrete, so improving in casting and pumping of the fresh concrete is achievable.

Structurally, foamed concrete as lightweight concrete reduces the dead loads of concrete constructions, therefore decreasing the size of structural elements and meaning that less reinforcing is applicable. Since the seismic force correlates with the construction mass ( $F = ma$ ), lightweight construction will have a smaller effect compared to a heavy construction building under the same seismic force (Chen et al., 2010).

Functionally, foamed concrete has excellent acoustic insulation, thermal insulation, and fire resistance. The insulation properties reduce the power consumption and noise of heating and air-conditioning systems in the buildings, consequently reducing CO<sub>2</sub> emission. Moreover, using foamed concrete improves the safety of construction buildings by high resistance to fire risk (Amran et al., 2015).

In terms of foamed concrete fabrication, reducing element size and reinforcement results in savings in the construction materials, manpower and transport costs (Amran et al., 2015).

While foamed concrete boasts numerous advantageous properties, it also presents certain drawbacks. One such disadvantage is its high permeability, which can accelerate corrosion in conventional steel reinforcement. Additionally, foamed concrete is prone to high drying shrinkage, it exhibits up to ten times greater drying shrinkage compared to conventional concrete, potentially leading to increased crack formation during the serviceability state. This disparity arises from the absence of coarse aggregates, higher cement content, and increased water content in foamed concrete. (Brady et al., 2001; Amran et al., 2020b). However, researchers have suggested that the performance of foamed concrete regarding drying shrinkage can be

improved. This enhancement can be achieved by partially substituting cement with supplementary materials such as silica fume, fly ash, and lime (Amran et al., 2015). Additionally, the addition of fibres to the foamed concrete mix is known to reduce drying shrinkage (Pillar & Repette, 2015; Yousefieh et al., 2017).

Moreover, the effects of various mixing, transporting, and pumping methods on the stability of the foam in foamed concrete mixes have not been thoroughly investigated. These methods play a crucial role in ensuring the production of large quantities of foamed concrete that meet design standards. Additionally, there is currently no standard for designing foamed concrete, which further complicates its application in construction. Establishing standardized guidelines would be beneficial in ensuring consistent quality and performance in foamed concrete structures.

### 1.3. Why Use Textiles as Reinforcement?

Textile reinforced concrete (TRC) is a composite material comprising of fine-grained concrete and textile material, typically made from multi-filament yarns known as roving. These filaments are commonly crafted from alkali-resistant glass, basalt, or carbon materials. The textile layer is embedded within the concrete, with a maximum aggregate size of 2 mm (Hartig et al., 2008; Graf et al., 2007). Compared to conventional steel bars, textiles offer several advantages, including the ability to construct lightweight and thin structural elements. Additionally, textiles do not require a minimum concrete cover for corrosion protection, as is the case with conventional reinforcement bars. Furthermore, textiles are often available in sheet form, making them easy to form to the desired geometry of the structural element (Schneider & Schätzke, 2006).

### 1.4. Problem Statement

While foamed concrete offers lightweight properties advantageous over conventional concrete, its high permeability, stemming from FC behaviour, accelerates corrosion processes in conventional steel. This corrosion concern was also highlighted by the

Institution of Structural Engineers (IStruct) in 2022, particularly in a report addressing the failure of reinforced autoclaved concrete on school roofs in the UK. This research focuses on mitigating this issue by presenting and examining textile as a lightweight reinforcement within the foamed concrete to enhance its structural, and durability properties.

### 1.5. Scientific Novelty

The scientific novelty of this research lies in its unique approach to theoretically and experimentally examining textile reinforced foamed concrete (TRFC) beams under three different failure scenarios, including tension failure with low and high reinforcement, as well as compression failure. By investigating flexural behaviour, deflection behaviour, and crack width and propagation under various failure patterns, this research aims to provide insights into the structural performance of TRFC beams. Additionally, the study includes a life cycle assessment (LCA) of the TRFC element to evaluate its environmental performance, contributing to a comprehensive understanding of both the structural and environmental aspects of TRFC beams.

### 1.6. Scope of Research

The scope of this thesis research involves conducting a comprehensive investigation into the structural performance and environmental implications of textile-reinforced foamed concrete (TRFC) beams. The study will thoroughly analyse the flexural and bond behaviour of TRFC beams under various failure scenarios, encompassing both theoretical analyses and experimental testing. Theoretical analyses will focus on predicting behaviour under tension failure with varying levels of reinforcement, as well as compression failure. The experimental component will entail testing of TRFC beams for flexural and bond behaviour, with the aim of identifying the most promising TRFC configurations for structural applications.

In Libya, the author's country of origin, the use of lightweight concrete materials in structural applications is still at an early stage. The research aims to bridge knowledge

gaps concerning the performance of foamed concrete and textile reinforcement in this context. Considering that most of the people live in a coastal environment, which is susceptible to corrosion, the study highlights the potential of Textile Reinforced Foamed Concrete (TRFC) to address corrosion concerns. Furthermore, it underlines TRFC's advantages, including its lightweight properties and thermal insulation capabilities, which are especially pertinent in Libya's extreme climate conditions.

### 1.7. Aim, Objectives, and Methodology

#### 1.7.1. Aim

The aim of this research is to produce and analyse the structural performance of textile reinforced foamed concrete beams. The study will undertake theoretical and experimental evaluations under different failure cases to determine the most appropriate configuration for structural applications. Additionally, the research will investigate the environmental and cost impacts linked to the developed textile reinforced foamed concrete mix.

#### 1.7.2. Objectives

To achieve the aim of the research, the study will pursue the following specific objectives:

- 1- Produce and determine the fresh and mechanical properties of the FC mixes with varying densities, water-to-cement ratios, and cement-to-sand ratios.
- 2- Theoretically design three potential different failure cases of AR glass textile reinforced foamed concrete (TRFC).
- 3- Experimentally examine the flexural and bond behaviour of textile reinforced foamed concrete.
- 4- Investigate the environmental and cost impacts of the textile reinforced foamed concrete.

### 1.7.3. Methodology

The research methodology consists of the following tasks, with the flowchart illustrated in Figure 1.4:

**Task 1:** Conduct a comprehensive review of existing literature on lightweight cellular concrete (foamed concrete) and textile reinforced concrete (TRC), with a critical focus.

**Task 2:** Design foamed concrete (FC) mix trials for all FC production stages using the absolute volumes method. The production process aims to achieve a foamed concrete mix with a density of no more than  $1800 \pm 50 \text{ kg/m}^3$  and a compressive strength within the range of 21 to 35 MPa, aligning with typical specifications for structural applications. Additionally, considering the integration of the foamed concrete into the fibre textile reinforcement, the workability target is set at greater than 300 mm. Furthermore, the lowest cement content that fulfils the targeted density, compressive strength, and workability was considered. The production of FC comprises five stages:

**Stage One:** Investigate the influence of water-to-cement ratios (0.3, 0.4, and 0.5) and cement-to-sand ratios (1:1, 1:1.5, and 1:2).

**Stage Two:** Examine the impact of incorporating waste toner as an additive into the foamed concrete mixes.

**Stage Three:** Investigate the effect of different FC mix densities (1200, 1400, 1600, and  $1800 \text{ kg/m}^3$ ).

**Stage Four:** Validate the experimental results obtained from the previous stages by comparing them with relevant findings from existing literature.

**Stage Five:** Determine the hardened properties of the selected foamed concrete mix. This includes the static modulus of elasticity test and the four-point flexural test to assess the mix mechanical properties.



- Task 3:** Provide a theoretical analysis predicting the flexural behaviour of simply supported AR glass textile-reinforced foamed concrete (TRFC) beams under three bending tests in three failure cases, including two cases of tension failure with low ( $Ten_1$ ) and high ( $Ten_2$ ) reinforcement, and one case of compression (Com) failure.
- Task 4:** Carry out three-point bending tests to assess the flexural behaviour of four simply supported beam samples, including textile-reinforced foamed concrete (TRFC), textile-reinforced foamed concrete with short fibre (TRFCS), textile-reinforced concrete (TRC) utilized as a control sample, and textile-reinforced concrete with short fibre (TRCS) also employed as a control sample, under three failure cases  $Ten_1$ ,  $Ten_2$ , and Com. Digital Image Correlation (DIC) is employed to measure displacements and track crack propagation.
- Task 5:** Examine the bonding behaviour of three AR-glass yarns interconnected by transverse yarns along the entire length of the foamed concrete specimens and compare with conventional fine-grained concrete, using the pull-out test.
- Task 6:** Investigate the environmental and cost impacts through a life cycle assessment (LCA) of foamed concrete with short fibre (FCS), fine-grained concrete (C), foamed concrete with fly ash (FCFA), and conventional concrete (CC). Furthermore, the comparison extends to TRFCS one-way slab with conventional reinforced concrete (CRC).

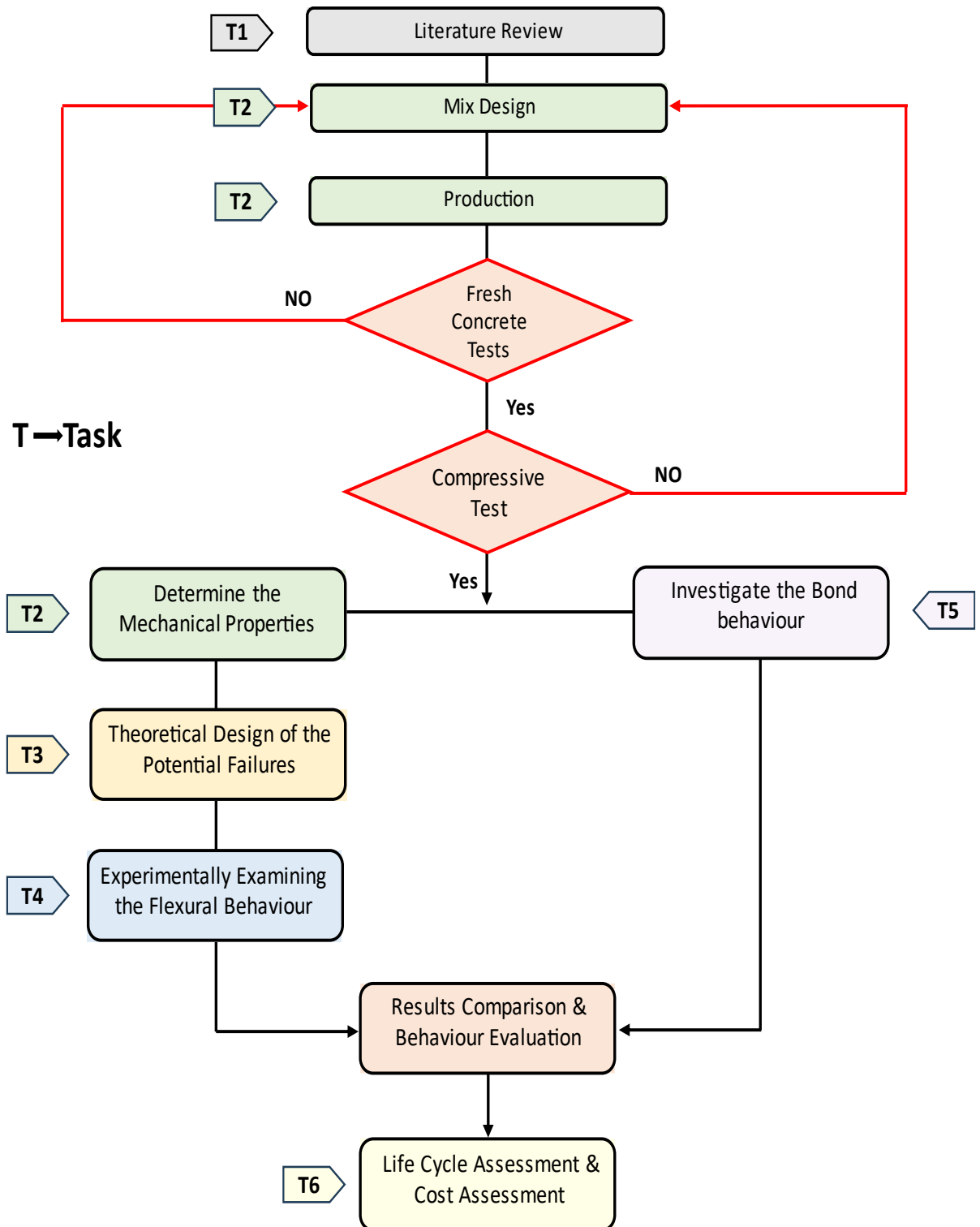


Figure 1.4: Research methodology

## 1.8. Outline of Thesis

The outline and contents of the thesis are summarised as follows:

**Chapter One** provides an overview of foamed concrete (FC) and textile reinforced concrete (TRC), including definitions, classifications, advantages, and challenges associated with steel reinforced foamed concrete. The chapter also outlines the rationale for utilizing FC with textile reinforcement and presents the aim, objectives, and methodology of the thesis.

**Chapter Two** A critical analysis of previous literature is conducted, focusing on three main areas: foamed concrete, textile reinforced concrete, and the evaluation of reinforced foamed concrete. This chapter provides a comprehensive understanding of the existing knowledge base and fills the gap in this area.

**Chapter Three** delves into the materials, mix design, and testing procedures relevant to foamed concrete. Emphasis is placed on elucidating the essential components, their proportions, and the testing protocols necessary for assessing the strength and properties of foamed concrete, with a focus on its suitability for structural applications.

**Chapter Four** A review of the design factors of textile reinforced concrete (TRC) is presented as guidelines for the theoretical analysis predicting the behaviour of AR glass textile reinforced foamed concrete (TRFC) under three distinct failure scenarios.

**Chapter Five** describes an experimental program involving flexural and pull-out tests on AR fibre textile-reinforced concrete. The aim is to evaluate the flexural behaviour, deflection behaviour, and crack propagation under various failure patterns, providing insights into the structural performance of TRFC beams.

**Chapter Six** an LCA of the textile reinforced foamed concrete (TRFCS) one-way slab is conducted, focusing on the production stage (cradle-to-gate). The chapter includes a comparison with conventional reinforced concrete slabs, considering embodied

energy and embodied carbon. Additionally, an economic assessment investigates the total cost of the prepared mixes.

**Chapter Seven** presents conclusions drawn from the research findings and provides recommendations for future work in this area.

## Chapter 2 Literature Review

### 2.1. Introduction

Concrete stands as the cornerstone of modern construction, prized for its unparalleled combination of durability, workability, strength, and the abundance of its constituent materials. Yet, amid its widespread usage, the imperative to advance concrete technology remains pressing. A pivotal facet of this evolution lies in the quest to reduce the inherent weight of concrete structures, thereby alleviating structural burdens and enhancing overall performance (Jones & McCarthy, 2005). The benefit of using lightweight concrete LWC is not limited to reducing the total structure load in multi-storey building only. However, LWC also boasts exceptional noise and thermal insulation properties, contributing to enhanced comfort and sustainability (Neville, 2010).

This literature review is structured into three main sections, each addressing a distinct aspect of concrete innovation: lightweight cellular concrete (foamed concrete), textile reinforced concrete, and evaluation of reinforced foamed concrete. Through the analysis of existing literature, the current research aims to produce a design framework for textile reinforced foamed concrete, accounting for various failure scenarios. This attempt not only fills a critical gap in understanding but also paves the way for the development of textile reinforced foamed concrete.

### 2.2. Lightweight Concrete (LWC) Background

Lightweight concrete (LWC) exhibits a density range of approximately 300-2000 kg/m<sup>3</sup>, with strength varying from 1 to over 60 MPa and thermal conductivities falling within the 0.2 to 1.0 W/mK range. These values are notably lower than those of conventional weight concrete, which typically has a density of 2100–2500 kg/m<sup>3</sup>, a strength ranging from 15 to over 100 MPa, and thermal conductivities between 1.6 and 1.9 W/mK (Neville, 2010).

The relatively low density of LWC can be achieved by incorporating air voids in three distinct locations: between coarse aggregates, excluding fine aggregates (no-fine concrete); within the coarse aggregates (lightweight aggregate concrete); and in the cement paste, excluding coarse aggregates (Aerated concrete) (Newman & Owens, 2003), as illustrated in Figure 2.1. In this research, the focus will be on utilizing aerated concrete, specifically the foamed concrete type.

Structural LWC's compressive strength is established according to the design requirements of a particular structure. Generally, the specified strengths lie between 21 and 35 MPa, with occasional instances where they may reach 48 MPa or beyond, though this is less frequent (ASTM C330, 2009; ACI 213R-03, 2003).

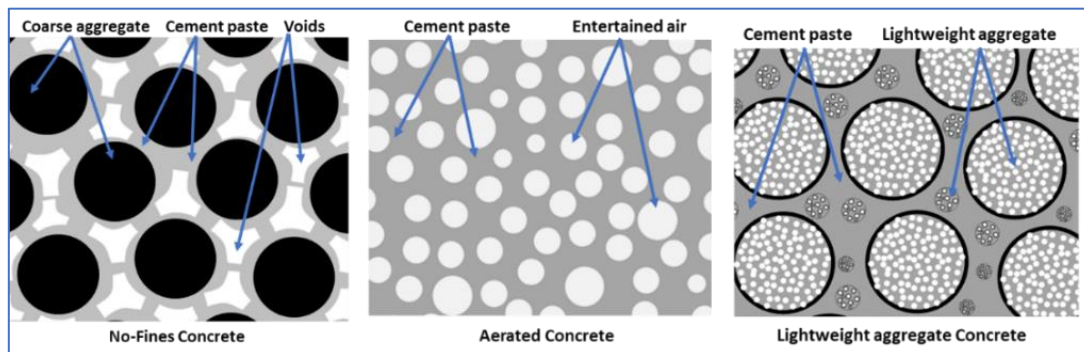


Figure 2.1: Lightweight concrete forms (Newman and Owens, 2003)

### 2.2.1. Aerated or Cellular Concrete

Aerated or Cellular concrete, identified by the American Concrete Institute (ACI 523.2R-96 Committee, 1997), is characterized as a lightweight material composed of cement, fine siliceous materials like fly ash, sand, or slag, mixed with water to create a slurry with a uniform cell or void structure. The voids in the paste result from either a mechanical incorporation of air or a chemical reaction. The primary advantages of aerated concrete over conventional concrete include weight reduction, high resistance to fire, excellent thermal and noise isolation, ease of application and pumping, and the absence of a need for compacting (Chica & Alzate, 2019).

According to Neville (2010), there are two main methods for producing cellular concrete:

- Chemical Reaction Method: This involves generating gas bubbles in the fresh mortar through a chemical reaction. Commonly, this reaction is induced by adding substances such as aluminium powder, zinc powder, or hydrogen peroxide.
- Foaming Agent Method: This method introduces air bubbles into the mortar by adding a foaming agent during mixing in a high-speed mixer. Alternatively, a stable preformed foam can be added to the mix in an ordinary mixer, as depicted in Figure 2.2.

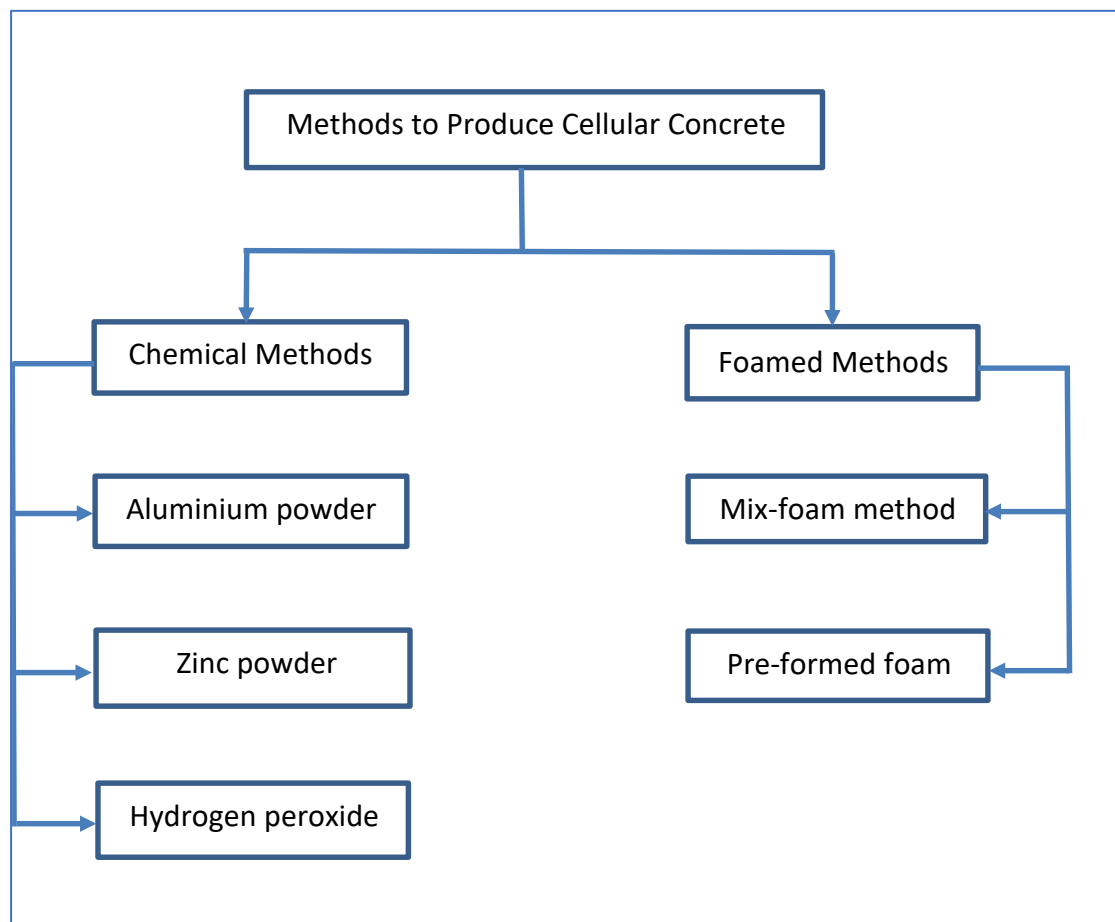


Figure 2.2: Methods to produce cellular concrete (Neville, 2010)

### 2.2.2. Foamed Concrete (FC)

Foamed concrete is characterized as lightweight cellular concrete featuring air voids that are generated and trapped within a mortar, achieved through the utilization of a suitable foaming agent (Amran et al., 2015; Ramamurthy & Nambiar, 2009). According to Nambiar and Ramamurthy (2007), the porous structure in foamed concrete is

accomplished through a mechanical process. Two primary methods are employed for this purpose: the mixed foam method and the preformed foam method.

Foamed concrete exhibits advantageous characteristics, including low self-weight, self-compacting nature, high flowability, fire resistance, and exceptional thermal and sound insulation, all attributed to the presence and distribution of air bubbles in the mortar (Pan et al., 2007). The type of foaming agent and the method of foam preparation significantly impact the creation of stable and uniformly distributed air voids in the foamed concrete mix (Ramamurthy & Nambiar, 2009).

The strength and stiffness of foamed concrete are significantly influenced by the type of cement used and the water-to-cement ratio, especially at specific densities. As density increases, strength and stiffness typically increase, while thermal insulation and water absorption tend to decrease. Therefore, it is crucial to carefully assess how the proportions in the mix design affect its strength, stiffness, shrinkage, thermal insulation, and density. The ratio of sand to binder (s/b ratio), and water-to-cement ratio are often determined through trial-and-error experimentation. However, the absence of standardized specifications for foam concrete production renders mass production impractical (Shankar et al., 2023).

The design flexibility of foamed concrete allows for a density range spanning 280–1800 kg/m<sup>3</sup>. Typically, conventional foamed concrete is proportioned to achieve relatively low compressive strengths (1- 10 N/mm<sup>2</sup>), making it suitable for applications such as void filling and non-structural purposes (Jones and McCarthy, 2005). Despite presenting economically, environmentally, and sustainably viable solutions, the utilization of foamed concrete in the structural construction sector remains relatively limited. This is attributed to a lack of awareness and confidence in the material's engineering properties (Raj et al., 2019).

In this research, the aim is to use the positive properties of preformed foamed concrete to design and produce a lightweight concrete with a density not exceeding 1800 kg/m<sup>3</sup> and a compressive strength within the range of 21 to 35 MPa. This will involve the production of a one-way textile reinforced foamed concrete slab.



### 2.3. Foamed Concrete Specifications

No standardized codes or regulations exist for foamed concrete, which would otherwise provide specifications for its properties, applications, and quality, including its use as a structural element with reinforcement (Shankar et al., 2023; Amran et al., 2020). Nonetheless, various guidelines and methodologies have been generally disseminated in literature focusing on cellular and lightweight concrete. The specific guidelines utilized in this research are detailed in Table 2.1. However, it is important to note that while foamed concrete falls under the category of lightweight concrete, relying solely on lightweight concrete guidelines may not be entirely appropriate due to the unique properties and characteristics of foamed concrete. As a result, a trial-and-error approach was employed in this research, given the absence of standardized specifications for foam concrete production.

*Table 2.1: Main published guidelines for lightweight concrete used in this research.*

Publishing Body	Year	Title of the specification
American Concrete Institute (ACI 523.3R-14)	2014	Guide for Cellular Concretes above 50 lb/ft <sup>3</sup> (800 kg/m <sup>3</sup> )
American Society for Testing and Materials (ASTM C330)	2009	Standard Specification for Lightweight Aggregates for Structural Concrete
American Concrete Institute (ACI 523.1R-06)	2006	Guide for Cast-in-Place Low-Density Cellular Concrete
American Concrete Institute (ACI 213R-03)	2003	Guide for Structural Lightweight-Aggregate Concrete
Transport Research Laboratory (TRL Limited)	2001	Specification for Foamed Concrete
American Society for Testing and Materials (ASTM C 495-99)	1999	Standard Test Method for Compressive Strength of Lightweight Insulating Concrete
American Concrete Institute (ACI 523.2R-96)	1996	Guide for Precast Cellular Concrete Floor, Roof, and Wall Units

### 2.4. Production of Foamed Concrete

#### 2.4.1. Constituent Materials

Figure 2.3 illustrates the primary materials required to prepare foamed concrete, comprising cement, fine aggregate (sand), and water, which together form the mortar. Unlike conventional concrete, foamed concrete does not incorporate any coarse

aggregate. The density of foamed concrete is predominantly regulated by the quantity of foam introduced into the mortar (Raj et al., 2019).



Figure 2.3: Materials for foam concrete (Raj et al., 2019).

#### 2.4.1.1. Cement

Cement serves as the primary binder in foam concrete. Various types of cement are utilized, including ordinary Portland cement, high alumina cement, rapid-hardening Portland cement, calcium chloroaluminate cement, and alkali-activated cement (Raj et al., 2019). Typically, the total amount of cement by weight in the foamed concrete mix ranges between 250- 500 kg/m<sup>3</sup>. However, for achieving higher strengths, recommendations suggest a cement content exceeding 500 kg/m<sup>3</sup> (Hilal et al., 2015).

#### 2.4.1.2. Additive

Foamed concrete, known for its high cement content, has prompted the search for partial replacements to mitigate its negative environmental impact and reduce costs. Silica fume and fly ash emerge as the two primary additives for enhancing foamed concrete properties, as revealed by previous research.

The inclusion of 10% silica fume in the mixture has shown significant enhancements in compressive strength and thermal conductivity, up to 400% and 30% respectively, compared to using cement alone with the same foam content. It is noteworthy that this improvement comes alongside an increase in foamed concrete density (Gökçe et

al., 2019). Moreover, the addition of polypropylene fibre and silica fume also leads to a notable increase in the compressive strengths of foamed concrete over curing time, particularly evident at higher foam concrete densities (Amran et al., 2020a). The substantial enhancement in foamed concrete strength may be attributed to the increase in density. It is crucial to recognize that this increase in density compromises the desirable lightweight properties of foamed concrete.

Fly ash has many effects on the foamed concrete mix properties including improving the mix consistency, reducing heat hydration, increasing the curing time, and enhancing the strength of foamed concrete (Pan et al., 2007; Hashemmoniri & Fatemi, 2023). Additionally, the water absorption rate decreases with the increase in the percentage of fly ash replacement for cement, attributed to the higher pozzolanic reaction and smaller particle size of fly ash compared to cement (Hashemmoniri & Fatemi, 2023). There is a marginal effect on foamed concrete density by adding fly ash (Gökçe et al., 2019). Nonetheless, the main drawback of fly ash lies in its cost, which is comparable to that of cement. Overall, in comparing the effects of silica fume and fly ash on foamed concrete properties, fly ash appears to offer distinct advantages.

Toner, a dry ink powder with a particle size ranging from 5 to 20  $\mu\text{m}$ , primarily consists of a brittle polyester resin acrylic copolymer with a low melting temperature of 110°C. Waste toner is sourced from used laser printers, and printers in universities, schools, and companies that print books, newspapers, and magazines generate tons of waste toner annually. The disposal of this waste toner incurs significant costs. Toner has recently been introduced as an additive for foamed concrete, but there is limited data and published research on its use in this application. Toner can be considered a sustainable and cost-effective material, often sourced from old printer cartridges or collected from expired and waste materials at little to no cost. Toner includes several additives to enhance flow and lubrication, such as iron oxide, ground sand, fluoropolymer powders, metal stearates (e.g., zinc stearate), fumed silica, magnetite, and carbon black (Alkurdi et al., 2021).

Short fibres, also known as dispersed fibres, are small, discrete lengths of fibres that are mixed into the concrete matrix. These fibres can be made from materials such as

steel, polypropylene, glass, carbon, or natural fibres. Short fibres are not continuous and are randomly distributed throughout the concrete mix. They vary in length, typically ranging from a few millimetres to several centimetres. Short fibres are mixed directly into the dry concrete mix to ensure that the fibres are evenly distributed throughout the mix, then providing uniform reinforcement. The primary function of short fibres is to improve the concrete's toughness and resistance to cracking. They help to control shrinkage cracks, enhance impact resistance, and improve the overall durability of the concrete. However, they do not provide as much tensile strength as textile reinforcements due to their shorter length and random distribution. The effect of the short fibre on the foamed concrete mix has been discussed in 2.5. Properties of Foamed Concrete section.

#### 2.4.1.3. Water

Water in the mixture should be free and clean from harmful amounts of salts, alkalis, acids, oils and organic matter as specified by ACI 523.2R-96 (1997). Its role in the mixture is pivotal, influencing both the stability and consistency of the mix. Unlike conventional mixes, the water-to-cement ratio ( $w/c$ ) in foamed concrete tends to be slightly higher. This ratio stands as a crucial factor in achieving optimal workability. However, this ratio is dependent upon several factors, including the required strength of the concrete, the use of plasticizing agents, and the type of binder. Typically, the ( $w/c$ ) ratio ranges between 0.4 and 0.8. Insufficient water content to fully hydrate the cement can lead to water being drawn out from the foam, potentially causing disintegration of mixture components (Brady et al., 2001).

Conversely, a higher ( $w/c$ ) ratio reduces the relative viscosity and weakens the bubble-maintaining capacity in cement paste. Additionally, it encourages the merging of bubbles into larger ones (Liu et al., 2016).

#### 2.4.1.4. Fine Aggregate

Natural, non-organic sand with a maximum size of 2.36 mm is commonly employed as the fine aggregate in foamed concrete mixtures to enhance stability and workability (Jones & McCarthy, 2005). The absence of coarse aggregate in foamed concrete mixtures is deliberate, as its inclusion could lead to foam collapse during mixing, potentially resulting in mix segregation. However, there is potential to explore alternative fine aggregate materials, such as fly ash, expanded polystyrene granules, and expanded clay, for producing foamed concrete using sustainable or waste materials (Brady et al., 2001).

#### 2.4.1.5. Foaming Agents

The type of foaming agent, whether synthetic or protein-based, significantly impacts the performance of foamed concrete production, influencing key aspects such as compressive strength, foam stability, thermal resistance, and pore structure. The most commonly utilized foaming agents are synthetic and protein-based surfactants, both designed to produce stable air bubbles that can withstand the physical forces involved in the foamed concrete manufacturing process (Falliano et al., 2018). Table 2.2 presents the main types of foaming agents and their properties used in foamed concrete.

Protein-based foaming agents typically generate robust, closed air bubbles, resulting in a high strength-to-density ratio. In contrast, synthetic surfactants produce larger bubbles with more open cells due to higher expansion. Synthetic foaming agents are advantageous for their insensitivity to the alkalinity of the mix, ease of formulation, consistent performance, stability, and lower cost (Brady et al., 2001; Amran et al., 2015). Foaming agents are generally mixed with water in ratios ranging from 1/5 to 1/25 (one part surfactant to 5-25 parts water) (Chun et al., 2007).

Table 2.2: Types and properties of surfactants used in foamed concrete (Brady et al., 2001; Amran et al., 2015)

Surfactant Type	Example composition	Properties	Foam Characteristics	Applications in foamed concrete	Price
Synthetic	Alkyl sulfates	Consistent, Stable and easy to formulate	Produces larger bubbles with open cells due to lower strength and higher expansion	Ideal for high-density foamed concretes, suitable for rapid and large-scale placement	Low
Protein	Keratin and hydrolysed animal proteins	Stabilised, variable & highly refined	Creates firm texture, stable, stronger foam with smaller closed-cell bubbles	Best for low-density foamed concretes, especially when waterproofing and high strength are needed	High

#### 2.4.1.6. Foam

Foam plays a crucial role in forming air voids trapped within the mortar in foamed concrete, produced by using an appropriate foaming agent (Amran et al., 2015; Ramamurthy & Nambiar, 2009). Nambiar and Ramamurthy (2007) highlight that the porous structure in foamed concrete is accomplished through a mechanical process. Two primary methods are employed to generate foam: the mixed foam method, involving the integration of the foaming agent with the matrix as demonstrated in Figure 2.4, and the preformed foam method, where the foaming agent is blended with water, creating foam before incorporation into the mix, as illustrated in Figure 2.5.

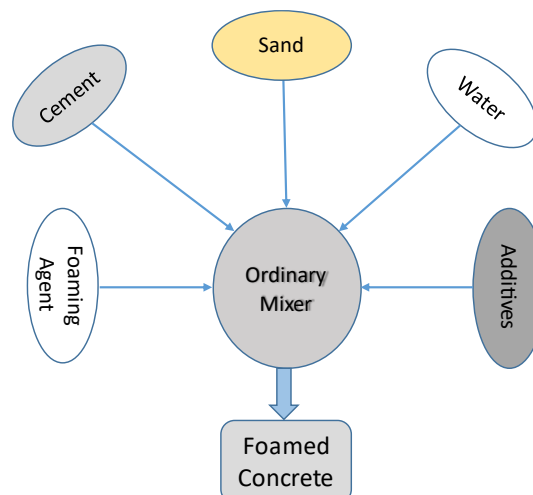
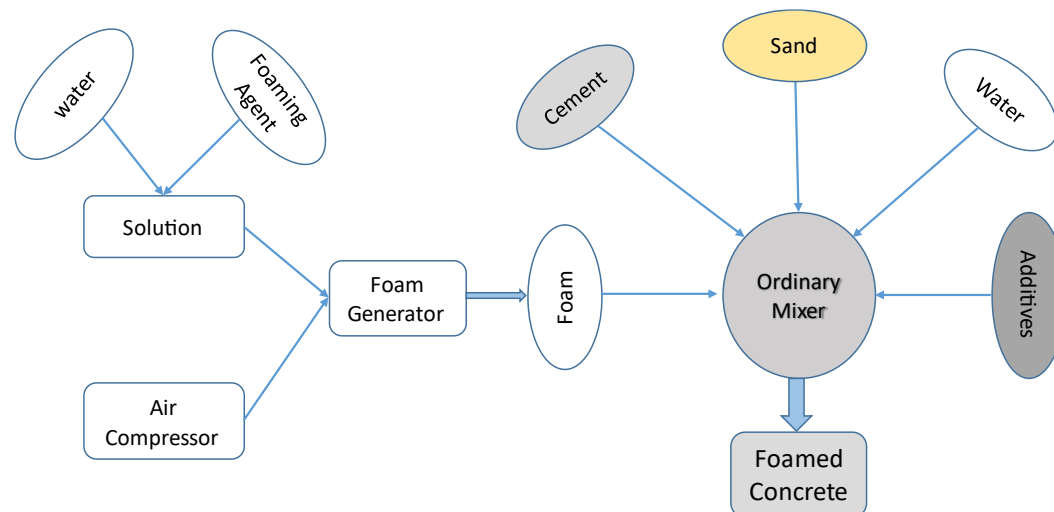


Figure 2.4: Foamed concrete production using the mixed foam method



*Figure 2.5: Foamed concrete production using the preformed method*

Both the mixed foam and preformed foam techniques are acknowledged as effective methods for producing high-quality foam concrete (Shankar et al., 2023). However, according to Ramamurthy & Nambiar (2009), the preformed foam method stands out by producing stable foam separately and then thoroughly blending it into the mixture. This stability is crucial as the foam must withstand the mortar pressure until the initial cement set occurs, allowing a solid structure of foamed concrete to form around the air voids. To ensure foam stability, the foam must withstand the mortar pressure until the initial cement set occurs, allowing a solid structure of foamed concrete to form around the air voids. For stability, the foam should have a density ranging between 40 and 50 g/Litre. The foam density measured by collecting a known volume of foam and weighing it to determine its mass per unit volume, ensuring accurate and consistent measurement.

Additionally, the stability of the foam determined by measuring the density of the foamed concrete before and after the curing process. Significant changes in density could indicate foam instability, such as collapse or excessive air loss. Furthermore, the compressive strengths of the foamed concrete tested after curing. Consistent and predictable strength results across different batches suggested stable foam. These procedures, outlined in (ACI 523.3R-14, 2014) and (Ramamurthy & Nambiar, 2009).

The preformed foam method offers a distinct advantage in that it enables precise measurement of foam density before its integration into the cementitious slurry.

Consequently, it provides greater control and accuracy in the production of foamed concrete compared to the mixed foam method.

The preformed foam can take two forms: dry or wet foam. Wet foam is created by spraying a foaming agent solution over a fine mesh. Typically, wet foam is characterized by larger-sized bubbles, ranging between 2– 5 mm, and is relatively less stable. On the other hand, dry foam is produced by mixing the foaming agent solution with water and then forcing compressed air into the mixing chamber. Dry foam stands out for its remarkable stability and small bubble size, typically smaller than 1 mm. This characteristic makes dry foam easy to blend with the concrete mixture (Ramamurthy & Nambiar, 2009). The dry foam is produced as depicted in Figure 2.6.

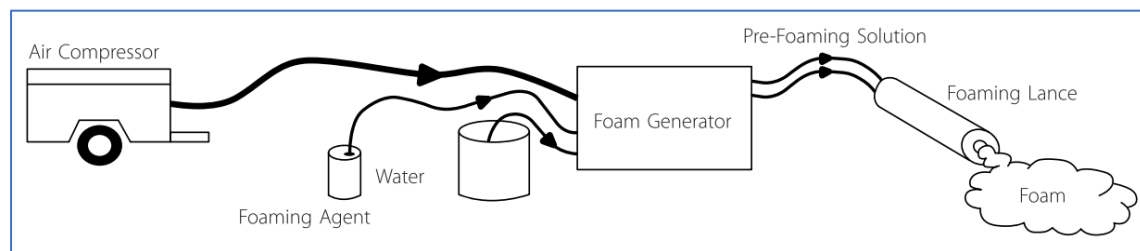


*Figure 2.6: Produce preformed foam from water, foaming agents and compressed air (World Pumps, 2017)*

#### 2.4.2. Preparation of Foamed Concrete

According to ACI 523.3R-14 (2014), the mixing process of foamed concrete should be conducted mechanically to ensure a uniform distribution of mixture components. However, excessive mixing should be avoided to prevent undesirable changes in density and consistency. Specific batching and mixing sequences are recommended, starting with the addition of water and water-soluble admixtures to the mixer, followed by cement, aggregate(s), and other admixtures. All ingredients, except the preformed foam, should be mixed to a uniform consistency before adding the foam, which is incorporated last. The mixing time typically ranges from 2 to 3 minutes, although it may vary depending on the output of the foam generator and the desired concrete density.



When preparing foamed concrete specimens, they should be placed in a mould in two nearly equal layers. Light tapping of the mould sides with a rubber hammer ensures the surface of the sample is level. The top surface should be finished immediately and covered with a plastic protection layer to prevent evaporation. Samples should not be removed from the moulds until the risk of damage has passed, and they should be ejected within 48 hours of moulding. Following moulding, the samples should be maintained at a temperature of  $21 \pm 5^{\circ}\text{C}$  for the first 24 hours. Subsequently, specimens are cured for 28 days under moist conditions, avoiding direct exposure to running water and stored at a relative humidity of  $50 \pm 20\%$  and a temperature of  $22 \pm 5^{\circ}\text{C}$ . These carefully controlled conditions ensure the proper development and durability of foamed concrete specimens.

The incorporation of fly ash and silica fume into foamed concrete has been observed to extend the curing time, primarily attributed to the substantial enhancement in foamed concrete strength (Pan et al., 2007; Amran et al., 2020; Hashemmoniri & Fatemi, 2023).

### 2.5. Properties of Foamed Concrete

Several factors significantly influence both the fresh and hardened state properties of foamed concrete. These include the type of foam agent utilized, the method of foam agent preparation to achieve a uniform distribution of air voids (bubbles), the foaming process itself, the precision of the mixture design calculation, and the overall production process of foamed concrete (Shankar et al., 2023).

The properties of foamed concrete can be categorized into fresh, physical, mechanical, and functional properties, all of which are influenced by the performance and quality of the manufacturing process. These properties will be elaborated upon in the subsequent sections.

### 2.5.1. Fresh Properties

Foamed concrete eliminates the need for compaction or vibration, unlike conventional concrete. During the fresh phase, the foamed concrete mix exhibits self-compacting properties. Therefore, parameters such as workability become crucial considerations. These aspects are typically influenced by factors such as the water-to-cement ratio ( $w/c$ ), additive materials, cement-to-fine aggregate ratio, plasticizers, and the type and volume of foam agents added (Brady *et al.*, 2001).

#### 2.5.1.1. Workability

Foamed concrete is recognized for its self-compacting nature, eliminating the requirement for vibration during placement. Nevertheless, it is imperative to assess the workability factor to ensure proper penetration of the foamed concrete through reinforcement or fill and to accurately take the shape of the shuttering form. This ensures that the foamed concrete achieves optimal placement and consolidation without the need for mechanical compaction. To assess the workability of foamed concrete mixes, visual examination of a viscosity is employed, unlike conventional concrete slump tests, which are not suitable for concrete mortar (Raj *et al.*, 2019).

An alternative method known as the spread ability test is utilized. In this procedure, a sample is placed in a small slump cone featuring dimensions of 70 mm top diameter, 100 mm bottom diameter, and 60 mm height. The cone is then raised vertically, and the spread in two directions is measured (Li & Li, 2013; Yang *et al.*, 2009).

Observations indicate that a high fibre content in foamed concrete leads to poor workability. It has been found that including fibre content within the range of 0.5% to 0.8% of the weight of the binder achieves a balance between performance enhancement and flowability. Additionally, increased foam content results in higher spread ability due to decreased solid content. Furthermore, substituting fly ash for ordinary Portland cement enhances spread ability owing to the small, round shape and smooth surface of fly ash grains. (Amran, 2020).

A limiting workability of 300 mm is suggested based on the recommendation by Alma'aitah and Ghiassi (2022). Their research involved conducting and reviewing around 80 mixes in textile reinforced concrete. Although there is no established standard for the workability of textile reinforced concrete, this research adheres to their suggestion that the spread ability diameter should be no less than 300 mm. This recommendation is grounded in the necessity for improved penetration of the concrete mix, which is essential for enhancing the bonding with embedded textiles. This improved bonding is critical for the composite material's overall performance, as it directly influences the structural integrity and durability of the textile reinforced concrete. Therefore, adhering to a high workability to ensures the optimal performance of the composite material.

The water-to-cement ( $w/c$ ) ratio in the base mix, crucial for achieving optimal workability, is influenced by several factors such as the type of binder(s) used, the desired strength of the concrete, and the presence of water-reducing or plasticizing agents. Typically falling within the range of 0.4 to 0.8, this ratio varies based on specific requirements. Higher ratios are necessary for finer-grained binders like fly ash due to their heightened absorption ability, while lower ratios are favoured for applications necessitating high strength or when superplasticizers are employed (Brady et al., 2001).

#### 2.5.1.2. Fresh Density

The fresh density, or wet density, of foamed concrete plays a pivotal role in mix design, serving as a primary factor in determining the density of all components. This process will be further elucidated in the Mix Design section in Chapter Three. According to BS EN 12350-6: 2019, the wet mix density of foamed concrete is typically calculated by filling and weighing a pre-weighted standard container of known volume with the fresh mix. Subsequently, the difference between the achieved and design densities should be assessed and limited to  $\pm 50 \text{ kg/m}^3$  (Bing et al., 2012).

The wet density is utilized to ascertain and prepare the volume of components in the design mix and to regulate the casting procedure. Conversely, the dry density governs

the physical, mechanical, and durability properties of hardened foamed concrete (Ramamurthy & Nambiar, 2009).

### 2.5.2. Physical Properties

In contrast to conventional concrete, the exclusion of coarse aggregate and the incorporation of foam significantly alter the physical properties of foamed concrete. Notably, properties such as drying shrinkage, density, and air-void system exhibit marked differences between foamed concrete and conventional concrete.

#### 2.5.2.1. Drying Shrinkage

Foamed concrete exhibits up to ten times greater drying shrinkage compared to conventional concrete. This disparity arises from the absence of coarse aggregates, higher cement content, and increased water content in foamed concrete. However, researchers have suggested that the performance of foamed concrete in terms of drying shrinkage can be enhanced. This improvement can be achieved by partially substituting cement with supplementary materials such as silica fume, fly ash, and lime, which possess lower heat of hydration (Amran et al., 2015). Additionally, the addition of fibres to the foamed concrete mix is known to reduce drying shrinkage. Fibres have the ability to retain and delay water evaporation within foamed concrete, thereby mitigating drying shrinkage (Pillar & Repette, 2015; Yousefieh et al., 2017). The drying shrinkage of foam concretes increases with an increase in foam volume (Gencel et al., 2021).

#### 2.5.2.2. Hardened Density

The designed hardened density of foamed concrete typically falls within the range of 280 to 1800 kg/m<sup>3</sup>, with corresponding compressive strengths ranging from 0.5 MPa to 40 MPa at 28 days. This variability in density is primarily influenced by the foam content within the mix (Bing et al., 2012). In a study conducted by Gökçe, Hatungimana and Ramyar (2019), the impact of fly ash and silica fume inclusion on

density was investigated. Fly ash and silica fume were replaced in percentages of 0, 10, and 20% by weight of cement, while the foam content in the mixture was 0, 31%, and 47% by volume. The findings revealed that fly ash addition had an insignificant effect on the density of the foam concrete mixture. However, the incorporation of silica fume led to a significant density increase, up to 20% compared to the control foamed concrete mixture. This notable rise in density led to reassessing the effect of silica fume addition.

The increase in density from 488 to 1024 kg/m<sup>3</sup> resulted in a substantial increase in fracture energy and tensile stress. Specifically, the fracture energy increased by approximately 800%, from 1.39 N/m to 12.54 N/m, while the maximal tensile stress increased by approximately 400%, from 0.112 MPa to 0.555 MPa (Kozłowski & Kadela, 2018). These findings suggest a strong correlation between density and mechanical properties in foamed concrete.

### 2.5.2.3. Air-Void Systems

The presence of air voids in foam concrete has a substantial impact on both its strength and density. These air voids are influenced by specific parameters such as their size, distribution, and volume percentage within the foamed mix. Recognizing the significance of air voids enables a more comprehensive understanding of how they affect the overall properties of foam concrete (Nambiar & Ramamurthy, 2007).

Protein foaming agents generate smaller isolated air bubbles compared to synthetic foaming agents (Panesar, 2013). Larger air voids in the mix reduce heat and sound conductivity, while smaller closed voids contribute to lower density and higher conductivity (Batool & Bindiganavile, 2017). Additionally, isolated small air voids lead to reduced water absorption, as disconnected voids impede water transport through the mix (Hilal et al., 2014).

Air void spacing, defined as the minimum distance between two voids, is a critical parameter influencing the foam concrete properties. Greater void spacing prevents voids from merging or overlapping, leading to improved strength and density.

Additionally, substituting fine aggregate with fly ash promotes a more uniform distribution of air voids, attributed to the finer particles of fly ash. These particles uniformly coat each air bubble, effectively isolating them from each other (Nambiar & Ramamurthy, 2007).

The instability seen in fresh foam concrete mixes is a result of internal forces acting on the bubbles and surrounding paste or mortar fractions. The buoyancy force, which is proportional to the size of the bubbles, causes bubbles to rise within lower density mixes, where larger bubbles are more prevalent. This buoyancy-driven movement contributes to the overall instability of the mix (Jones et al., 2016).

According to Dhasindrakrishna et al. (2021), the collapse of fresh foam concrete is influenced by two primary factors. Firstly, the yield stress of the interstitial paste determines its ability to maintain shape and resist deformation. Decreasing yield stress indicates reduced structural integrity, making collapse more likely. Secondly, foam content, with reduced foam content leading to decreased resilience and increased susceptibility to collapse.

### 2.5.3. Mechanical Properties

#### 2.5.3.1. Compressive Strength

The compressive strength of foamed concrete is influenced by various factors, including density, void characteristics, curing conditions, and ingredient properties (Tambe & Nemade, 2022). A decrease in dry density significantly reduces foamed concrete strength. Additionally, factors such as air void systems, foaming agents, water-to-cement ratio ( $w/c$ ), cement-to-sand ratio, and supplementary materials also impact compressive strength (Amran et al., 2015).

The water-to-cement ratio plays a crucial role in enhancing compressive strength, with an optimal range typically falling between 0.4 and 0.8. However, low water-to-cement ratios may impede complete cement hydration. The ratio of cement to sand also

affects strength, typically ranging from 0.5 to 1 for foamed concrete, depending on its intended applications (Nambiar & Ramamurthy, 2006; Amran et al., 2015).

Foaming agents are key determinants of compressive strength, with protein-based agents generally yield higher strengths due to the properties of the small air bubbles they generate compared to synthetic foaming agents (Panesar, 2013; Brady *et al.*, 2001).

Partial replacements of cement with silica fume or fly ash have been found to enhance compressive strength (Hilal et al., 2015; Pan et al., 2007). However, the rate of strength gain is slower with the addition of silica fume or fly ash, requiring a longer curing period to reach ultimate strength compared to mixtures using only Portland cement (Kearsley & Wainwright, 2002). Additionally, the inclusion of polypropylene short fibres and silica fume has been shown to further strengthen foamed concrete (Amran, 2020). Noticeably silica fume does not only affect compressive strength but greatly increases the density of foamed concrete mix (Gökçe et al., 2019).

A comparison of previous research studies reveals a consistent trend: an increase in compressive strength with a rise in density. However, noteworthy variations were observed, particularly in the study by Pan et al. (2007), which exhibited a more pronounced strength increase at lower densities compared to other findings. This discrepancy can be attributed to the utilization of ultra-fine mineral admixtures in their experiment. The inclusion of these ultra-fine minerals elevated the viscosity of the fresh foamed concrete mixture, enhancing its ability to support sand particles and thus preventing segregation. Another study by Li et al. (2023) also supports this notion, indicating that ultra-fine slag significantly improved both compressive strength and the strength-to-density ratio in foamed concrete. Consequently, it is recommended to further investigate the impact of ultra-fine mineral admixtures on foamed concrete strength with different densities to better understand their effects.

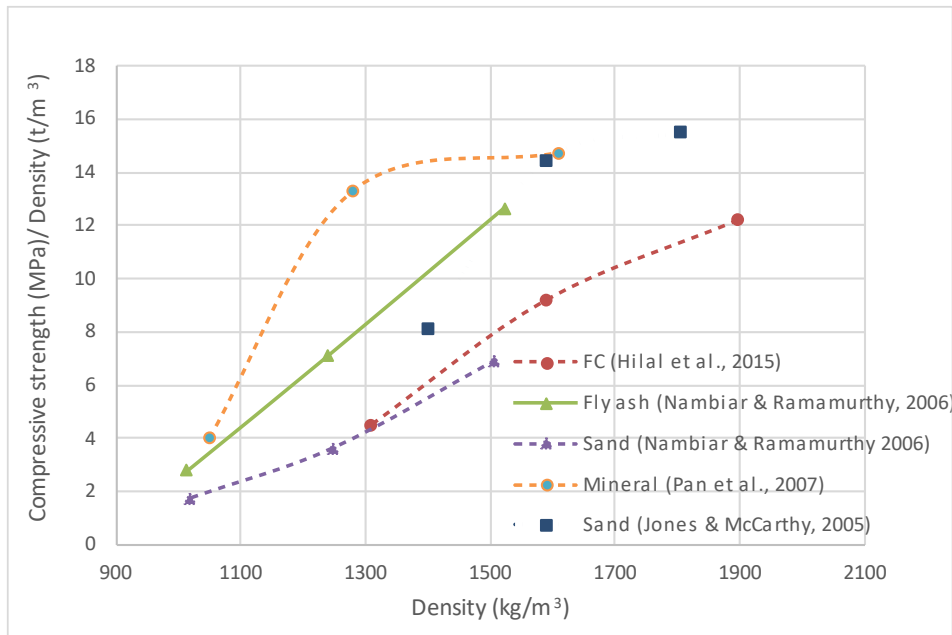


Figure 2.7: Strength to strength density ratios for different foamed concrete mixes

### 2.5.3.2. Flexural and Tensile Strength

Flexural and tensile strengths are crucial parameters in the analysis and design of concrete structures, often specified in industry codes and standards alongside compressive strength. Typically, these strengths show improvement with increasing compressive strength (Bing et al., 2012). Similarly, in the case of foamed concrete, tensile and flexural strengths also exhibit improvements (Amran et al., 2015).

The addition of polypropylene fibres, as highlighted by Bing et al. (2012), can substantially enhance the tensile strength of foamed concrete by up to threefold. The effectiveness of fibres is influenced by factors such as length, quantity, and size, with an optimal combination contributing to increased tensile capacity. Furthermore, fibres play a crucial role in transforming the behaviour of foamed concrete from brittle to ductile, thereby enhancing both flexural strength and overall toughness.

In beam flexural tests, it was observed that foamed concrete beams exhibited greater deflection at failure, ranging from 13% to 20% more than conventional concrete beams. However, it was noted that reinforced foamed concrete beams showed limited resistance to shear forces (Tan et al., 2011).



Recent studies have shown that while the introduction of a 2% by volume fibre content does enhance flexural capacity compared to control samples, further increases to 5% do not yield significant further improvements. Hence, it is advisable to limit the fibre content in foamed concrete elements to 2% to achieve optimal characteristics, as observed in experimental campaigns (Falliano et al., 2019).

#### 2.5.3.3. Modulus of Elasticity

The modulus of elasticity plays a critical role in determining the elastic properties of concrete, directly impacting the performance and serviceability of concrete structures. This parameter is primarily influenced by the properties of the cement paste and the type of aggregate used (Zheng et al., 2008).

In foamed concrete, the density serves as the most influential factor affecting the modulus of elasticity. For example, dry densities of 400 and 1600 kg/m<sup>3</sup> result in modulus of elasticity values ranging around 1.0 and 11 GPa, respectively. This significant variation in modulus can be attributed to the differing densities of the foamed concrete mixtures. Additionally, studies have shown that incorporating polypropylene fibres into foamed concrete can have a positive impact on its stiffness, further enhancing its modulus of elasticity (Brady et al., 2001).

### 2.5.4. Functional Properties

#### 2.5.4.1. Thermal Conductivity

Foamed concrete offers significantly lower thermal conductivity, with reported reductions of up to 30% in thermal conductivity when compared to conventional concrete. This characteristic makes foamed concrete an attractive option for applications requiring enhanced thermal insulation (Brady et al., 2001).

The thermal conductivity of foamed concrete tends to increase with its density. For instance, foamed concrete with a density of 500 kg/m<sup>3</sup> exhibits a thermal conductivity of 0.08 W/mK, while one with a density of 1800 kg/m<sup>3</sup> has a thermal conductivity of

0.68 W/mK (Gökçe et al., 2019). This trend can be attributed to the presence of more voids in lower density foamed concrete, which act as insulating barriers, thereby reducing thermal conductivity.

Moreover, studies have shown that replacing a portion of the cement in foamed concrete with supplementary materials such as fly ash or silica fume can affect its thermal conductivity. For example, replacing 20% of cement with fly ash can lead to a reduction in thermal conductivity of up to 40%. Conversely, replacing cement with silica fume may increase thermal conductivity by up to 37% (Gökçe et al., 2019). The rise in thermal conductivity associated with the use of silica fume in foamed concrete mixes may be attributed to the increase in density.

Additionally, the incorporation of short fibres can disrupt the continuity of heat transfer paths within the concrete matrix, resulting in improved insulation properties for foamed concrete (Wijesinghe et al., 2024).

#### 2.5.4.2. Acoustic Insulation Resistance

The ability of foam concrete to resist the transmission of airborne sound is influenced by its density and the frequency of the sound. Unlike conventional concrete, foam concrete exhibits higher sound absorption capabilities (Zhang et al., 2015). According to sound transmission theory, sound frequencies are reflected based on the density and thickness of the wall, resulting in greater sound reflection in denser concrete elements (Amran et al., 2015; Laukaitis & Fiks, 2006). Additionally, the inclusion of fibres in foam concrete creates frictional resistance against sound waves, resulting in a decrease in the amplitude of transmitted sound as the energy transforms into thermal energy due to this friction (Wijesinghe et al., 2024).

While foam concrete can offer superior sound insulation performance compared to conventional concrete, it is essential to mention that the extent of this improvement may differ depending on factors for instance the density. Denser foam concrete tends to exhibit better sound insulation properties due to increased mass and sound reflection capabilities. Therefore, claims of foam concrete boasting significantly better

insulation capabilities should be interpreted with consideration of the specific density and other relevant factors (Tambe & Nemade, 2022).

#### 2.5.4.3. Fire Resistance

It has been documented that foamed concrete can offer comparable fire resistance to conventional concrete. However, exposure to elevated temperatures can result in excessive shrinkage due to rapid evaporation (Amran et al., 2015). The fire resistance of foamed concrete is generally influenced by its density, with lower densities exhibiting greater resistance. Notably, it has been observed that foamed concrete with densities of  $950 \text{ kg/m}^3$  and  $1200 \text{ kg/m}^3$  can endure fire for 3.5 hours and 2 hours, respectively (Jones & McCarthy, 2005).

While existing literature highlights the superior fire resistance of foamed concrete, further investigation is warranted to elucidate the underlying mechanisms of this property. Moreover, there is a need to explore the characteristics of foamed concrete reinforced with various fibres and to evaluate the outcomes of foamed concrete supported by other materials (Raj et al., 2019).

## 2.6. Textile Reinforced Concrete (TRC)

### 2.6.1. Introduction

Textile reinforced concrete (TRC) is described as a composite material, which is a combination of textile material and fine-grained concrete. It has been considered as a construction material for more than ten years. Generally, structural elements of textile reinforced concrete contain layers of textile fabrics of multi-filament yarns (so-called roving), which are commonly manufactured from carbon, basalt, or alkali-resistant glass materials. The textile layers are embedded in a fine-grained concrete with a maximum size of fine aggregate of 2 mm (Graf et al., 2007; Hartig et al., 2008). TRC provides the opportunity to build thin and lightweight elements for structural use. Also, it does not require a minimum concrete cover to protect against corrosion, compared to steel reinforcement bars. Furthermore, TRC is typically available as sheets that facilitate it to form and take the geometry of the element (Schneider & Schätzke, 2006).

### 2.6.2. Textile Reinforced Concrete Material

#### 2.6.2.1. Fine Grained Concrete

The cementitious material plays a crucial role in enhancing the bond between the textile reinforcement layers and the concrete matrix by facilitating increased penetration of fine-grained concrete between filaments (Hegger & Voss, 2004). Several factors, including the particle size of the cementitious matrix and the textile's geometry, influence the penetration of the concrete matrix (Dolatabadi et al., 2010).

Typically, the maximum grain size utilized is smaller than 2 mm, classifying the mixture as mortar. Moreover, the incorporation of replacement materials such as silica fume and fly ash not only improves the consistency and stability of the mixture but also enhances its mechanical properties (Bramshuber et al., 2006).

The key advantage of utilizing textile reinforcement lies in the ability to construct lightweight and thin elements. In the context of this research, the fine-grained concrete under examination is foamed concrete, specifically chosen for its compatibility with textile reinforcement. Furthermore, foamed concrete is lighter than conventional fine-grained concrete, offering improved sound and heat resistance compared to its conventional counterpart.

#### 2.6.2.2. Textile

Textile refers to materials made from continuous long filaments or fibres woven, knitted, or otherwise constructed into a fabric-like structure. These textiles are used to reinforce concrete, providing enhanced strength and ductility. Textile can be made from a variety of materials, including alkali-resistant glass (AR-glass), carbon, aramid, basalt, and metals. Textiles provide a structured reinforcement that enhances tensile strength transforming the behaviour of concrete into a more ductile form, whereas short fibres primarily improve crack resistance and toughness (Bing et al. 2012; Mobasher, 2016).

The textile fabrication method and the fineness of the yarn significantly influence the interaction between the filaments. Textiles fabrications are predominantly produced as filaments or twisted yarns. In Figure 2.8, the left image (a) shows filament yarn, which is a bundle of elementary fibres called filaments. Each yarn consists of several hundred to thousands of single filaments. The fineness of the yarn, indicated as tex (grams per 1000 meters), depends on the number of filaments, the average filament diameter, and the fibre density. The right image (b) shows twisted yarn, which is composed of filaments twisted together. Filament yarns stand out as the superior choice for reinforcement due to their minimal structural elongation (Gries et al., 2006).

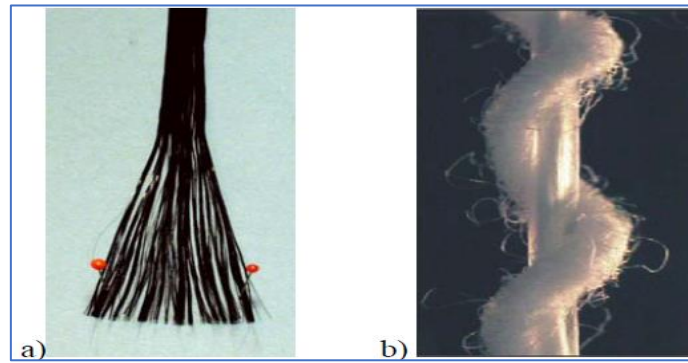


Figure 2.8: Yarn construction: a) filament yarn, b) twisted yarn (scale for the photographs 0.1 - 0.2 mm per pixel). (Gries et al., 2006)

When it comes to textile materials, alkali-resistant glass fibres (AR-glass), carbon, aramid, basalt, and metal textiles are among the most used. Figure 2.9 shows different types of textile materials (Gries et al., 2006).

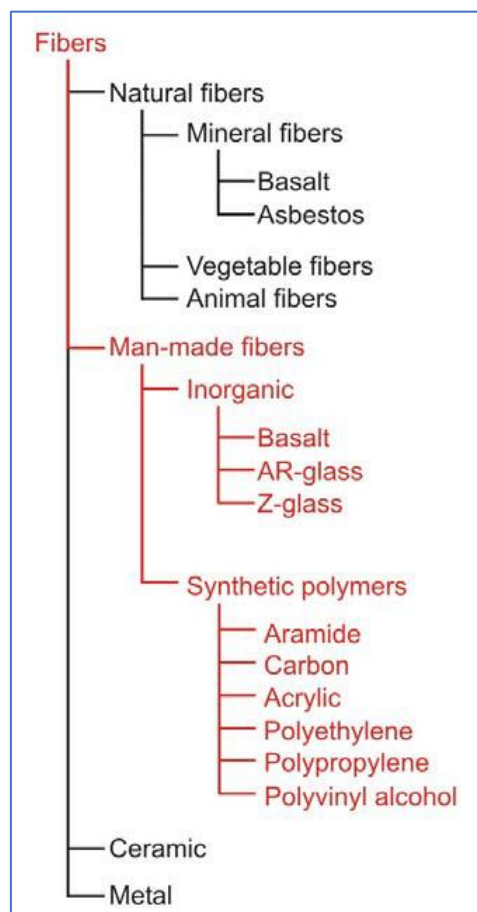


Figure 2.9: Different types of textile materials (Gries et al., 2006)

Textile materials predominantly consist of a two-dimensional structure known as bi-axial textiles. In this configuration, two directions play a key role: the warp ( $0^\circ$ )

direction, situated lengthwise in the reinforcing direction, and the weft (90°) direction, positioned crosswise, as illustrated in Figure 2.10 (Peled et al., 2008).

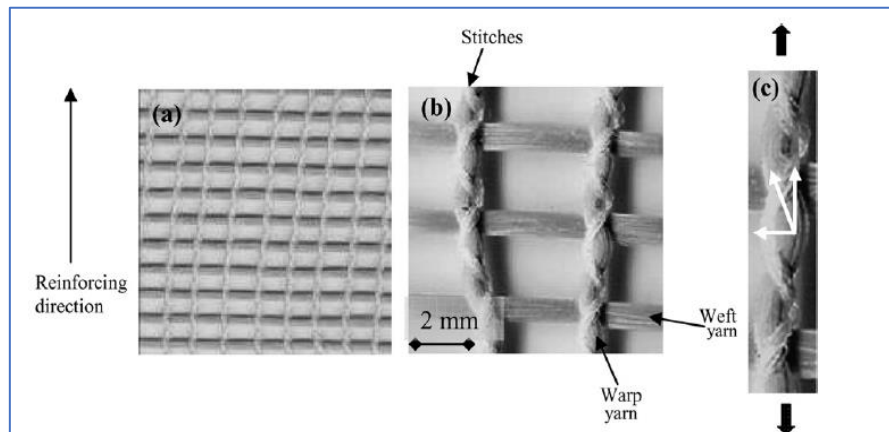


Figure 2.10: Warp & weft directions in bi-axial textile (Peled et al., 2008)

In specific instances, exemplified in Figure 2.11, a multi-axial warp knit textile is presented, comprising eight layers that provide flexibility in their orientation (0°, 90°, +45°, -45°). The 0° direction aligns with the warping direction, and the threads adjusted at different angles are denoted as the weft. This design allows for a versatile arrangement of layers, catering to specific reinforcement requirements (Gries et al., 2006).

The extensive benefits of utilizing multi-axial warp knit textiles are comprehensively discussed in Section 2.6.4.3, specifically focusing on their role in addressing transverse loading influences.

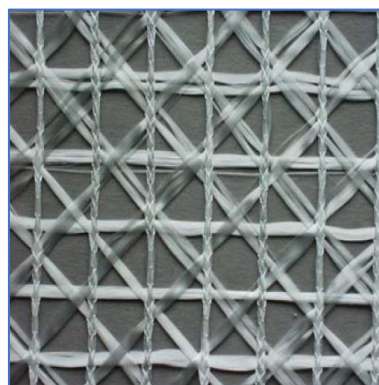
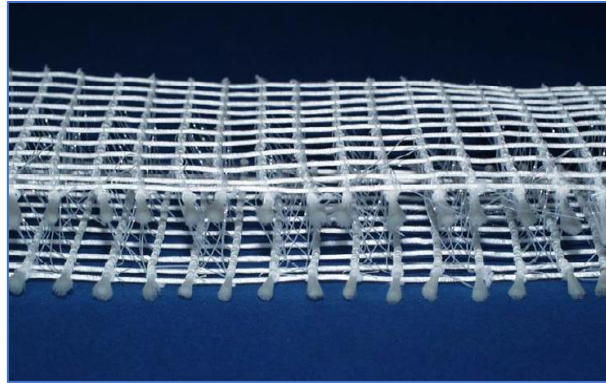


Figure 2.11: Warp & weft directions in multi-axial textile (Gries et al., 2006)

Additionally, three-dimensional warp knit textiles are crafted using two textile fabrics interconnected, as depicted in Figure 2.12. This innovative three-dimensional textile finds primary application in reinforcing thin concrete elements, where each fabric is typically positioned close to the surface (Gries et al., 2006).



*Figure 2.12: Three-dimensional textile (Gries et al., 2006)*

### 2.6.3. Filament Material and Properties

The properties of filament, yarn (roving), and textile materials are essential determinants of the characteristics of composite textile-reinforced concrete. In the following sections, the three main textile types will be discussed.

#### 2.6.3.1. Alkali-Resistant (AR)-Glass Filament Yarns

AR-glass filament yarns exhibit resistance to the corrosive alkaline factors present in concrete. Derived from melting silica sand, clay, and limestone at temperatures up to 1350 °C, the size of the glass fibres is crucial for subsequent processes, enhancing yarn properties, adhesion, and stress transfer between filaments and the matrix material. The basic mechanical properties of AR-glass, depending on yarn fineness, include a tensile strength of up to 1400 N/mm<sup>2</sup>, linear elastic elongation of up to 2%, and a modulus of elasticity ranging between 70 and 80 kN/mm<sup>2</sup>. Although its density is relatively high at 2.8 kg/dm<sup>3</sup> compared to carbon or aramid, AR-glass demonstrates good adhesion to concrete, presenting a favourable cost-performance ratio (Gries et al., 2006).



### 2.6.3.2. Carbon Filament Yarns

Carbon filament yarns, produced from polyacrylonitrile through polymerization and thermal treatment, boast a high modulus of elasticity and tensile strength compared to AR-glass. With a modulus of elasticity between 200 and 450 kN/mm<sup>2</sup> and tensile strength ranging from 2000 to 5000 N/mm<sup>2</sup>, carbon fibres have a low density of 1.8 kg/dm<sup>3</sup>. They exhibit minimal creeping, low heat expansion and conductivity, good electrical conductivity, and high resistance to acid, alkaline, and organic solvents. Despite these advantages, the adhesion to concrete is not as robust as that of AR-glass. Carbon fibres also pose challenges in processing due to their sensitivity to lateral stresses, leading to more frequent filament breaks (Gries et al., 2006).

### 2.6.3.3. Aramid Filaments

Aramid filaments, created through the polycondensation of aromatic dicarbon acids with aromatic diamines, possess exceptional tensile strength and modulus of elasticity. With a tensile strength of about 3000 N/mm<sup>2</sup> and a modulus of elasticity ranging between 60 and 130 kN/mm<sup>2</sup>, aramid fibres offer a lower density of 1.4 kg/m<sup>3</sup>, reduced brittleness, and higher impact resistance compared to carbon and glass fibres. However, aramid fibres are susceptible to heat expansion, which can result in a significant difference in expansion between the reinforcing material and the concrete. This discrepancy leads to reduced adhesion between aramid fibres and concrete, limiting their usage. Additionally, aramid fibres exhibit low resistance to alkaline solutions (Gries et al., 2006).

In this research, Alkali-Resistant (AR)-Glass fibres were chosen for their properties, aimed at inducing various failure cases in relatively small textile-reinforced foamed concrete beams. Detailed explanations of this selection and its implications will be provided in Chapter Four and Chapter Five.

## 2.6.4. Textile Reinforced Concrete Bearing Capacity

### 2.6.4.1. Impregnation Influence

Textile reinforced concrete (TRC) presents significant potential for constructing lightweight and load-bearing structures. Through the use of noncorrosive textile reinforcement, such as alkali-resistant (AR) glass or carbon fibres, the need for substantial concrete cover is minimized. The mechanical performance of textile-reinforced concrete (TRC) is intricately influenced by various characteristics of the textile fabrics. Key factors include the fibre material, the cross-sectional area of the roving, and the binding type of warp-knitted fabrics, such as tricot or plain stitch bond. Of particular importance is the impregnation process.

Impregnation, also known as coating, involves applying a protective layer to textiles to stabilize their inner structure and shape, ultimately fixing the textile's form. Its primary impact lies in enhancing the tensile strength of a textile reinforced component by amplifying the activation of the roving's inner filaments. Without impregnation, only the outer part of the roving, and selective filaments, directly engage with the surrounding concrete. Consequently, the stress-bearing capacity is lower at the centre of the roving, with only the load-bearing filaments effectively contributing, leading to potential separation from unloaded parts. In contrast, impregnated textiles facilitate a more uniform load distribution among filaments, resulting in heightened load-bearing capacity and a smoother response to applied loads (Gries et al., 2016). Figure 2.13 visually depicts the influence of coating on stress distribution within the filaments.

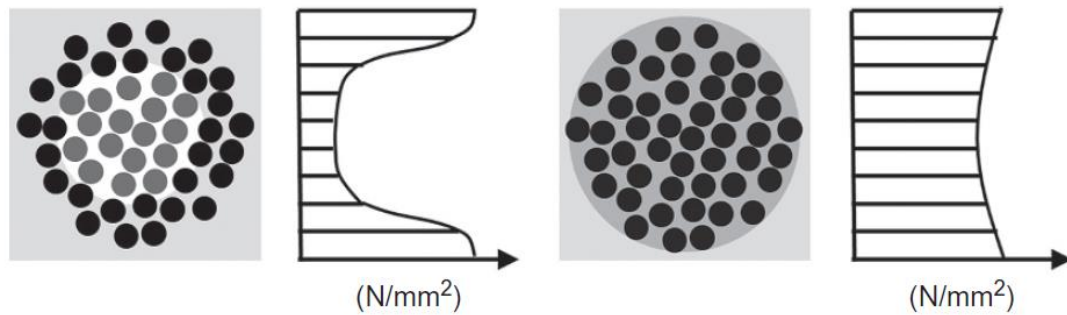


Figure 2.13: Cross-section of Roving Without Impregnation (Left) and With Impregnation (Right) (Gries et al., 2016)

Hegger et al. (2006) conducted research involving tensile tests on impregnated and non-impregnated textile-reinforced concrete, as well as individual filaments, roving, and textiles, to assess their bearing capacity. Drawing insights from previous studies, their findings indicate that impregnation (coating) significantly enhances the bearing capacity of textile-reinforced concrete. Notably, the tensile performance of impregnated textile-reinforced concrete closely aligns with that of individual filaments, suggesting a substantial improvement in the bonding between the impregnated textile and the concrete mortar within the composite as illustrated in Figure 2.14.

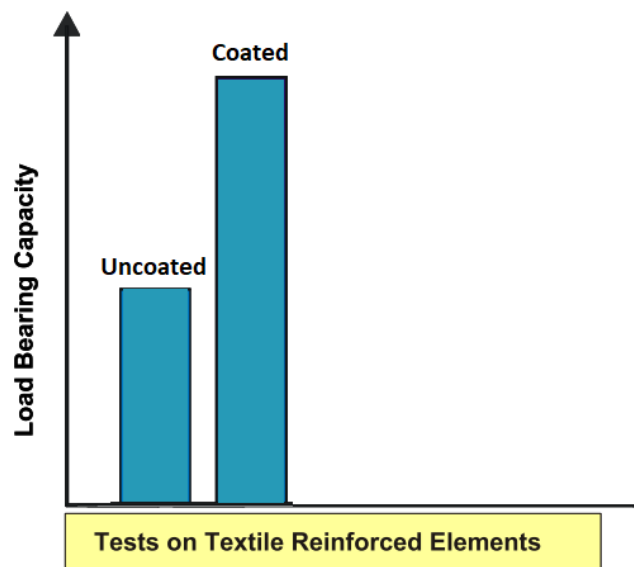


Figure 2.14: Comparison of the tensile strength between coated and uncoated textile in TRC element (Hegger et al., 2006)

The type of impregnation material applied, with options including epoxy resin, styrene-butadiene, or no impregnation, plays a pivotal role in determining the

material's overall behaviour. For instance, in the case of 3300-tex carbon yarns (measured in grams per kilometre length, g/km, denoted as "tex"), wherein the yarns are impregnated with epoxy-resin, composite tensile tests have demonstrated maximum textile stress of up to 3000 MPa. The stress level observed closely matches the material strength of carbon fibres, indicating a nearly complete activation of the yarn, even encompassing the inner filaments that lack direct contact with the concrete matrix. In contrast, a 3300-tex carbon yarn with impregnation of styrene-butadiene rubber (SBR), achieves lower textile stresses in the composite, nearly 2000 MPa. The reduced efficiency of the yarn with SBR impregnation is attributed to inferior bond properties, resulting in reduced activation of the inner filaments. This results in an extended anchorage length within the composite and a partial pullout of the inner filaments (Hegger & Will, 2016).

#### 2.6.4.2. Filament, Yarn (Roving) Influence

Textile are manufactured from many filaments (roving). These filaments do not act under the tensile strength as a homogeneous material. The tensile strength capacity of a TRC composite is mainly affected by the bonding mechanism between filaments (roving) and matrix. It can be said that tensile strength failure mostly occurs in the TRC composite due to the debonding between the filaments and the matrix (Xu & Li, 2007). Previous studies have been conducted to demonstrate the difference between the tensile strength of a filament itself and the strength tensile of the TRC composite. They showed that the filament strength is around double the strength of the TRC composite, see Figure 2.15. Furthermore, the failure mechanism of TRC is influenced by filament damage and uncertainties in their properties that may arise during the production phase. Additionally, failure can occur due to inadequate bonding between the filaments themselves or between the roving and the concrete mixture (Hegger et al., 2006).

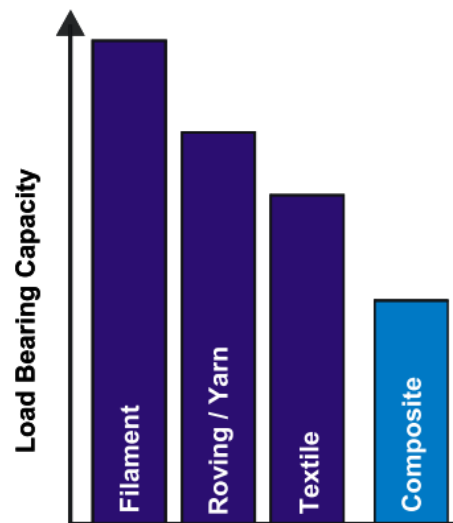


Figure 2.15: Comparison of the tensile strength of a filament, roving, textile with composite section (Hegger et al., 2006)

#### 2.6.4.3. Transverse Loading Influence

The load-bearing capacity of textile reinforcement under additional transverse loading experiences varying reductions attributed to the use of different textile fibre materials. In a tensile test, despite the identical geometrical properties of carbon and alkali-resistant (AR) glass textiles, the carbon textile-reinforced concrete exhibited greater sensitivity to biaxial stresses compared to the AR glass sample. Tests were conducted with the textile oriented at five different angles:  $0^\circ$  (conventional case),  $22.5^\circ$ ,  $45^\circ$ ,  $67.5^\circ$ , and  $90^\circ$ . Figure 2.16 illustrates the relationship between the ratios ( $k_{0\alpha}$ ), representing load-bearing capacities between sloped textile reinforcements and the textile aligned in the load direction ( $0^\circ$ ). Notably, when the textile was oriented at  $45^\circ$ , the carbon textile-reinforced concrete lost 60% of its bearing capacity, whereas the AR glass textile-reinforced concrete lost only 40% (Hegger & Voss, 2004).

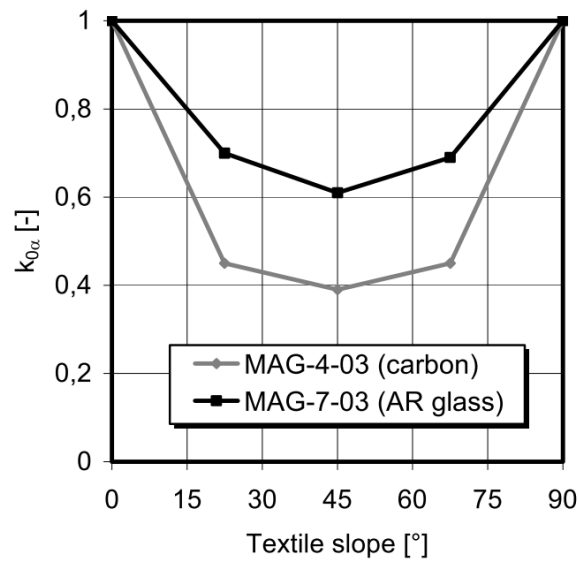


Figure 2.16: Effect of orientated 0°, 22.5°, 45°, 67.5°, 90° carbon and AR glass textile reinforced concrete in tensile tests (Hegger & Voss, 2004)

This effect becomes especially apparent in complex structures like shell elements, where textiles are oriented in diverse directions. Similarly, in straight elements like beams, transverse forces such as shear forces, exert an influence on the behaviour of textile reinforcement bearing capacity. In response to these challenges, employing a multi-axial warp-knit textile, encompassing different axials (0°, 90°, +45°, -45°), offers a viable solution to address transverse forces. This concept is akin to 3D textile reinforced concretes (TRCs), which utilize three-dimensional warp-knit textiles. These textiles, as depicted in Figure 2.12, consist of two linked fabrics. The efficacy of employing multi-axial textiles has been substantiated by studies such as those conducted by El Kadi et al. (2020).

### 2.6.5. Textile Bond

The properties of textile-reinforced concrete (TRC) composites are notably contingent on the interaction between the textile and the matrix. This bond behaviour plays a crucial role in dictating the overall performance of the composite, influencing its strength, toughness, and ductility (Banholzer et al., 2006). Typically, a robust bond tends to lead to reinforcement fracture, yielding high strength yet limited ductility and relatively brittle characteristics. In contrast, a less robust bond is more likely to induce

fibre pullout, resulting in a more ductile composite with diminished strength (Peled, 2016).

The bond between the textile and the concrete matrix is measured by the friction between the external filaments, connected to the matrix, and the concrete mortar. However, textiles are inherently non-homogeneous materials, and the bonding between filaments within the textile significantly influences its performance as a cohesive unit (Graf et al., 2007).

As depicted in Figure 2.17, an optical examination illustrates the bonded textile roving within a cementitious matrix. Here, only the outer part of the filaments is anchored in the concrete, allowing the core filaments to slide easily within the roving, particularly at low friction levels. Additionally, the cementitious matrix does not completely penetrate the core of the filaments (Reinhardt et al., 2006).

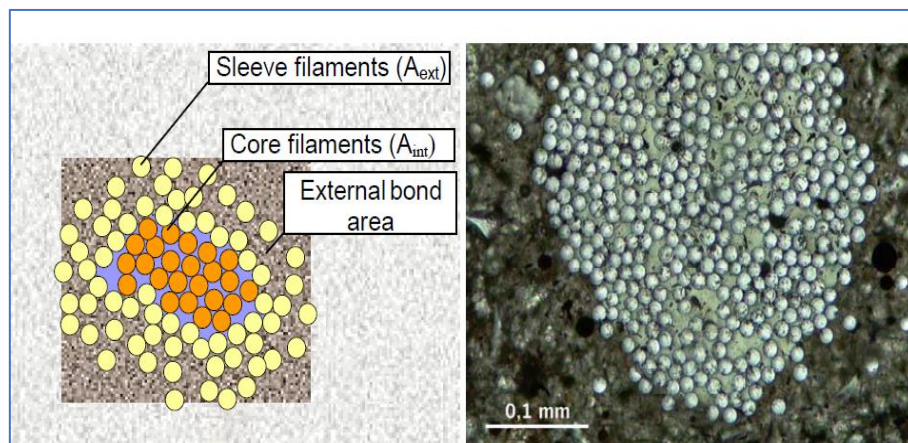


Figure 2.17: Roving with inner bond & outer bond (Reinhardt et al., 2006)

To enhance the reinforcing efficiency of Textile-Reinforced Concrete (TRC), epoxy resin impregnation can be employed. After impregnation with epoxy resin, the filaments may behave as a rigid, thin unit. Furthermore, covering the impregnated textile with sand can maximize the ultimate pull-out force, attributed to the heightened friction between the filaments and the concrete matrix (Xu & Li, 2007).

### 2.6.6. Pull-out Test

The stiffness of the fibre interface mortar system plays a crucial role in determining toughening mechanisms. In brittle mixtures, when the ultimate strain capacity of the fibres surpasses that of the matrix, the fibres act as bridges across matrix cracks. This bridging effect reduces stress concentration at the matrix crack, and the response of the debonding phase relies on the length of cylindrical shear microcracks formed at the interface. Additionally, the interface's ability to transmit traction across a matrix crack contributes to the overall toughening process. As fibres bridge matrix cracks, the processes of debonding and pullout contribute to toughening and energy dissipation (Mobasher, 2016).

Barhum & Mechtcherine (2013), investigated the pull-out test of a single yarn interconnected by transverse fibres in their study. Ghiassi et al. (2016), emphasized the importance of a comprehensive examination of pull-out behaviour in fabrics embedded in mortar, including the influence of transverse fibres on bond performance, to develop accurate constitutive models. The current pull-out test builds upon this previous research. It involves a thorough exploration of the bonding behaviour of three AR-glass yarns interconnected by transverse fibres along the entire length of concrete specimens. The key aspects of the current pull-out test include embedding the textile material along the length of the concrete specimens and utilizing three textile yarns interconnected by transverse fibres.

### 2.6.7. Stress-Strain Diagram of Textile Reinforced Concrete

Mobasher (2016) and Hegger et al. (2006) presented a comprehensive stress-strain diagram for textile-reinforced concrete (TRC) under uniaxial loading, delineated into four distinct stages, as illustrated in Figure 2.18.

- **Uncracked Composite Material (State I):**

In this initial stage, the composite remains uncracked, with the tensile strength primarily carried by the fine-grained concrete. The stiffness loading in this phase aligns with the E-modulus of the fine concrete.



- **Multiple Cracking - State II a:**

As the applied tensile strength surpasses the concrete tensile strength, the cracking process initiates, and the entire tension force is transferred to the textile reinforcement. Additional cracks are exhibited as the tension force increases, with crack width and distance decreasing due to enhanced bonding between textile reinforcement filaments and the concrete matrix.

- **Stabilized Crack Pattern - State II b:**

In this stage, the cracks stabilize, and no further cracks emerge. With increased loading, the filaments strain to resist this force, and the stress-strain curve roughly parallels that of the pure textile.

- **Failure state (State III):**

A ductile deformation area (State III) is absent in TRC tensile tests due to the lack of plastic capacity in the materials used (AR-glass, Carbon). Consequently, the composite fails in a brittle manner upon reaching the tensile failure strain of the reinforcement.

Overall, the stress-strain diagram of TRC exhibits a pattern similar to that of conventional concrete, particularly characterized by brittleness.

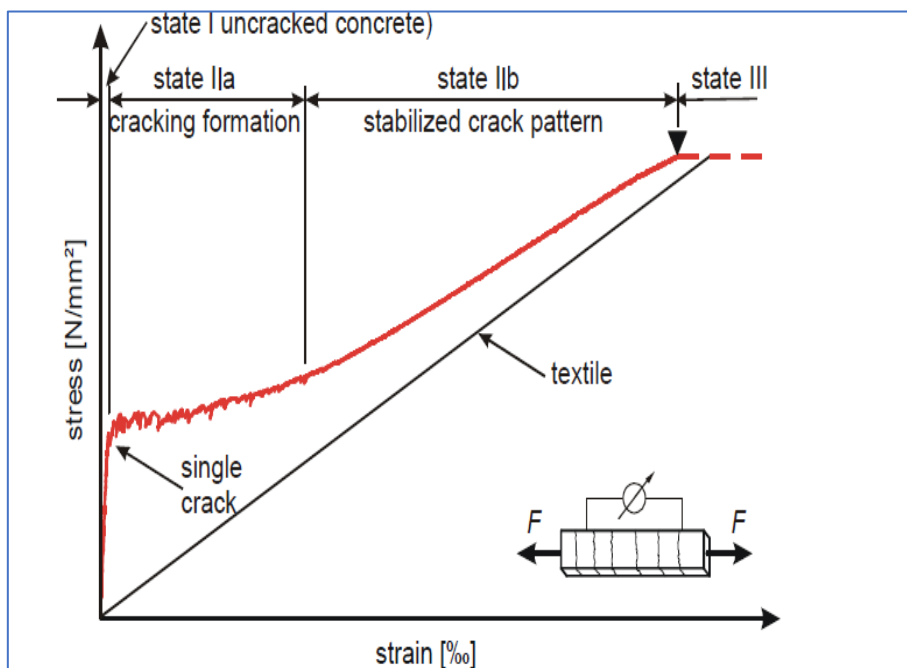


Figure 2.18: Stress-strain diagram of TRC under uniaxial loading (Hegger et al., 2006)

### 2.6.8. Textile Form Flexibility

In addition to the inherent strength of fabrics, the choice of impregnation significantly influences their form flexibility. When dealing with straight, rectangular structural components like facade panels (depicted in Figure 2.19), formed by casting fresh concrete into moulds, high-form stability of fabrics proves advantageous. This stability simplifies the production process, facilitating tasks such as placing textile fabrics and controlling their position within the formwork. Epoxy-resin impregnation enables the creation of form-stable reinforcement elements, exemplified in Figure 2.20. However, in the case of textile reinforced concrete (TRC) structures with curved geometries, such as shell structures requiring heightened form flexibility, the conventional high-form stability of fabrics becomes impractical. In these scenarios, the utilization of nonimpregnated fabrics proves more suitable for achieving the necessary adaptability and flexibility in conforming to the intricate curves of the structure (Hegger & Will, 2016).



*Figure 2.19: Examples of lightweight TRC structures (ventilated facade panels) (Hegger & Will, 2016)*

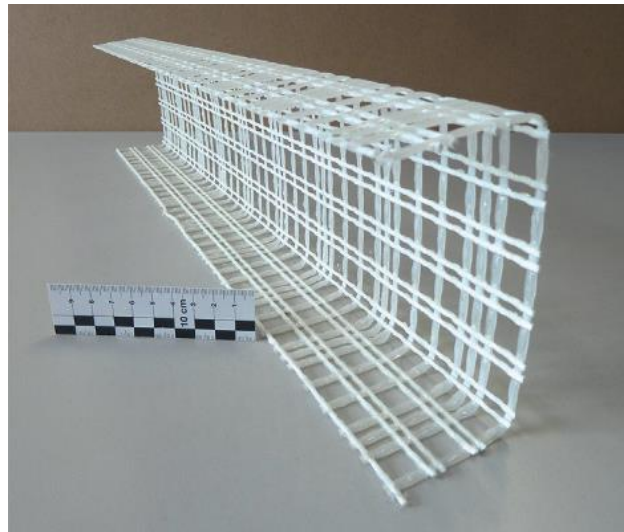


*Figure 2.20: AR-glass textile impregnated with epoxy-resin (Hegger & Will, 2016)*

### 2.6.9. Textile Reinforced Concrete (TRC) Design

Matrix cracking has a limited impact on the strength of impregnated textiles, whereas the interaction is more pronounced in the strength of non-impregnated textiles (Ferrara et al., 2021). Consequently, in the context of impregnated textiles, there exists a theoretical possibility to predict the bending strength and ultimate tensile strength of textile reinforced concrete, relying on the material characteristics of the composite components (Bensadoun et al., 2017; Rempel et al., 2015). However, the anticipation of cross-sectional strength for nonimpregnated textile fabrics becomes challenging when relying on predictions based on composite components and equilibrium conditions. Therefore, establishing the cross-sectional strength characteristics for textile reinforced concrete (TRC) structures reinforced with nonimpregnated fabrics necessitates experimental determination. This involves conducting tests on specimens that precisely mirror the cross-sectional layout applied in the specific structural design under consideration (Hegger & Will, 2016).

In 2016, Hegger and Will presented a design example of beam and slab elements utilizing impregnated carbon textiles. Figure 2.21 depicts a façade textile reinforced concrete (TRC) panels measuring  $3.20 \times 4.50$  m with a thickness of 30 mm. The textile reinforcement is carbon fabric comprised of 3300 tex roving impregnated with epoxy

resin. The spacing between roving is 60 mm in the 0-degree direction and 62 mm in the 90-degree direction of the textile.



Figure 2.21: Large-sized TRC facade panels (Hegger & Will, 2016)

The facade panels are affixed to the building's load-bearing structure through two stiffening ribs, each with an increased thickness of 10 cm as illustrated in Figure 2.22. Horizontal wind loads are carried by the slabs in a unidirectional manner between these ribs. Consequently, the design calculations can be executed using a simply supported beam model, characterized by a rectangular cross-section with a unit width.

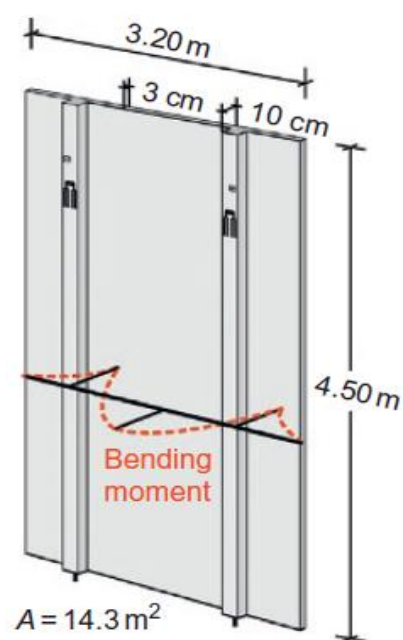


Figure 2.22: Backside of one TRC panel with supporting lines (Hegger & Will, 2016)

As previously discussed, it is indeed possible to predict the bending strength and ultimate tensile strength of textile-reinforced concrete using impregnated fabrics. This approach is grounded in the material behaviour of both the reinforcement and concrete, drawing an analogy to conventional steel-reinforced concrete cross-sections. Schladitz et al. (2012) delineate a comparable approach for evaluating retrofitted steel-reinforced structures using textile-reinforced concrete. To estimate the ultimate bending capacity ( $M_u$ ) for a specific cross-sectional layout, concrete compression tests, and yarn tensile tests have been conducted experimentally, as illustrated in Figure 2.23.

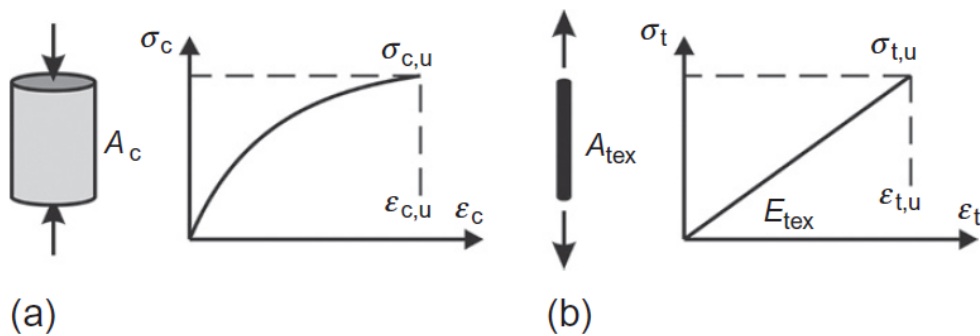


Figure 2.23: Experimentally determine the material characteristics (a) the concrete compression and (b) the impregnated yarn tension (Hegger & Will, 2016)

In Figure 2.23  $\epsilon_{cu}$  is the ultimate concrete strain;  $\sigma_c$  is the ultimate concrete stress;  $\epsilon_{tu}$  is the ultimate textile strain;  $E_{tex}$  is the textile young's modulus of elasticity.

Figure 2.24 provides a diagrammatic representation of the cross-sectional model for the TRC beam element. In computing the bending capacity ( $M_u$ ), a linear strain distribution across the cross-sectional height is assumed. Additionally, the tensile strain ( $\epsilon_{t,0}$ ) is constrained to the rupture strain ( $\epsilon_{tu}$ ) observed in yarn tests, considering a reinforcement failure of the composite cross-section ( $\epsilon_{t,0} \leq \epsilon_{tu}$ ). The determination of the compressive strain ( $\epsilon_c$ ) at the top of the TRC cross-section requires an iterative process. It involves adjusting the strain profile iteratively to ensure the equilibrium of internal normal forces is satisfied.

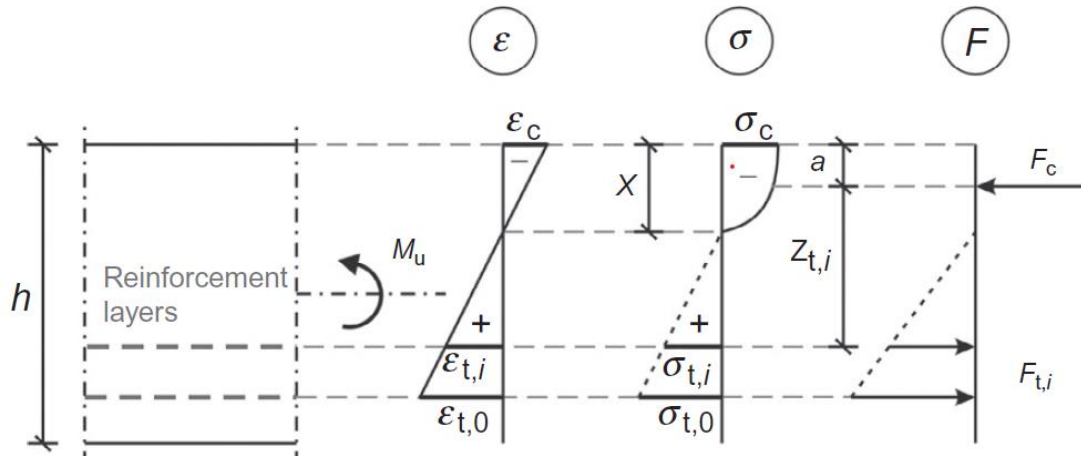


Figure 2.24: Cross-sectional model for the TRC beam element diagram

In Figure 2.24  $h$  is the height;  $\varepsilon_c$  is the concrete ultimate strain;  $\varepsilon_{t,0}$  and  $\varepsilon_{t,i}$  are the lowest and highest textile strain layer respectively;  $X$  is the neutral axis depth;  $\sigma_c$  is the concrete stress;  $\sigma_{t,0}$  and  $\sigma_{t,i}$  are the textile stresses;  $F_c$  is the compressive force;  $F_{t,i}$  is the tension force;  $Z_{t,i}$  is the lever arm between the forces.

In the initial phase of the calculation process, the stress distribution derived from the assumed strain profile is evaluated. The integration of compressive stresses ( $\sigma_c$ ) over the compressive zone ( $X$ ) yields the resulting compressive force ( $F_c$ ). The calculations are determined as follows:

$$F_c = \int_0^{\varepsilon_c} \sigma_c(\varepsilon) d(\varepsilon) \quad (2.1)$$

$$F_{t,i} = A_{tex} \sigma_{t,i} \quad (2.2)$$

$$F_c - \sum_i F_{t,i} = 0 \quad (2.3)$$

The ultimate bending capacity ( $M_u$ ) can be calculated by multiplying the internal tensile forces ( $F_{t,i}$ ) with their corresponding lever arms ( $Z_i$ ), which are related to the compressive force ( $F_c$ )

$$M_u = \sum_i F_{t,i} Z_{t,i} \quad (2.4)$$

#### 2.6.10. TRC Ultimate Flexural Strength and Flexural Strain Review

In examining the flexural strength and strain, the influence of short fibre and textile type is considered, with the concrete compressive strength set at approximately 30

MPa (matching the targeted compressive strength in the current research). Determination of ultimate flexural strength and flexural strain employs equations (2.5) and (2.6), respectively (ASTM D790, 2010). The literature details are given in Table 2.3.

$$\sigma_f = \frac{3PL}{2bd^2} \quad (2.5)$$

where  $\sigma_f$  is flexural stress in the fibres at the midpoint (MPa);  $P$  is the load at a given point on the load-deflection curve (N);  $L$  is the supported span (mm),  $b$  is the width of beam tested (mm), and  $d$  is the depth of beam tested (mm).

$$\varepsilon_f = \frac{6Dd}{L^2} \quad (2.6)$$

where  $\varepsilon_f$  is the strain at failure (mm/mm);  $D$  is the maximum deflection of the centre of the beam (mm);  $L$  is the supported span (mm), and  $d$  is the depth (mm).

*Table 2.3: Literature details and references*

Textile Type	Short Fibers	Reference
Glass	PVA 2%	(Alma'aitah & Ghiassi, 2022)
Glass	Glass 2%	(Alma'aitah & Ghiassi, 2022)
Glass	PP 2%	(Alma'aitah & Ghiassi, 2022)
Glass	-	(Alma'aitah & Ghiassi, 2022)
Carbon	-	(Halvaei et al., 2020)
Carbon	-	(Halvaei et al., 2020)
Carbon	-	(Halvaei et al., 2020)
Carbon	-	(Alrshoudi, 2021)

Comparing published studies reveals a noticeable positive impact of short fibres on ductility behaviour and, to some extent, on flexural loads. Figure 2.25 clearly illustrates that samples containing short fibres consistently display higher strain readings, particularly surpassing the 0.02 strain limit. This observation informs the incorporation of short fibres into foamed concrete in ongoing research to examine their impact on textile reinforced foamed concrete (TRFC).

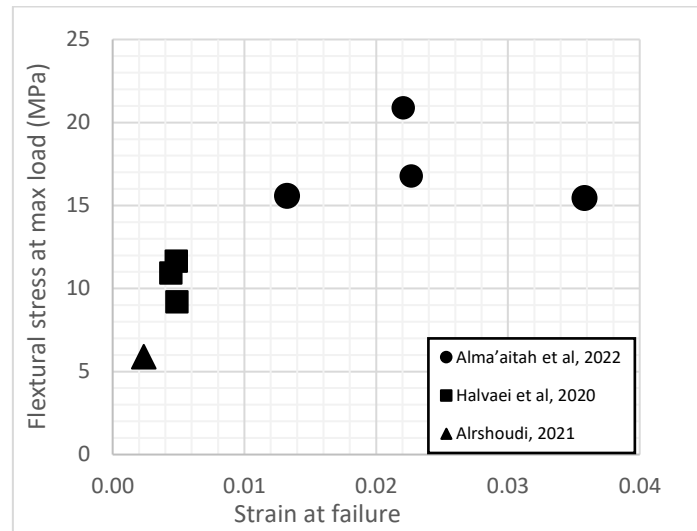


Figure 2.25: Comparison of the ultimate flexural strength and flexural strain at failure of the selected literature.

#### 2.6.11. Textile Reinforced Concrete (TRC) Durability

Textile Reinforced Concrete (TRC) holds vast potential for diverse applications, subjecting it to a wide array of mechanical and environmental loads. Its applicability spans various contexts, exposing it to a multitude of stresses and environmental conditions based on specific use cases. When considering structural durability, particular attention is given to mechanical loads concerning cracking, as cracks significantly enhance fluid and gas transport in concrete. Unlike conventional steel reinforcement, TRC is not susceptible to the accelerated corrosion process caused by cracks. Additionally, TRC offers the notable advantage of well-controlled crack widths, which are considerably smaller compared to structures reinforced conventionally (Mechtcherine, 2016).

In contrast to traditional reinforcement steel, the vulnerability to durability issues in TRC is associated with the robustness of the bond between the textile reinforcement and the fine-grained concrete matrix, along with the cohesion among the individual filaments of the textile (Portal et al., 2015). The difficulties of fabric reinforcement bonding become more pronounced when exploring various types of single fibres with high and low modulus, each featuring distinct geometries. This complexity arises from the role played by yarns transverse to the load direction and the intricate geometries of the individual reinforcing yarns comprising the fabric (Peled, 2016).



As outlined in the Bond Textile Section, the interaction between textile and fine-grained concrete is strengthened through impregnation, involving the coating of the textile reinforcement. Notably, in certain instances, overlaying the impregnated textile with sand proves effective in maximizing the ultimate pull-out force. This enhancement is credited to the increased friction between the filaments and the concrete matrix.

The water absorption of TRC exhibits an upward trend with the increasing fineness of multifilament yarns, while it decreases with a higher quantity of polymer used to coat the yarns. These trends primarily stem from variations in the capillary system formed within multifilament yarns. Notably, the oxygen permeability coefficient of crack-free (no visible cracks) TRC specimens is influenced by the polymer coating of the textile, with minimal dependence on the fineness of multifilament yarns. Embedding coated textiles into the composite, as opposed to uncoated textiles, leads to a substantial reduction in permeation coefficients up to 65% (Mechtcherine & Lieboldt, 2011).

Regarding chloride migration, there is currently limited information available on the chloride permeability of TRC. The notable higher resistance exhibited by both cracked and uncracked TRC against the penetration of chloride ions can be ascribed to factors such as their elevated cementitious material content, low water-to-cement ratio, self-limiting crack width, and consequently, the self-healing capability of the cracks. While these findings are promising, further research is imperative to deepen the understanding of these mechanisms and enhance the overall knowledge in this area (Mechtcherine, 2016). which especially regarding the combined effects of mechanical and environmental loads, is currently insufficient. The intricate interplay between these factors has not been adequately explored. Given the diverse array of textile and matrix types in use, the durability of TRCs is anticipated to exhibit considerable variation (Alma'aitah et al., 2021).

The potential for utilizing textile reinforced concrete (TRC) in structural elements and buildings subjected to intense mechanical or environmental stresses is considerable. Current perceptions suggest that TRC can deliver robust, enduring performance and advantageous transport properties even in a cracked state. Furthermore, there is

promising evidence that, in numerous cases, TRC may exhibit superior resistance to aggressive environments when compared to conventional reinforced concrete. However, apart from exposure to alternating freezing and thawing, there is a notable absence of information regarding the impact of aggressive environments on the mechanical properties of TRC materials. Exploring these effects would be crucial to a more comprehensive understanding of TRC's behaviour under diverse environmental conditions (Mechtcherine, 2016). Therefore, there is a pressing need for more thorough investigations in this domain to enhance our understanding and provide insights into the varied performance of TRC under different conditions.

#### 2.6.12. Textile Reinforced Concrete (TRC) Manufacturing Methods

The manufacturing process of TRC involves the incorporation of textile reinforcement and a concrete matrix, creating a cohesive composite element. Various methods are employed for the production of textile reinforced concrete, with options including manual hand lay-up and the pultrusion method (Mobasher et al., 2009).

##### 2.6.12.1. Hand Lay-up Method

The hand lay-up method, also known as the contact moulding technique, stands as one of the oldest and simplest approaches for crafting a textile reinforced concrete (TRC) composite element. Recognized for its historical significance, this technique offers accurate control over textile placement compared to alternative methods. The procedural steps involve meticulous preparation of the mould, followed by the casting of the concrete cover. Subsequently, the textile layer is manually laid up, and in the ensuing step, the concrete mix is cast to ensure its penetration through the textile layer. The final stage encompasses finishing the concrete surface. It is necessary that each of these steps occurs in sequence for optimal results (Mobasher et al., 2009).

### 2.6.12.2. Pultrusion Method

The pultrusion technique is employed to create fabric-cement laminate composites. The manufacturing process commences as the fabric traverses a paste infiltration chamber. Subsequently, it is pulled through a series of rollers, effectively squeezing the mixture into the openings of the fabric. The excess mixture is then removed, and the composite laminates are formed. Additional pressure is applied by the rollers to enhance the penetration of the paste between the fabric openings. The paste must maintain adequate fluidity to effectively permeate the fabric openings, and simultaneously, the mixture should be sufficiently dense to adhere to the fabric.

This method allows for the production of fabric-cement sheets with varying lengths, thicknesses, and widths, providing a versatile approach to crafting composite materials, as illustrated in Figure 2.26 (Mobasher et al., 2009).

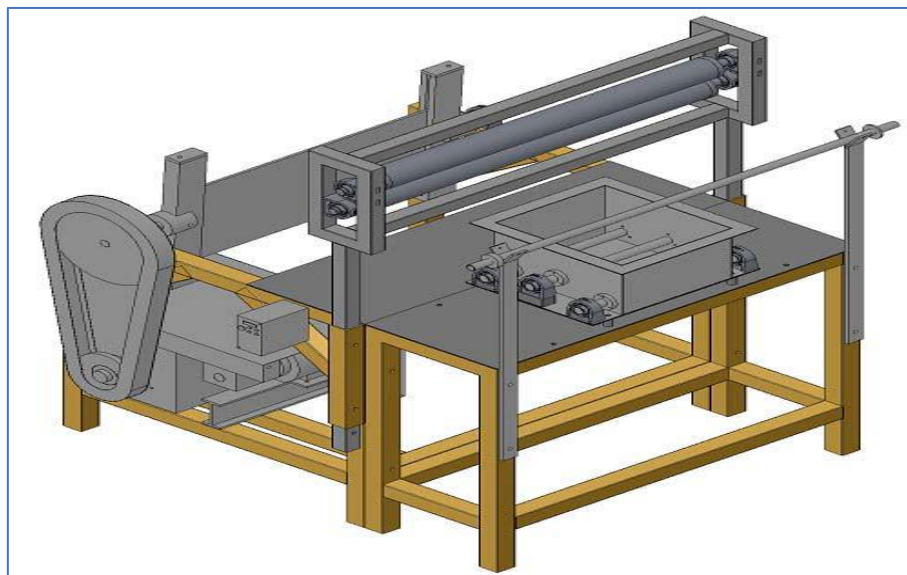


*Figure 2.26: Pultrusion machine (Mobasher et al., 2009)*

To establish a link between the hand lay-up and pultrusion methods and the ongoing research focusing on textile reinforcement with foamed concrete, it is crucial to consider the properties of foamed concrete. As discussed earlier, the bubbles in foamed concrete are sensitive, particularly during mixing and casting. An important characteristic of foamed concrete is its ability to self-compact, eliminating the need for external vibrations during the casting process.

In this context, the pultrusion method, which typically involves a series of rollers and additional pressure to enhance penetration, may present challenges for foamed concrete. The mechanical actions associated with pultrusion could potentially negatively impact the structure of foamed concrete. On the contrary, the hand lay-up method, with its manual and controlled approach, appears to be more suitable for accommodating the sensitivity of foamed concrete.

Therefore, considering the specific requirements of foamed concrete, the hand lay-up method emerges as a more fitting choice, aligning with the aim of the current research on textile reinforcement with foamed concrete.

### 2.6.13. Textile Reinforced Concrete (TRC) Applications

Textile reinforced concrete (TRC) stands as a composite construction material wherein textile reinforcement is integrated into a fine concrete matrix. An advantageous characteristic of textile reinforcement lies in its reduced susceptibility to corrosion, eliminating the need for a minimum concrete cover. This feature enables the fabrication of slender construction components and layers. The effectiveness of the fibre material can be maximized by finely tuning the volume proportion and orientation of the long fibres in alignment with tensile stress directions. TRC finds versatile applications, ranging from the production of thin-walled facade elements and load-bearing integrated formwork to tunnel linings and the reinforcement of existing structures, such as reinforced concrete (Mechtcherine, 2016).

The utilization of TRC extends to a diverse array of prefabricated products, encompassing both architectural (non-loadbearing) and structural (loadbearing) elements. Architectural applications include exterior cladding panels, parapet walls, and sound barriers, while structural applications comprise, among others, post-tensioned pedestrian bridge segments, and load-bearing sandwich panels. The growing popularity of prefabrication solutions based on TRC can be attributed to the significant reduction in concrete consumption, embodied energy of building components, and end-of-life waste (Papanicolaou, 2016).

### 2.6.13.1. Exterior Cladding and Façade Panels

Exterior cladding systems and facade panels are prominent applications of textile-reinforced concrete (TRC) products. TRC technology offers numerous advantages for the building envelope industry, including high-finished surface quality and aesthetics, remarkable mechanical properties, freeform design, reduced product thicknesses (typically ranging from 20–30 mm), enhanced durability characteristics, and a commendably low environmental impact. These features collectively position TRC as a compelling choice for achieving both structural integrity and aesthetic appeal in exterior cladding and facade systems (Papanicolaou, 2016).

Opting for textile reinforcement over conventional steel introduces a plethora of architectural design possibilities. This choice is underpinned by the advantages of reduced dead load weight and the elimination of the need for intricate facade anchors. Furthermore, textile reinforcement exhibits significantly higher corrosion resistance when compared to conventional steel reinforcement (Curbach et al., 2006). Noteworthy instances of TRC applications in facade panels include:

- Implementation as exterior cladding panels, showcased by the installation at Aachen University in Germany (Figure 2.27).
- Utilization in the construction of an office building in Dortmund, Germany, highlighted in Figure 2.28.

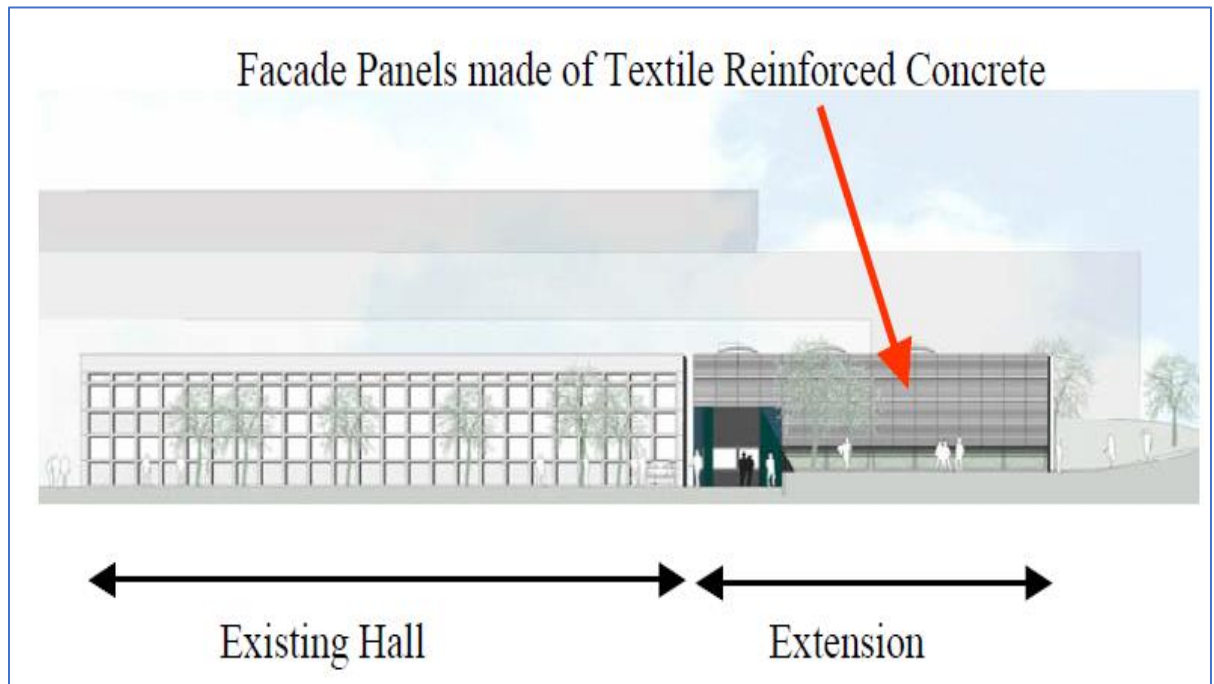


Figure 2.27: New extension of the testing hall of the Structural Concrete Institute Aachen University (Curbach et al., 2006)



Figure 2.28: Office building, Dortmund, Germany (Curbach et al., 2006)

### 2.6.13.2. Sandwich elements

The sandwich elements consist of two bearing shells enveloping an inner insulation layer. The construction process mirrors that of conventional reinforced concrete elements. Textile reinforcement is positioned in the formwork, and subsequently filled with high strength fine concrete. Before this, anchors connecting the facing elements with the reinforced concrete bearing elements are put in place. After the hardening

of the facing shells, the reinforced concrete bearing element is then poured, resulting in the creation of sandwich elements, illustrated in Figure 2.29 (Curbach et al., 2006).

The sandwich elements require the integration of bracing substructures to counteract deformations and bowing effects. However, advancements in design have led to the development of larger, compact, lightweight, and self-supporting elements that retain the heat protection and sound insulation properties of textile-reinforced concrete (TRC) facade panels. This is achieved by incorporating an insulating material layer between two slender TRC surfaces. This innovative approach represents a departure from conventional reinforced precast concrete sandwich panels, which are favoured for their prefabrication advantages, including structural, thermal, and sound efficiency, as well as enhanced durability characteristics (Papanicolaou, 2016).

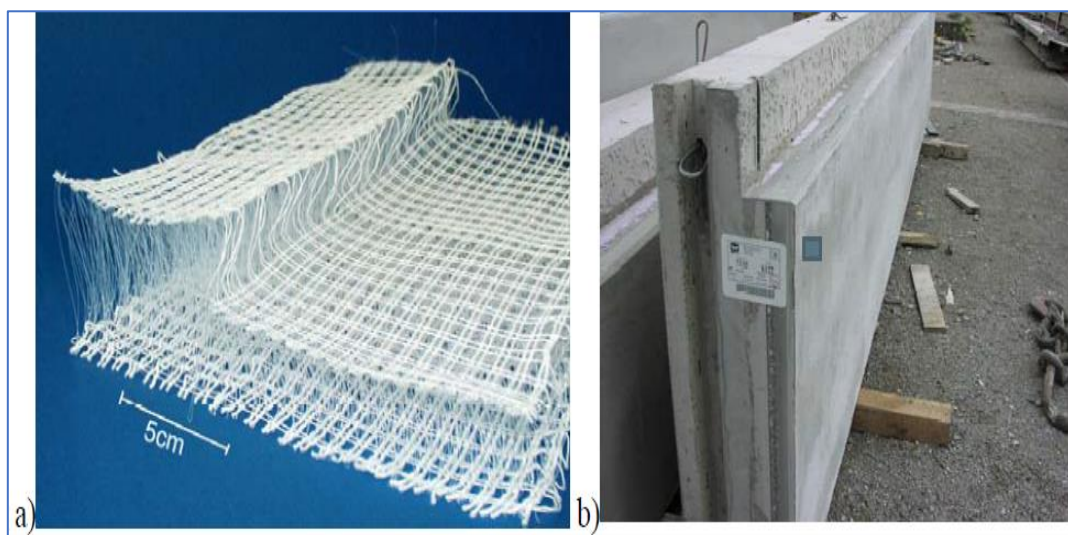


*Figure 2.29: Sandwich elements made of TRC: a) profiled spacer fabric, b) completed sandwich element (Curbach et al., 2006)*

A study was conducted to investigate the performance of sandwich composite elements, comprising a textile reinforced layer and an aerated concrete core, subjected to both quasi-static and intermediate strain rate impact loading. The selection of an aerated concrete core was based on its characteristic features as a lightweight, ductile material with excellent thermal properties. The results indicate that the sandwich composite utilizing aerated concrete exhibits promising potential as a building material for affordable and sustainable construction, particularly in seismic zones (Dey et al., 2015).

### 2.6.13.3. Decentralised Wastewater Treatment Plants

Decentralized wastewater treatment concrete plants find widespread use in economically viable applications, particularly in sparsely populated areas in Germany. The elevated demand for such concrete plants underscores concerns about the corrosion susceptibility associated with conventional steel reinforcement. Consequently, the adoption of textile reinforced concrete (TRC) is a strategic choice, given its remarkable corrosion resistance, as illustrated in Figure 2.30 (Curbach et al., 2006).



*Figure 2.30: Decentralised wastewater treatment plants made of textile reinforced concrete (Curbach et al., 2006)*

### 2.6.13.4. Barrel Shells

The versatility and formability of textile-reinforced concrete materials make the production of complex geometries easier and more conceivable. An illustrative example of this capability is evident in the production of a barrel shell, as depicted in Figure 2.31 (Hegger & Voss, 2008).





*Figure 2.31: Barrel shell is made of textile reinforced concrete (Hegger and Voss, 2008)*

#### 2.6.13.5. Cycle-Path and Footbridge

The Institute of Concrete Structures at Dresden University, Germany, collaborated with a local contractor to design and construct a small, innovative textile reinforced concrete footbridge catering to pedestrians and cyclists. This project serves as an indication of the practical application of the ideas within textile reinforced concrete research. The outcomes highlight the unique attributes of textile reinforced concrete (TRC), with a focus on its advantageous low weight relative to load capacity and its capability to support slender constructions. The cycle path and footpath represent a single-span girder, employing a segment construction method with internal post-tensioning of textile-reinforced concrete. The superstructure boasts an average span width of 8.60 m, providing a robust solution, while the width of 2.50 m accommodates the needs of pedestrians and cyclists alike, as illustrated in Figure 2.32 (Curbach et al., 2006).



*Figure 2.32: Textile reinforced concrete bridge (Curbach et al., 2006)*

## 2.7. Review of Reinforced Foamed Concrete

In a comprehensive study conducted by Lee et al. (2018), the flexural behaviour of foamed concrete beams and slabs was thoroughly investigated and compared with conventional concrete samples, with emphasis on three distinct reinforcement ratios: under-reinforced, balanced-reinforced, and over-reinforced, all employing conventional steel reinforcement. While the foamed samples exhibited lower load-carrying capacity compared to conventional concrete beams, they were still able to achieve their theoretical design moment at the yield point. However, it was observed that foamed concrete slabs and beams displayed higher deflection ability than their conventional counterparts, owing to the lightweight nature and lower stiffness of foamed concrete, except in cases of over-reinforcement. In instances of over-reinforcement, it is anticipated that the deflection behaviour between foamed concrete and conventional concrete would be similar, as the load is borne by an equivalent amount of steel reinforcement in both cases.

The failure mode of conventional concrete samples was consistently attributed to flexural failure, whereas foamed concrete exhibited a combination of flexural and shear failure. This discrepancy can be attributed to the absence of coarse aggregate in foamed concrete, leading to reduced friction and interlocking behaviour, which may contribute to flexural shear failure.

In May 2019, the UK's Standing Committee on Structural Safety (SCOSS) issued a safety alert titled "FAILURE OF REINFORCED AUTOCLAVED AERATED CONCRETE (RAAC) PLANKS" following the sudden collapse of a school flat roof in 2018. Subsequently, The Institution of Structural Engineers (IStruct) in 2022 conducted a thorough assessment and investigation into this issue. The RAAC panels in question are made of Autoclaved Aerated Concrete (AAC), a lightweight, precast, cellular concrete with a density ranging from 600 to 800 kg/m<sup>3</sup>, compressive strength between 2 and 5 MPa, and reinforced with conventional steel.

The report highlighted several performance defects observed in RAAC panels. High deflection of panels is a common issue, often leading to transverse cracking, with

longitudinal cracking also observed in many cases. Transverse cracks near the bearing, particularly within the end 300mm, may indicate high shear stresses or bond failure, serving as a potential warning sign of a failing panel. Corrosion of reinforcement poses a significant risk, especially when located near supports. Given the nature of RAAC construction, corrosion can have a more pronounced impact on the structural capacity of the panel compared to conventional concrete. Furthermore, reinforcement corrosion may result in large pieces of AAC detaching, posing a safety hazard to occupants.

In a three-point-bending test experiment, glass fibre textile reinforced foamed concrete beams were investigated, incorporating short polymer fibres. The foamed concrete densities ranged from 400 to 800 kg/m<sup>3</sup>. The addition of short polymer fibres resulted in a modest increase in the flexural capacity of the tested beams (Falliano et al., 2019).

In a study investigating foamed concrete reinforced with basalt and carbon textile, conducted at foamed concrete densities ranging approximately between 740 and 800 kg/m<sup>3</sup>, it was found that transverse grid fibres effectively anchored fibres in the main direction. Specimens reinforced with a carbon grid demonstrated superior flexural stiffness when compared to those reinforced with a basalt grid, owing to the higher modulus of elasticity of the carbon textile (Hulimka et al., 2017).

An experiment was conducted to explore the load-carrying capacity of alkali-resistant fibre textile reinforced foamed concrete. Foamed concrete specimens were produced with densities of 650 kg/m<sup>3</sup>, 1150 kg/m<sup>3</sup>, and 1650 kg/m<sup>3</sup>. The findings indicate that the load-carrying capacity in bending rose with both the density of the foamed concrete and the number of reinforcement layers (Serudin et al., 2022).

To address the issues identified in previous literature, it is important to recognize that high deflection in lower densities of foamed concrete (ranging from 600 kg/m<sup>3</sup> to 800 kg/m<sup>3</sup>) often results in increased transverse and longitudinal cracking. Transverse cracks near the bearing may signify high shear forces or bond failure within the foamed concrete matrix. Therefore, increasing the density of Foamed concrete is

recommended, as it correlates with enhanced stiffness. So, it can help to reduce the transverse and longitudinal cracks in foamed concrete. Additionally, incorporating textile reinforcement is advised to address the corrosion issues associated with conventional steel reinforcement.

Furthermore, previous studies on textile reinforcement in foamed concrete lacked theoretical calculations to predict experimental results. Additionally, failure modes, such as tension and compression failures, were not adequately addressed.

In the current research, both theoretical and experimental studies will be conducted on reinforced foamed concrete across three reinforcement scenarios: two cases involving tension failure with low and high reinforcement, and one case involving compression failure. These studies aim to provide a comprehensive understanding of the behaviour of reinforced foamed concrete under different loading conditions and failure modes.

## 2.8. Summary

- Foamed concrete offers several advantages over conventional concrete, such as its low self-weight, self-compacting nature, high flowability, fire resistance, and excellent thermal and sound insulation properties.
- The porous structure of foamed concrete significantly influences its properties, with factors such as the foam producing method, choice of foaming agent, and additives playing crucial roles in shaping this structure.
- Additive materials like fly ash, silica fume, and short fibres have been shown to enhance the properties of foamed concrete. However, it is important to note that in some cases, these additives can also have adverse effects. For instance, silica fume may increase the density of foamed concrete, while the inclusion of short fibres can negatively impact workability.
- Despite its advantages, foamed concrete also comes with certain disadvantages, such as high drying shrinkage and less stiffness compared to conventional concrete, which can result in more cracks during the serviceability state.
- There is a need for further research to develop foamed concrete code designs. Additionally, more studies should focus on the porous structure in foamed concrete.
- Textile reinforced concrete (TRC) offers the opportunity to create lightweight and slender elements. When incorporating foamed concrete with the textile (TRFC), the resulting composite provides even greater benefits, including reduced weight and improved sound and heat resistance compared to conventional fine-grained concrete used in TRC elements.
- Impregnation plays a pivotal role in enhancing the bonding performance between the impregnated textile and the concrete mortar, as well as ensuring the high-form stability of fabrics. Furthermore, within impregnated textiles, there exists a theoretical possibility to predict the bending strength and ultimate tensile strength of textile reinforced concrete based on the material characteristics of the composite components.

- The influence of aggressive environments on the mechanical properties of textile reinforced concrete (TRC) elements remains largely unexplored, highlighting a significant gap in current research.
- Higher deflection observed in lower densities of foamed concrete often precipitates an escalation of transverse and longitudinal cracks, consequently amplifying shear forces. To mitigate this concern, increasing the density of foamed concrete emerges as a recommended strategy, effectively minimizing the occurrence of such issues.
- Further investigation into reinforced textile foamed concrete across various failure scenarios is essential to raise a deeper comprehension of structural element performance.

## Chapter 3 Foamed Concrete: Materials, Mix Design, Testing for Strength and Properties

### 3.1. Introduction

This chapter delves into the comprehensive exploration of the materials, mix design, and testing procedures relevant to foamed concrete. Foamed concrete, as described by Amran et al. (2015) and Ramamurthy & Nambiar (2009), is a lightweight cellular concrete characterized by air voids entrapped in a mortar using a suitable foaming agent with a wide range of construction applications. This chapter focuses on the essential components, their proportions, and the subsequent testing processes required to evaluate the strength and properties of foamed concrete. The goal is to formulate foamed concrete mixes tailored for effective utilization in structural applications.

### 3.2. Materials Used

#### 3.2.1. Cement

The primary binder for the foamed concrete in this study was Portland cement CEM I-52,5, conforming to BS EN 197-1:2011. The research encompassed a cement content range of 340 kg/m<sup>3</sup> to 780 kg/m<sup>3</sup>, with the typical cement content in foamed concrete falling between 250 and 500 kg/m<sup>3</sup>. It is worth noting that exceeding 500 kg/m<sup>3</sup> of cement is recommended for achieving higher compressive strength, as suggested by Hilal et al. (2015). The analysis of the chemical composition of the cement utilized in this study was conducted in the university laboratory by Alma'aitah and Ghiassi in 2022. Refer to Table 3.1 for detailed information.

Table 3.1: Chemical composition of cement (Alma'aitah & Ghiassi, 2022).

Chemical Composition of Cement	Percentage (%)
Cl-	0.05
SO <sub>3</sub>	3.34
CaO	64.72
SiO <sub>2</sub> , Al <sub>2</sub> O <sub>3</sub> , Fe <sub>2</sub> O <sub>3</sub>	27.34
Na <sub>2</sub> O	0.23
MgO	1.09
PO <sub>4</sub> <sup>3-</sup>	-
K <sub>2</sub> O	0.63
SiO <sub>2</sub>	-
Si	-
CaCO <sub>3</sub>	-
Loss on ignition	-
Others	2.6

### 3.2.2. Sand

Natural, non-organic sand subjected to sieving, excluding particles larger than 2.36 mm, served as the fine aggregate to enhance stability and workability in the foamed concrete mixture, aligning with the recommendations of Jones & McCarthy (2005). The sand utilised adhered to BS EN 12620:2002 standards. Notably, coarse aggregate was omitted in foamed concrete production, given that the fine air void structure cannot effectively accommodate larger-sized (heavyweight) aggregate, potentially causing segregation.

### 3.2.3. Water

Freshwater sourced from the tap was used in concrete mixing for wetting the aggregate, initiating chemical reactions with the cementitious binder, and lubricating the mixture to ensure easy workability. Neville (2010) noted the absence of a defined standard for mixing water quality, emphasising the importance of cleanliness while avoiding excessive organic or inorganic substances.



Potable water played a crucial role in the foam production process. This holds particular significance when utilizing a protein-based foaming agent, as done in this research, as any organic contamination can detrimentally affect the foam's quality and, by extension, the resulting concrete (ACI 523.2R-96, 1997). It is imperative that the water used in the mixture is free from harmful levels of salts, alkalis, acids, oils, and organic matter. The water to cement (w/c) ratio of the base mix, crucial for achieving proper workability, is influenced by factors such as the type of binder(s), desired concrete strength, and the use of water-reducing or plasticizing agents. Typically falling between 0.4 and 0.8, this value ensures adequate hydration of the cement (Brady et al., 2001). Three water to cement ratios were used 0.3, 0.4 and 0.5 in foamed concrete mix. Figure 3.1 illustrates the materials utilized in the foamed concrete mix.

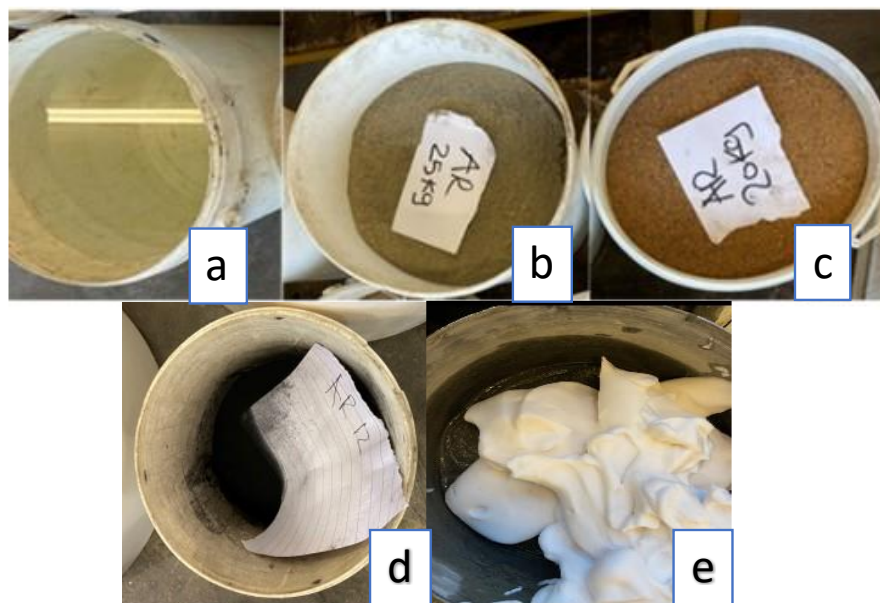


Figure 3.1: Used materials: (a). Water (b). cement (c). sand (d). toner (e). foam.

#### 3.2.4. Foaming Agent

Different foaming agent types, specifically synthetic and protein-based surfactants, play a crucial role in influencing the performance of foamed concrete production. These agents impact key aspects such as compressive strength, foam stability, thermal resistance, and pore structure of the resulting foamed concrete. The commonly used foaming agents include both synthetic and protein-based options, each with distinct

characteristics. Protein-based foaming agents, despite being more expensive, produce strong, closed-air bubbles and offer a high strength to density ratio. In contrast, synthetic foaming agents exhibit insensitivity to mixed alkalinity, ease of formulation, consistent performance, and stability (Falliano et al., 2018; Amran et al., 2015). The surfactants are typically mixed with water in a ratio range of 1/5 to 1/25. Despite the higher cost in the UK market, this research selects a protein-based foaming agent due to its desirable properties (Chun et al., 2007).

Propump 26, a protein-based foaming agent, was employed in this research. Figure 3.2 illustrates the foam production process including the foaming agent, foam machine, and the resultant foam product. The foam was produced according to the manufacturer's specifications: the foaming agent was mixed with water at a ratio of one part surfactant to 25 parts water. Following this, the solution was expanded using compressed air to achieve foam with a density ranging between 40 and 50 g/Litre. Importantly, each Litre of Propump 26 yielded approximately 500 Litres of foam.



Figure 3.2: Foam producing: (a). Foaming agent (b). Foam machine (c). Foam

### 3.2.5. Waste Toner

Toner, a dry ink powder with a particle size of 5 – 20  $\mu\text{m}$ , is primarily composed of a brittle polyester resin acrylic copolymer with a low melting temperature of 110  $^{\circ}\text{C}$  (Alkurdi et al., 2021). In this study, toner was employed as an additive to partially

replace 5%, 7.5%, and 10% of the cement by weight in the foamed concrete mix. Waste toner cartridges were collected from university offices (see Figure 3.3); however, some toner was purchased due to the shift to online education during the COVID-19 pandemic.



*Figure 3.3. Waste toner cartridges*

### 3.3. Mix Design, Production, and Tests

Amran et al. (2015), note that standardized methods for achieving specific properties in foamed concrete mixes are not yet established. Nevertheless, trial and error approaches were employed to formulate an appropriate mix. The mix proportions were calculated with a focus on achieving and controlling density, involving considerations such as the water-to-binder ratio, partial replacement of cement with additives, and the binder-to-fine aggregate ratio.

Similarly, to conventional weight concrete mix, the amount of the materials utilised to produce an appropriate mix of foamed concrete should follow reasonable procedures. The foamed concrete mix design was based on the absolute volume of its components. The constituents of the foamed concrete mix were determined by factors such as wet density, water-to-cement ratio, and cement content. Once the quantities were calculated, dry raw materials were mixed in a standard mixer (ACI 523.3R-14, 2014).

### 3.3.1. Mix Design Calculation

In the Absolute Volume method, the mix proportioning process commences with the determination of wet density, cement-to-sand ratio (C:S), water-to-cement ratio (w/c), and cement content. The steps of the Absolute Volume method for mix design are detailed in Table 3.2. To further illustrate the mix design procedure, an example is provided below:

- Wet density of required foamed concrete = 1400 kg/m<sup>3</sup>
- Cement: Sand (C:S) ratio = 1:2 = 0.5
- Water/Cement (w/c) ratio = 0.5
- Specific gravity of cement = 3.15
- Specific gravity of sand = 2.65
- Unit weight of water = 1000 kg/m<sup>3</sup>
- The total mass of raw materials = 1 m<sup>3</sup> x 1400 kg/m<sup>3</sup> = 1400 kg

Table 3.2: Absolute volume method for mix design

Material	Weight (kg)	Calculation	Absolute Volume (m <sup>3</sup> )
Cement	400	$400 \times \frac{1}{3.15 \times 1000}$	0.127
Sand	800	$800 \times \frac{1}{2.65 \times 1000}$	0.301
Water	200	$200 \times \frac{1}{1 \times 1000}$	0.2
Total =			0.628

The air volume required to be filled by foam is calculated as 1 m<sup>3</sup> minus 0.628, resulting in 0.372 m<sup>3</sup>. The foam volume is equal to 0.372 m<sup>3</sup>, which is equivalent to 372 Litres. According to the foaming agent specifications (Propump 26), each Litre of foaming agent yields approximately 500 Litres of foam. Therefore, the amount of foaming agent required to produce 372 Litres of foam is calculated as:

$$\frac{372}{500} = 0.744 \text{ Litre}$$

The foaming agent was mixed with water at a ratio of one part surfactant to 25-part water. Consequently, the amount of water required to produce foam is determined as 25 multiplied by 0.744, equalling 18.6 Litres. An example of mix design calculations is provided in Appendix A.

### 3.3.2. Foam Production

The production of foam using the pre-formed foam method is a straightforward and cost-effective approach. All equipment typically employed in conventional concrete production can be adapted for foamed concrete production, with the foam generator being the only additional requirement. In this study, Propump 26, a protein-based foaming agent, was utilized. The foam was produced according to the manufacturer's specifications: the foaming agent was mixed with water at a ratio of one part surfactant to 25 parts water and stirred well for 4 to 5 minutes. Following this, the solution was expanded using compressed air. The pressure used was 6 bar, and the flow rate of the foam was 150 Litres per minute, as indicated by the foam generator manual. The resulting foam should have a density ranging between 40 and 50 g/Litre. The foam density was measured by collecting a known volume of foam and weighing it to determine its mass per unit volume, ensuring accurate and consistent measurement of the foam density. Subsequently, the preformed foam was introduced into the cementitious mixture and mixed for approximately 2 minutes. This procedure yielded a homogeneous foamed concrete mix (ACI 523.3R-14, 2014; Ramamurthy & Nambiar, 2009).

### 3.3.3. Foamed Concrete Production

Standardized methods for achieving specific properties in foamed concrete mixes have not been established yet (Amran et al, 2015). The flow chart in Figure 3.4 elucidates the process of producing dry foam and foamed concrete. Similarly, to conventional heavyweight concrete mixes, the material quantities needed for a suitable foamed concrete mix should follow rational procedures. Once the quantities were determined,

dry raw materials were mixed in a standard mixer. Following this, mixing water was gradually added to the mixture over 2-3 minutes, ensuring a continuous process until a homogeneous mix with no lumps was achieved. Subsequently, the preformed foam was introduced using a foam generator and mixed into the wet slurry for approximately 2 minutes. This procedure yielded a homogeneous foamed concrete mix, as illustrated in Figure 3.5 (ACI 523.3R-14, 2014).

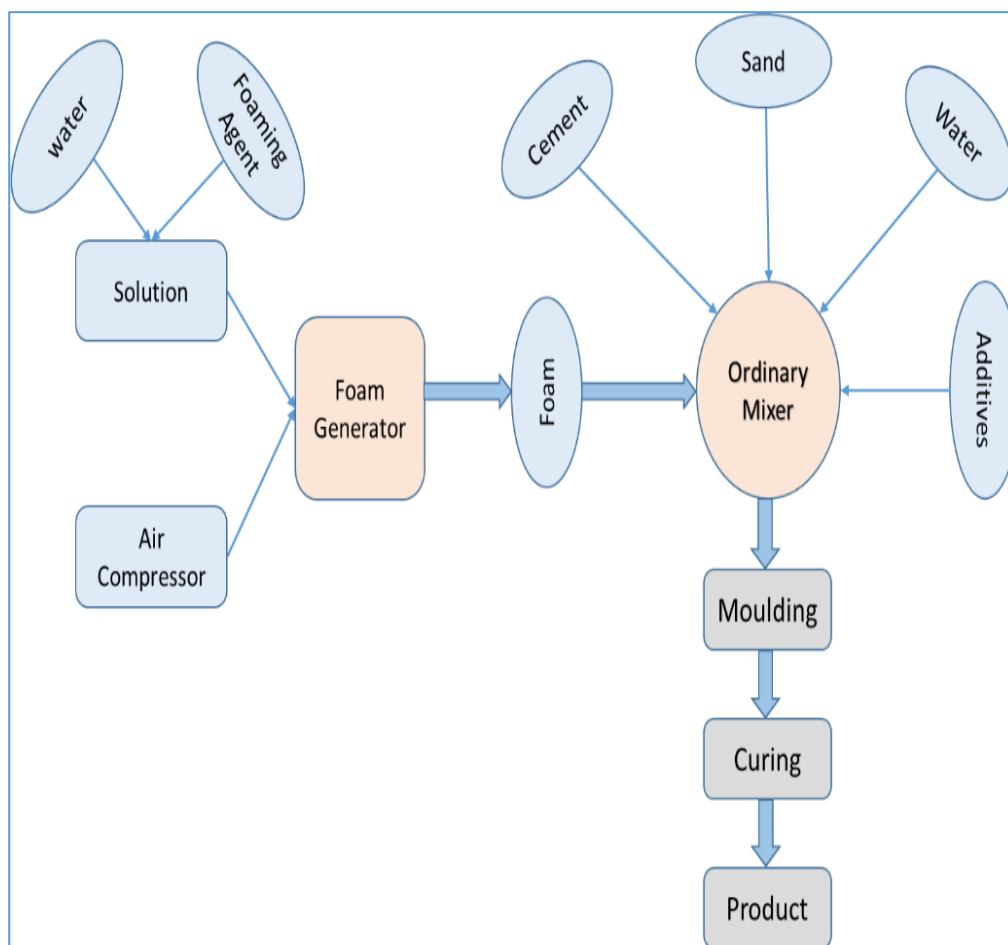


Figure 3.4: Production of dry foam and foamed concrete



Figure 3.5: Foamed concrete production

The fresh plastic density of the mixture is promptly measured upon completion of the mixing process following the guidelines outlined in BS EN 12350-6: 2019. This involves weighing the foamed concrete sample in a pre-weighed container of known volume. Verify whether the plastic density falls within the specified tolerance limit of  $\pm 50 \text{ kg/m}^3$ . If the measured plastic density is outside this limit, produce additional foam, and promptly incorporate it into the mix until the target density is attained. However, mixes with plastic densities below the specified limits are not considered. The fresh density is determined by filling the pre-determined volume and weight container with foamed concrete. Subsequently, any excess concrete is removed from the top of the container, and the surface is levelled without compaction. The container is then weighed to determine the plastic density using the following equation:

$$\rho_t = \frac{M_2 - M_1}{V} \quad (3.1)$$

where  $\rho_t$  is the target plastic density ( $\text{kg/m}^3$ );  $M_2$  is the combined mass of container and samples (kg);  $M_1$  is the mass of empty container (kg);  $V$  is the volume of the container ( $\text{m}^3$ ).

#### 3.3.4. Sampling and Curing

Cubes, cylinders, and prism moulds were prepared prior to the mixing process, with release oil applied to all internal surfaces using a brush. The foamed concrete mix was then evenly placed in two nearly equal layers within the moulds. Subsequently, the

sides of the moulds were lightly tapped with a rubber hammer until the surface of the sample achieved a level plane. Figure 3.6 illustrates the process of preparing and applying release oil on the samples and placing foamed concrete mix. Following this, promptly finish the top surface and cover it with a plastic protective layer to prevent evaporation. After moulding, maintain the samples at a temperature of  $21 \pm 5^\circ\text{C}$  for the initial 24 hours. Subsequently, remove all specimens from the moulds and cure them in water until the testing day (BS EN 12350-1, 2000) , as depicted in Figure 3.7.



Figure 3.6: Prepare and apply release oil on the specimen, then position the foamed concrete mix.





Figure 3.7: Specimens curing in water

### 3.3.5. Workability Test

The assessment of workability in foamed concrete mix can be visually conducted by examining its viscosity. Unlike conventional concrete slump tests, assessing the slump of concrete mortar is not appropriate (Raj et al., 2019). Instead, the workability of foamed concrete can be determined through the spread ability method. In this procedure, a sample is placed in a small slump cone, as depicted in Figure 3.8, with a top diameter of 70 mm, a bottom diameter of 100 mm, and a height of 60 mm. The cone is then raised vertically, and the spread in two directions is measured. The variance between these two measurements typically falls within a margin of approximately 5 mm, during the workability tests, only one replicate was tested (Li & Li, 2013; Yang et al., 2009).



Figure 3.8: Spread ability of the foamed concrete mix

### 3.3.6. Hardened Density Test

In accordance with BS EN 12390-7:2009, the density of hardened concrete ( $\rho$ ) after 28 days of water curing was determined using the following equation, and its value was adopted as the mean average value from three 100 mm cubes.

$$\rho = \frac{M_a}{M_a - M_w} \times 1000 \quad (3.2)$$

where  $\rho$  is the hardened concrete density ( $\text{kg/m}^3$ );  $M_a$  is the weight of the specimen in air (kg);  $M_w$  is the weight of the specimen in water (kg).

### 3.3.7. Compressive Strength

Foamed concrete is designed to achieve a specific density instead of focusing on compressive strength, as is the case with conventional concrete. As discussed in the literature review, the compressive strength of foamed concrete is significantly influenced by factors such as density, cement/sand ratio, and water/cement ratio. Cube specimens measuring 100 x 100 x 100 mm underwent compressive strength testing after 28 days of curing, following the guidelines of BS EN-12390-3: 2019. These specimens were carefully positioned and centred beneath the loading plate, ensuring even surfaces contacted with the loading plates, as depicted in Figure 3.9. The testing apparatus was calibrated to apply minimal load values specifically between 10 and 50 N/Sec. The failure loads were documented, and concrete compressive strengths were

computed utilizing Equation (3.3). The compressive strength of the samples was determined to the nearest 0.1 N/mm<sup>2</sup>.



Figure 3.9: Compressive test for cubes

$$f_c = \frac{F}{A_c} \quad (3.3)$$

where  $f_c$  is the compressive strength (N/mm<sup>2</sup>);  $F$  is the maximum load at the failure (N);  $A_c$  is the cross-sectional area on which the load is applied (mm<sup>2</sup>).

### 3.3.8. Static Modulus of Elasticity ( $E$ ):

The static modulus of elasticity ( $E$ ) of the foamed concrete mix was measured using 150 × 300 mm cylinder samples. Three specimens, following the guidelines of BS EN-12390-13:2013, were tested at 28 days. Each sample was equipped with a compress meter featuring two steel rings for clamping to the sample, a spherically seated lever unit, and two-gauge length bars to measure axial deformation, as depicted in Figure 3.10. The testing involved three loading cycles:

- The test samples were placed in the machine, and a base stress ( $\sigma_b$ ) of 0.5 MPa was applied for 20 seconds.

- Subsequently, the stress was gradually increased at a rate of 0.5 MPa/s until reaching one-third of the compressive strength ( $\sigma_a$ ) (the compressive strength was estimated before conducting the test).
- The stress was maintained for 20 seconds, recording the strain ( $\varepsilon_a$ ).
- Before reducing the stress at the same rate (0.5 MPa/s) to equalize the base stress ( $\sigma_b$ ), the strain ( $\varepsilon_b$ ) at this point was recorded, completing the first cycle.
- Two additional cycles were carried out.
- The readings from the three cycles were averaged.
- The modulus of elasticity ( $E$ ) in MPa was calculated using Equation  $E = \frac{\sigma_a - \sigma_b}{\varepsilon_a - \varepsilon_b}$

(3.4).

$$E = \frac{\sigma_a - \sigma_b}{\varepsilon_a - \varepsilon_b} \quad (3.4)$$

where  $\sigma_a$  is the upper loading stress (MPa) (where  $\sigma_a = f_c / 3$ );  $\sigma_b$  is the base stress (i.e., 0.5 MPa);  $\varepsilon_a$  is the strain under( $\sigma_a$ );  $\varepsilon_b$  is the strain under( $\sigma_b$ ).



Figure 3.10: Static modulus of elasticity test

### 3.3.9. Four-point flexural test

The flexural strength of plain foamed concrete mixes was determined at 28 days, measuring the maximum load at failure, and identifying the location of fracture. Three foamed concrete prism (100 × 100 × 500) mm specimens were subjected to testing in accordance with BS EN 12350-5:2019. The prisms were centrally positioned on the supports under the four-point loading machine, as illustrated in Figure 3.11. Loading commenced when all the loading and supporting rollers were uniformly in contact with the test samples. The stress rate was maintained within the range of 0.04 MPa/s to 0.06 MPa/s. Flexural strength results were determined using Equation (3.5).

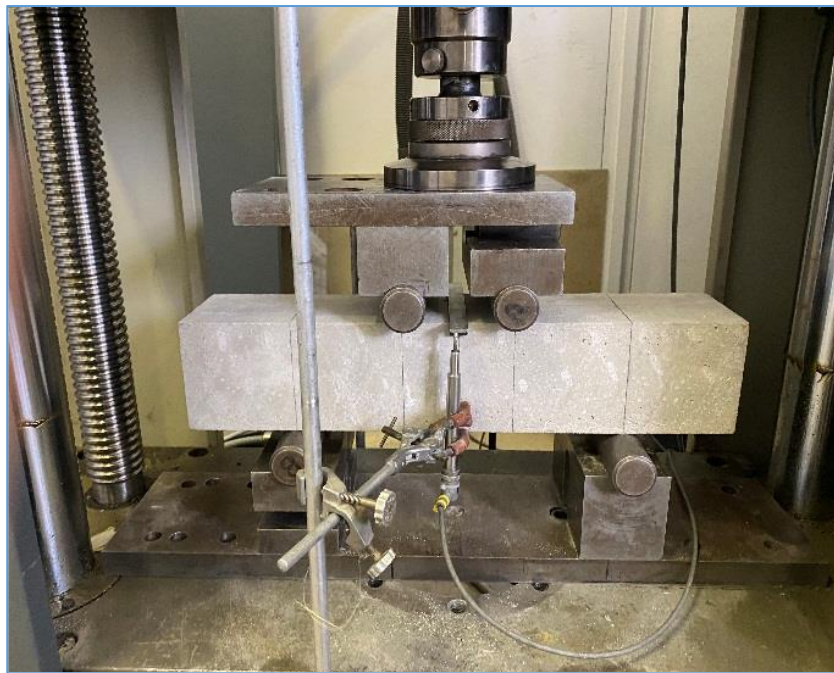


Figure 3.11. Four-point flexural test for plain FC prism

$$f_{ct} = \frac{F x l}{b x d^2} \quad (3.5)$$

where  $f_{ct}$  is the flexural strength (MPa);  $F$  is the maximum load (N);  $l$  is the distance between the lower rollers (mm);  $b$  is the width of the specimen (mm);  $d$  is the depth of the specimen, as oriented for testing (mm).

### 3.4. Experimental Program for Foamed Concrete (FC) Development

The objectives of the test programme are geared towards comprehending the mixing procedure (pre-foamed mix) and establishing an appropriate mix design, considering factors such as compressive strength, mixture workability, and cement content. The compressive strength of structural concrete is determined based on the design specifications of a given structure. Typically, the specified strengths fall within the range of 21 to 35 MPa, occasionally reaching up to 48 MPa or even higher, although not commonly (ACI 213R-03, 2003).

In this study, the foamed concrete (FC) intended for use as a one-way slab element was designed to attain a target density of approximately  $1800 \text{ kg/m}^3$  through the absolute volume method. The primary emphasis was on achieving a compressive strength within the range of 21 to 35 MPa, aligning with typical specifications for structural applications. Furthermore, considering the integration of fibre textile reinforcement into the foamed concrete mix, the workability target was set at greater than 300 mm, as recommended by Alma'aitah & Ghiassi (2022).

A total of eighteen mixes will undergo testing, utilizing a scenario designed to optimize both time and material utilization. The experimental program for foamed concrete development spans four distinct stages.

The first stage explores the influence of the water-to-cement ratio (w/c) and the cement-to-sand ratio (C:S). In the second stage, the impact of incorporating waste toner as an additive is examined. The third stage investigates the effect of mix densities.

Finally, in the fourth stage, the experimental results undergo validation by comparing them with relevant findings from existing literature. Additionally, in this stage, the evaluation of hardened properties involves comprehensive testing, including a static modulus of elasticity test and a four-point flexural test.

It is noteworthy that before each stage, a small trial mix is conducted to ensure accurate mix calculations.

### 3.4.1. Impact of Water-to-Cement Ratio and Cement-to-Sand Ratio

In the initial stage, design mixes using the absolute volume method are carried out to achieve the desired density. This phase explores the influence of three water-cement ratios ( $w/c$ ) and three cement-sand ratios ( $C:S$ ), all aiming for an initial selected density of  $1800 \text{ kg/m}^3$ , as depicted in Figure 3.12. The three water-to-cement ratios tested are 0.3, 0.4, and 0.5, while the three cement-to-sand ratios are 1:1, 1:1.5, and 1:2.

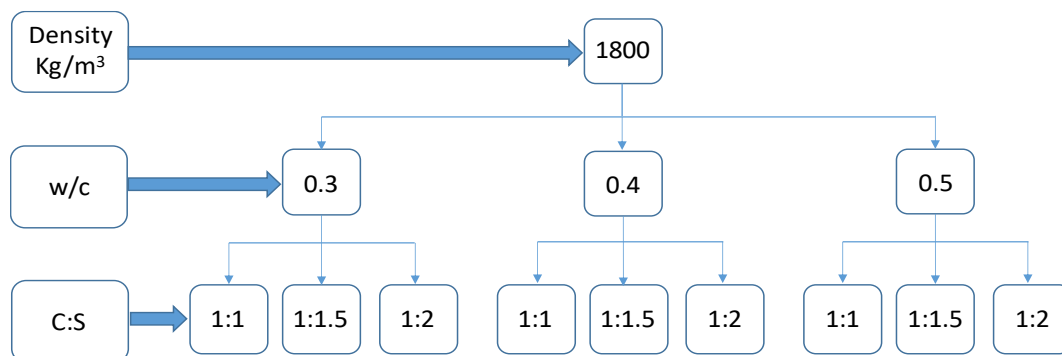


Figure 3.12: Experimental program: impact of water-to-cement ratios ( $w/c$ ) and cement-to-sand ratio ( $C:S$ ) on a density of  $1800 \text{ kg/m}^3$

The test program involved creating 27 foamed concrete (FC) cube samples with the goal of developing lightweight mixes. The objective was to achieve a 28-day compressive strength exceeding 21 MPa and ensure suitable workability. Nine distinct mix proportions were designed for this purpose, as outlined in Table 3.3.

Table 3.3: FC mixes with a targeted density of 1800 kg/m<sup>3</sup> and three different (w/c) and (C:S) ratios

Mix Name	(w/c)	C:S	Cement (kg/m <sup>3</sup> )	Sand (kg/m <sup>3</sup> )	Water (L)	Foam (L)
FC-1	0.3	1:1	783	783	235	222
FC-2	0.4	1:1	750	750	300	179
FC-3	0.5	1:1	720	720	360	140
FC-4	0.3	1:1.5	643	964	193	239
FC-5	0.4	1:1.5	621	931	248	203
FC-6	0.5	1:1.5	600	900	300	170
FC-7	0.3	1:2	546	1091	164	252
FC-8	0.4	1:2	529	1059	212	221
FC-9	0.5	1:2	514	1029	257	192

The compressive strength test was conducted on 10 × 10 × 10 cm cube specimens in accordance with the guidelines outlined in BS EN-12390-3:2019, while hardened density was determined following BS EN 12390-7:2009 after 28 days. Table 3.4 presents the mean compressive strength and mean hardened density, along with their respective standard deviations (S. D). Notably, the FC-7 mix was excluded from the analysis due to the complete non-integration of its components, as illustrated in Figure 3.13.

Table 3.4: Properties of FC mixes with a targeted density of 1800 kg/m<sup>3</sup> and different (w/c) and (C:S) ratios

Mix Name	Mean Density (kg/m <sup>3</sup> )	S. D	Mean Comp Strength (MPa)	S. D	Workability (mm)
FC-1	1832	11.1	33.9	1.7	175
FC-2	1752	10.2	31.9	2.2	310
FC-3	1784	6.4	24.1	2.3	340
FC-4	1843	6.7	32.3	1.3	155
FC-5	1782	11	28.1	1.1	305
FC-6	1844	7.5	20.6	2.4	325
FC-7*	-	-	-	-	-
FC-8	1825	6	20.9	2.4	260
FC-9	1804	6.6	19.5	1.4	310

The FC-7\* mix was excluded due to the complete non-integration of its components.





Figure 3.13: Excluded non-integrated mix (FC-7 mix)

The mean compressive strength is plotted against three water-to-cement ratios and three cement-to-sand ratios for foamed concrete mixes targeting a density of  $1800 \text{ kg/m}^3$ , as depicted in Figure 3.14. In general, there is an improvement in workability with an increase in the water-to-cement ratio. However, it is important to note that this improvement is accompanied by a decrease in compressive strength. For instance, FC-1 with a (w/c) of 0.3, FC-2 with a (w/c) of 0.4, and FC-3 with a (w/c) of 0.5 exhibit spread abilities of 175, 310, and 340 mm, respectively, and possess compressive strengths of 33.9, 31.9, and 24.1 MPa, respectively.

FC-1, FC-4, and FC-8 mixes were excluded due to poor workability issues, measuring 175, 155, and 260 mm, respectively. A statistical analysis of the densities and compressive strengths of the FC-2, FC-3, FC-5, FC-6, and FC-9 mixes was conducted. The analysis involved performing t-tests using DATAtab (DATAtab, 2024) to compare the selected mixes against the specified criteria. The objective was to determine if any mixes meet the requirements of having a compressive strength above 21 MPa and a density below  $1850 \text{ kg/m}^3$  (density was increased by  $50 \text{ kg/m}^3$ ).

### Hypotheses:

For density:

- Null hypothesis ( $H_0$ ): The mean density is greater than or equal to  $1850 \text{ kg/m}^3$ .
- Alternative hypothesis ( $H_1$ ): The mean density is less than  $1850 \text{ kg/m}^3$ .

For compressive strength:

- Null hypothesis ( $H_0$ ): The mean compressive strength is less than or equal to 21 MPa.
- Alternative hypothesis ( $H_1$ ): The mean compressive strength is greater than 21 MPa.

**T-Test Formula:**

$$t = \frac{\bar{x} - \mu}{\frac{s}{\sqrt{n}}} \quad 3.6)$$

where  $\bar{x}$  is the sample mean;  $\mu$  is the criteria mean;  $s$  is the sample standard deviation and  $n$  is the sample size.

- **Example Calculation for FC-5 mix density and compressive strength:**

$$t_{density} = \frac{|1850 - 1782|}{\frac{11}{\sqrt{3}}} = 10.709$$

$$t_{compressive\ strength} = \frac{|28.1 - 21|}{\frac{1.06}{\sqrt{3}}} = 11.6$$

The t-test was performed for FC-2, FC-3, FC-5, FC-6, and FC-9 mixes. The Table 3.5 summarizes the calculated t-values for density and compressive strength. The calculated t-values were compared against the critical t-value according to DATAtab to determine significance. For one-tailed tests at a significant level of 5% ( $\alpha = 0.05$ ) and a degree of freedom ( $df = n - 1 = 2$ ), the critical t-value is 2.92.

Table 3.5: FC-2, FC-3, FC-5, FC-6, and FC-9 mixes t-values for density and compressive strength

Mix Name	t-value (Density)	Density reject ( $H_0$ )	t-value Comp Strength	Strength Reject ( $H_0$ )
FC-2	16.9	True	8.8	True
FC-3	7.9	True	4.7	True
FC-5	10.7	True	11.6	True
FC-6	0.37	False	0.3	False
FC-9	4	True	1.3	False

The analysis indicates that FC-2, FC-3, and FC-5 mixes have t-values larger than critical t-value, meaning their properties meeting the targeted density and compressive strength criteria. Among the accepted mixes (FC-2, FC-3, and FC-5), FC-5, with a (w/c) ratio of 0.4 and a (C:S) ratio of 1:1.5, was preferred for the next stage experimental program due to its lower cement content, as shown in Table 3.3.

It is essential to note that for the foamed concrete mix with a water-to-cement ratio of 0.3 and a targeted density of 1800 kg/m<sup>3</sup>, the use of a plasticizer is recommended to enhance workability. Moreover, from an environmental perspective, the substitution of waste materials for cement, particularly when the cement-to-sand ratio is 1:1, is a significant consideration.

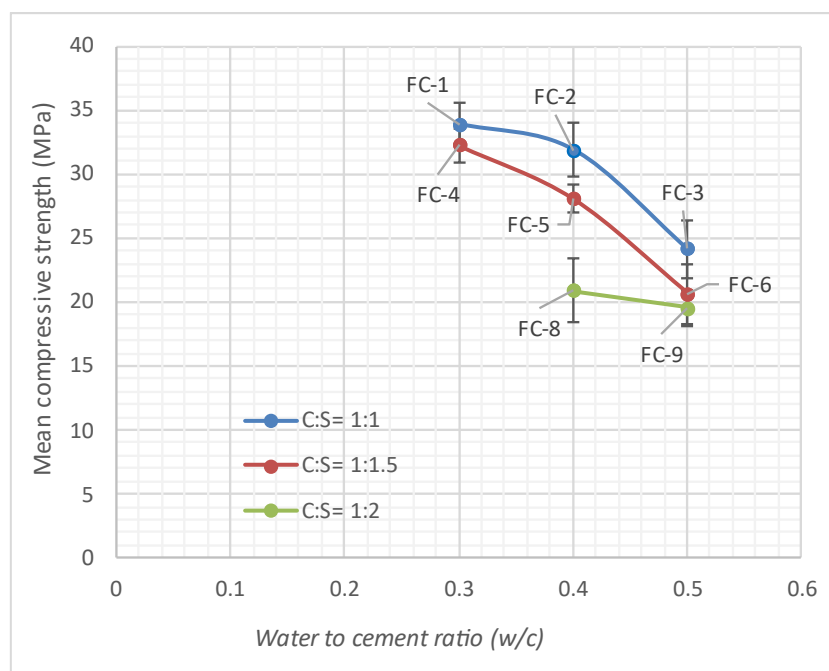


Figure 3.14. FC compressive strength with a targeted density of 1800 kg/m<sup>3</sup> and different (w/c) and cement: sand (C:S) ratios

### 3.4.2. Effect of Waste Toner

The second stage involves an in-depth investigation into the impact of replacing cement weight with waste toner on the optimized foamed concrete mix (FC-5) identified in the first stage. The emphasis will be on evaluating the compressive strength and density of

the FC-5 mix. The substitution of cement weight will be carried out using three distinct mass percentages of waste toner: 5%, 7.5%, and 10%, as depicted in Figure 3.15.

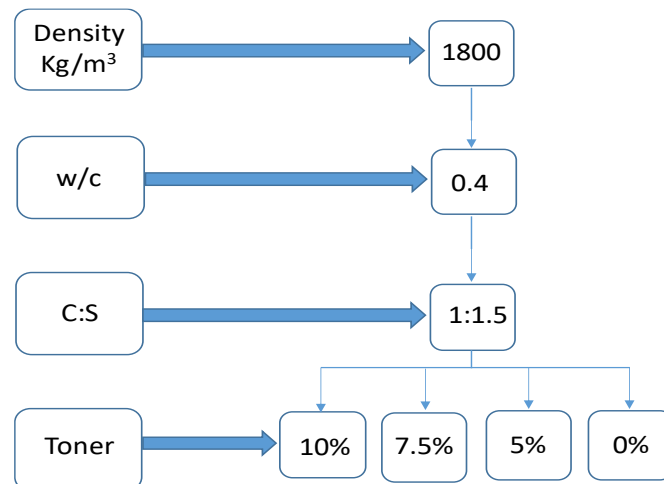


Figure 3.15: Experimental program: impact of three toner percentages on a density of 1800 kg/m<sup>3</sup>

In this phase, twelve cubes of foamed concrete were manufactured for examination in accordance with the study guidelines. Table 3.6 details the components of the sample mixes.

Table 3.6: FC mixes with a targeted density of 1800 kg/m<sup>3</sup> and three different toner percentages

Mix Name	Toner (%)	Binder (kg/m <sup>3</sup> )	Toner (kg/m <sup>3</sup> )	Cement (kg/m <sup>3</sup> )	Sand (kg/m <sup>3</sup> )	Water (L)	Foam (L)
FC-5	0	621	0	621	931	248	203
FC-10	5	621	31	590	931	248	199
FC-11	7.5	621	47	574	931	248	197
FC-12	10	621	62	559	931	248	140

The compressive strength test has been conducted to examine the potential of using toner as an additive to partially replace cement in the foamed concrete mix. Four different mixes were produced. Toner was used to replace 5%, 7.5% and 10% of the cement by weight. The target density was 1800 kg/m<sup>3</sup> and the cement content was between 621 and 559 kg/m<sup>3</sup>. Table 3.7 presents the mean compressive strength and mean hardened density after 28 days, along with their respective standard deviations (S. D).

Table 3.7. Effect of three percentages of toner on FC mean compressive strength and density.

Mix Name	Toner (%)	Mean Density (kg/m <sup>3</sup> )	S. D	Mean Comp Strength (MPa)	S. D
FC-5	0	1782	11	28.1	1.1
FC-10	5	2062	8.7	37.1	1.1
FC-11	7.5	2079	8.1	36.9	0.9
FC-12	10	2085	5	38.5	1.3

The test results reveal a notable increase, in compressive strength values with the addition of toner content in the mixture. Simultaneously, there was a significant rise in the sample densities compared to the control sample (FC-5), as indicated in Table 3.7. The average mean compressive strength of FC-10, FC-11, and FC-12 is 37.5 MPa, signifying a comprehensive improvement of 33.5% compared to the control sample (FC-5), as depicted in Figure 3.16.

All samples with toner and targeted for a density of 1800 kg/m<sup>3</sup> exhibit densities exceeding 2000 kg/m<sup>3</sup> (surpassing the density set in the study guidelines). These outcomes suggest an enhancement in the compressive strength of foamed concrete after the addition of waste toner, attributed to the increased density. This increase in compressive strength due to heightened concrete density aligns with findings presented by Nambiar & Ramamurthy (2006) and those by Jones and McCarthy (2005).

The t-test analysis of the mean densities and mean compressive strengths of the FC-5, FC-10, FC-11, and FC-12 was conducted. The analysis confirms that only FC-5 satisfies both the density and compressive strength criteria.

The 10% toner replacement by cement weight, i.e. the lowest cement content, was selected for use in the subsequent research stage (employing different density mixes of 1200, 1400, and 1800 kg/m<sup>3</sup>) to examine the toner's effect on foamed concrete densities lower than 1800 kg/m<sup>3</sup>.

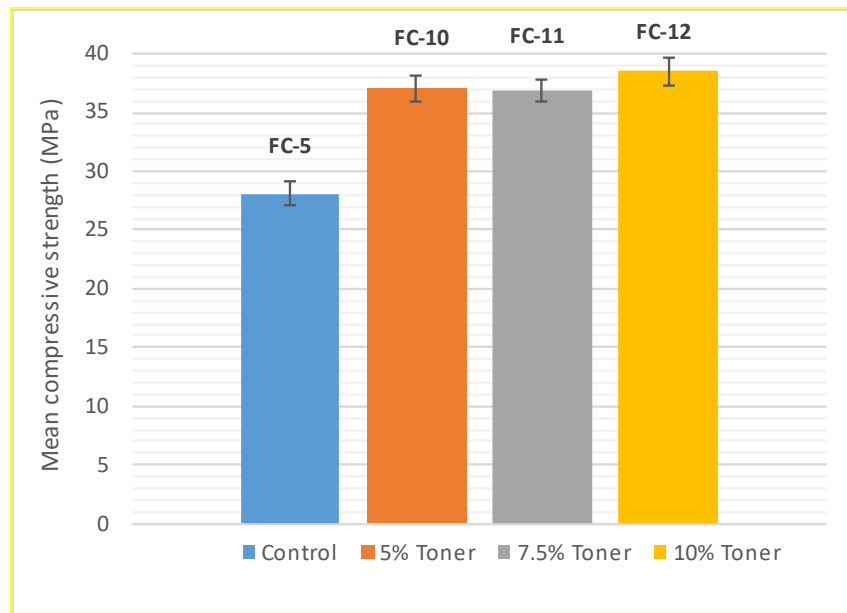


Figure 3.16: Compressive Strength of FC-5, FC-10, FC-11, and FC-12 samples at 28 days

### 3.4.3. Effect of Density

The third stage investigates four different targeted densities using the selected mix from the previous stages ( $w/c$  of 0.4,  $C:S= 1:1.5$ , and toner percentage of 10%), as shown in Figure 3.17.

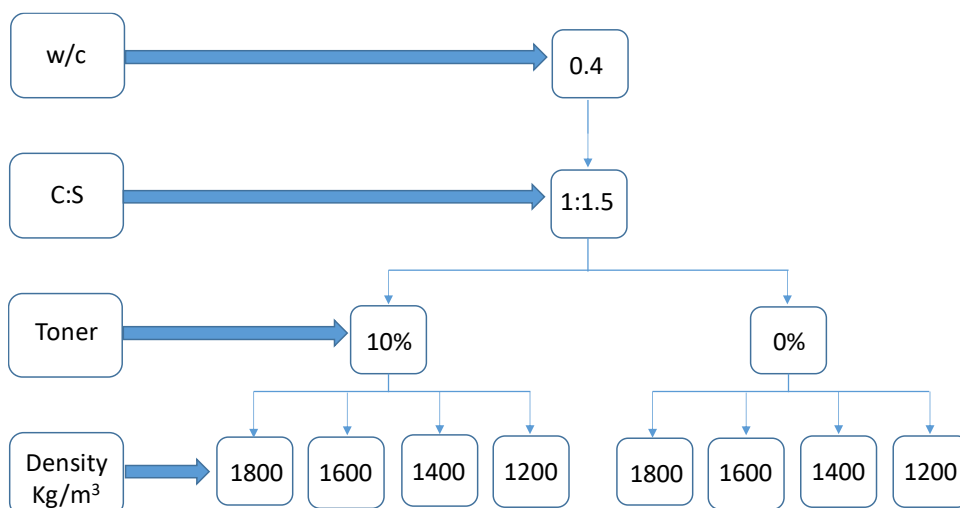


Figure 3.17: Experimental program: impact of different densities with ( $w/c$ ) of 0.4, ( $C:S= 1:1.5$ ), and toner percentage of 10%

In this phase of the experiment, the program involved the creation of a series of 24 foamed concrete cube samples. Toner was incorporated to substitute 10% of the cement by weight, maintaining a water-to-cement ratio ( $w/c$ ) of 0.4 and a cement-to-sand ratio ( $C: S$ ) of 1:1.5. The intended densities for the samples ranged from 1200, 1400, 1600 and 1800  $\text{kg/m}^3$ . For detailed information on the foamed concrete component mixes, please refer to Table 3.8.

Table 3.8: FC mixes with different densities with ( $w/c$ ) of 0.4, ( $C: S = 1:1.5$ ), and a toner percentage of 10%

Mix Name	Targeted Density ( $\text{kg/m}^3$ )	Binder ( $\text{kg/m}^3$ )	Toner ( $\text{kg/m}^3$ )	Cement ( $\text{kg/m}^3$ )	Sand ( $\text{kg/m}^3$ )	Water (L)	Foam (L)
FC-5	1800	621	0	621	931	248	203
FC-12	1800	621	62	559	931	248	140
FC-13	1600	552	0	552	828	221	292
FC-14	1600	552	55	497	828	221	284
FC-15	1400	483	0	483	724	193	380
FC-16	1400	483	48	435	724	193	3734
FC-17	1200	414	0	414	621	166	469
FC-18	1200	414	41	373	621	166	463

Across all sample results, the mean compressive strength values show an increase with toner inclusion compared to control samples of the same target densities. Nevertheless, it is notable that toner inclusion has led to an increase in actual density, with the specimen's density rising by approximately 20% in all mixes incorporating toner, as depicted in Figure 3.18 and detailed in Table 3.9.

Table 3.9: FC mean compressive strength and density of different targeted densities.

Mix Name	Targeted Density ( $\text{kg/m}^3$ )	Mean Density ( $\text{kg/m}^3$ )	S. D	Mean Comp Strength (MPa)	S. D
FC-5	1800	1782	11	28.1	1.1
FC-12	1800	2085	5	38.5	1.3
FC-13	1600	1602	22.4	18.0	0.3
FC-14	1600	1909	9.9	32.9	1.
FC-15	1400	1428	15	8.8	0.5
FC-16	1400	1697	12.6	19.9	0.7
FC-17	1200	1151	9.5	3.4	0.1
FC-18	1200	1371	25.2	6.1	0.7

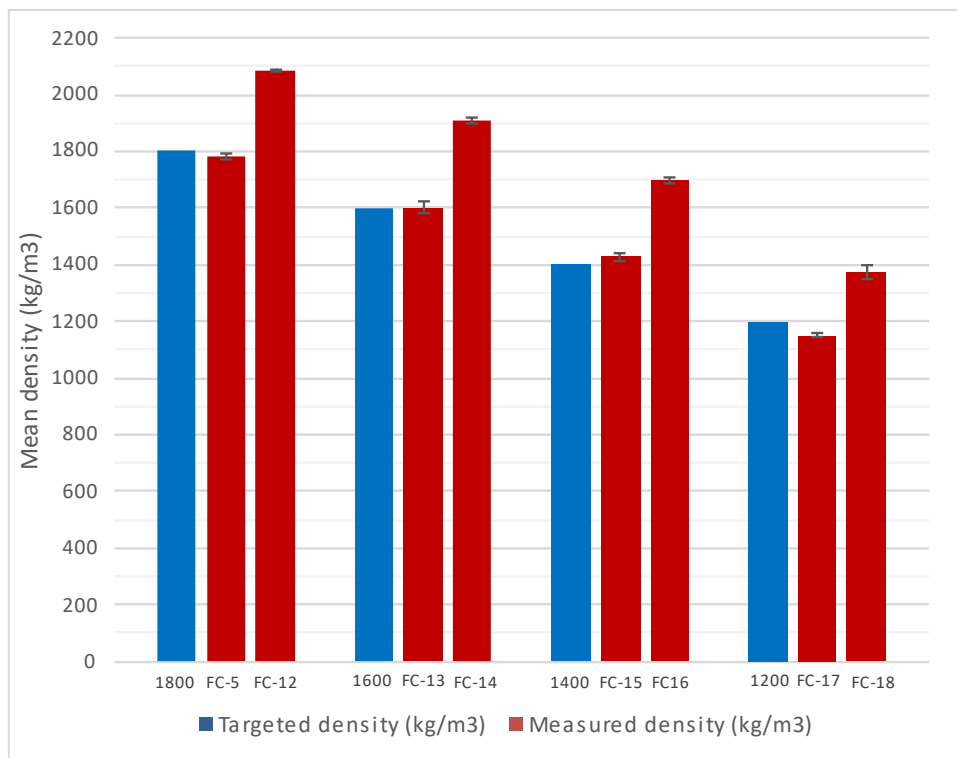


Figure 3.18: Effect of toner on different foamed concrete density

The mean compressive strength is graphed against density for foamed concrete mixes targeting densities of 1200, 1400, 1600, and 1800 kg/m<sup>3</sup>, as illustrated in Figure 3.19. FC-17, FC-18, FC-15, FC-13, and FC-16, having compressive strengths of 3.4, 6.1, 8.8, 18, and 19.9 MPa, respectively, were excluded due to falling below the specified compressive strength limit of 21 MPa. Additionally, FC-12 and FC-14 mixes were excluded due to higher density values, measuring 2085 kg/m<sup>3</sup> and 1909 kg/m<sup>3</sup>, respectively. To validate these findings, a t-test analysis of the mean densities and compressive strengths for the mixes was conducted. The results confirm that only FC-5 meets both the density and compressive strength criteria.

Consequently, the chosen foamed concrete mix is FC-5, featuring a (w/c) ratio of 0.4, a (C:S) ratio of 1:1.5, and 0% toner content. The mean density and compressive strength of the selected mix are 1782 kg/m<sup>3</sup> and 28.1 MPa, respectively.



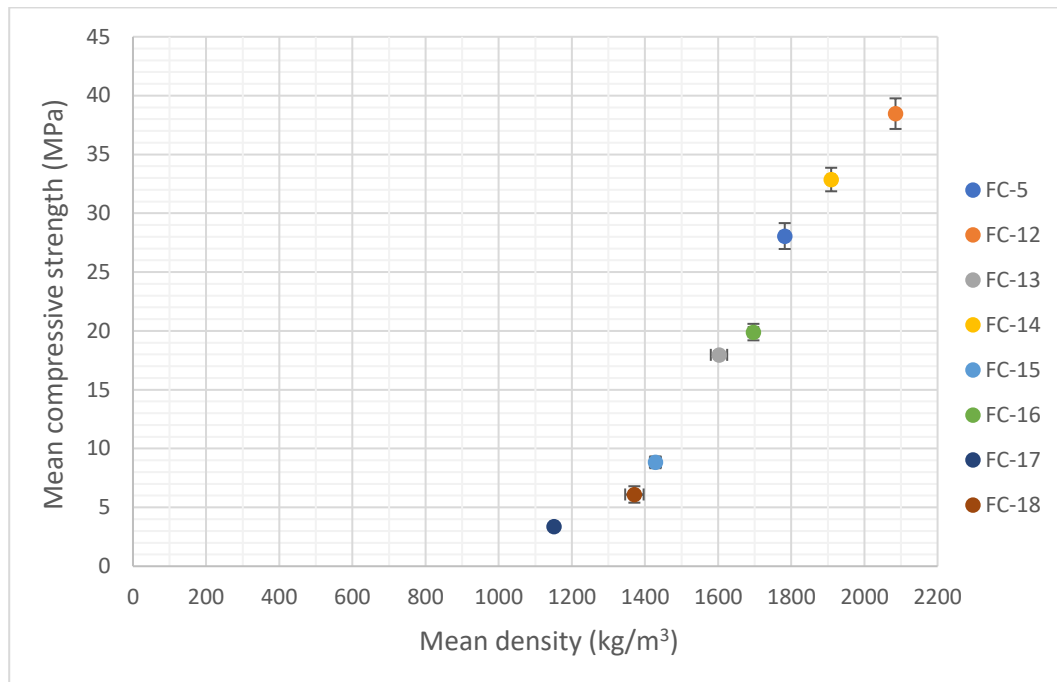


Figure 3.19: FC compressive strength with different targeted densities at 28 days

#### 3.4.4. Validating Experimental Results with the Literature

The selected mix (FC-5) from earlier stages, distinguished by a density of 1800 kg/m<sup>3</sup>, (*w/c*) ratio of 0.4, (*C:S*) ratio of 1:1.5, and toner percentage of 0%, is subjected to validation. This validation primarily focuses on comparing the strength-to-density ratios of the FC-5 mix at 28 days with foamed concrete mixes from the literature. For this comparative analysis, additional mixes from the current experimental set that share identical (*w/c*) and (*C:S*) ratios but exhibit lower densities are taken into consideration, as detailed in Table 3.10:

Table 3.10: Current study mixes that will be compared with the literature mixes.

Mix Name	Mean Density (kg/m <sup>3</sup> )	Mean Comp Strength (MPa)
FC-5	1782	28.1
FC-13	1602	18.0
FC-15	1428	8.8
FC-17	1151	3.4

The study's compressive strength to density ratio results is compared to relevant research studies. Notably, the findings exhibit similarities with studies conducted by Pan et al., (2007), (Fly ash) Nambiar & Ramamurthy, (2006), and (Sand) Jones & McCarthy, (2005). Specifically, this similarity is observed in cases where the density exceeds 1600 kg/m<sup>3</sup>. However, the results from the present study are appreciably higher than those reported by Nambiar & Ramamurthy (2006) using sand and Hilal et al. (2015) in their study on foamed concrete, as illustrated in Figure 3.20. This comparison highlights the resemblance of the FC-5 mix in terms of its strength-to-density ratio within the broader context of foamed concrete research.

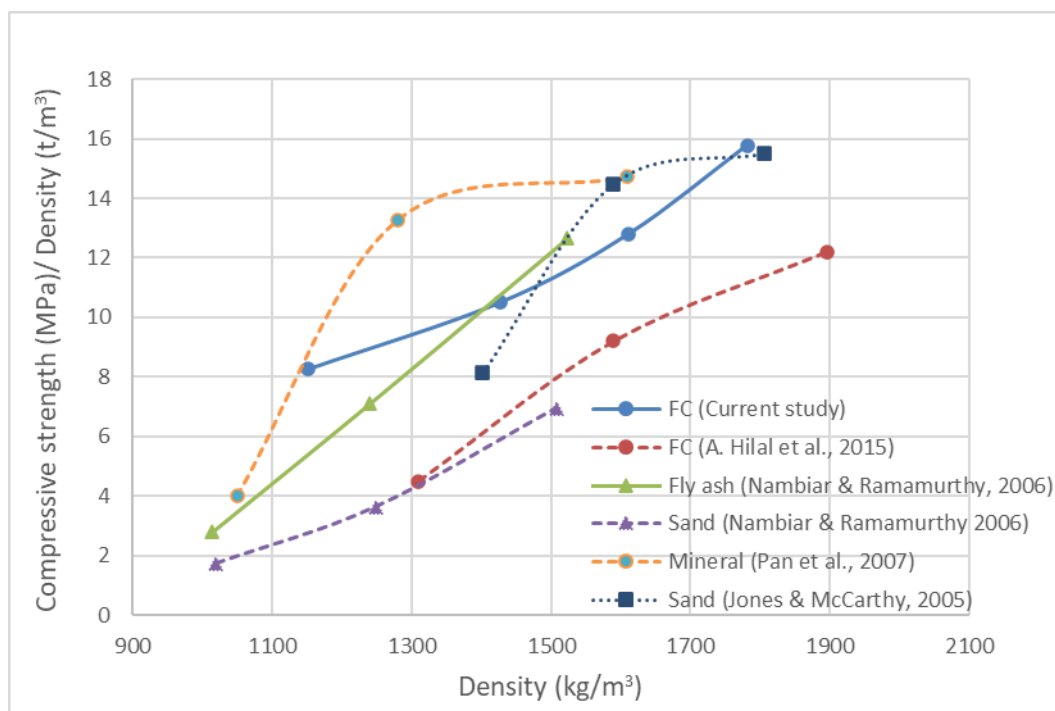


Figure 3.20: Strength to density ratios for different foamed concrete mixes

Overall, FC-5 foamed concrete mix is potentially suitable for use as a lightweight concrete for structural purposes since its density does not exceed  $1800 \text{ kg/m}^3$  and its 28-day compressive strengths are in excess of 21 MPa (Kosmatka et al., 2002, ACI 213R-03, 2003).

Also, in the fourth phase of this experimental program, the evaluation of hardened properties involved comprehensive testing, including a static modulus of elasticity test and a four-point flexural test. These tests were conducted on the selected foamed concrete mix from the preliminary stages, denoted as FC-5. This mix is characterized by a density of  $1800 \text{ kg/m}^3$ , (w/c) ratio of 0.4, (C:S) ratio of 1:1.5, and a toner percentage of 0%, as outlined in Table 3.11.

*Table 3.11: FC-5 foamed concrete mix hardened properties.*

Concrete Mix	Compressive Strength (MPa)	Modulus of Elasticity (GPa)	Ultimate Strain	Flexural Strength (MPa)
FC-5	28.1	10.464	0.00394	1.93

These tests provided essential data on the performance of the FC-5 mix, critical for its integration into the theoretical prediction of textile-reinforced foamed concrete (TRFC), as detailed in Chapter 4.

### 3.5. Research Programme

This research aims to comprehensively evaluate the structural performance, environmental impacts, and cost implications of textile reinforced foamed concrete. To achieve this goal, the research program will encompass the following key areas:

- **Structural Behaviour of the TRFC Beams**

Theoretical and experimental investigation into the flexural behaviour of textile reinforced foamed concrete beams through three-point bending flexural tests conducted across various failure scenarios. Additionally, the program will explore the bonding between the textile and foamed concrete via pull-out tests. The objective is to identify the most suitable configuration for structural applications.

- **Environmental and Cost Assessment of the TRFC**

Examination of the environmental and cost impacts of textile reinforced foamed concrete slabs through life cycle assessment (LCA) and cost analysis.

### 3.6. Summary

- The chapter begins by detailing the materials used in foamed concrete, the Portland cement CEM I-52.5 is the primary binder. The chemical composition of cement, fly ash, silica fume, and limestone, as analysed in the university laboratory, is presented. The incorporation of natural sand and freshwater from the tap, along with the use of a protein-based foaming agent called Propump 26, is discussed in detail. Additionally, the innovative use of waste toner as an additive in different proportions to partially replace cement is introduced.
- The mix design process is elucidated through the Absolute Volume method, outlining calculations for cement, sand, and water quantities. The foaming agent's role in producing dry foam and the subsequent production of foamed concrete are explained, with an emphasis on maintaining the target density and workability. Following production, the chapter covers sampling, curing, and the workability test, highlighting the importance of visual examination and spread ability. Subsequent sections detail the density test, compressive strength testing, static modulus of elasticity, and four-point flexural tests as standardized methods for evaluating foamed concrete properties.
- The experimental program for foamed concrete development unfolds in four stages. The initial stage explores the impact of water-to-cement and cement-to-sand ratios on achieving a target density of  $1800 \text{ kg/m}^3$ . The second stage investigates the effects of waste toner in different proportions on an optimized foamed concrete mix. The third stage examines the influence of varying densities, focusing on  $1200$ ,  $1400$ ,  $1600$ , and  $1800 \text{ kg/m}^3$ .
- In the final phase, key tests, including static modulus of elasticity and four-point flexural tests, were performed on FC-5, a selected foamed concrete mix with a density of  $1800 \text{ kg/m}^3$ , ( $w/c$ ) ratio of  $0.4$ , and ( $C:S$ ) ratio of  $1:1.52$ . Additionally, the properties of FC-5, particularly its compressive strength-to-density ratio, were scrutinized in comparison to pertinent research studies. This comparative analysis establishes the robustness and competitiveness of the FC-5 mix, showcasing its

strength-to-density ratio within the broader landscape of foamed concrete research.

- Each stage entails comprehensive testing and analysis of compressive strength, density, (w/c) ratio, and workability to unravel the intricate relationships between mix proportions and material properties. As a general trend, there is an enhancement in workability with an elevation in the water-to-cement ratio. Nevertheless, it is crucial to acknowledge that this improvement is combined with a reduction in compressive strength and density.
- In conclusion, this chapter serves as a comprehensive guide to foamed concrete, covering materials, mix design, and testing procedures. The systematic experimental program provides valuable insights for optimizing foamed concrete mixes tailored to specific applications and performance requirements.

## Chapter 4 Theoretical Prediction of Textile Reinforcement Foamed Concrete (TRFC):

### 4.1. Introduction

Textile reinforcements, utilized as the main reinforcement in reinforced concrete structures, are broadly acknowledged as innovative materials. Therefore, there are presently no specific design codes available for textile reinforced concrete (TRC) elements. However, several research studies have been carried out on textile reinforced concrete. They suggest that the impregnation or coating, involves applying a protective layer such as epoxy resin onto textiles to stabilize their inner structure and shape, has the greatest effect on the material properties of the TRC composite and its application. This chapter will aim to cover the theoretical calculated prediction of AR glass textile reinforced foamed concrete (TRFC) in three potential different failure cases. To experimentally achieve and examine the structural behaviour of these failures will be the subject of the next chapter. There are two cases of tension failure with low and high reinforcement and one case of compression failure. All tests were carried out in three-point flexure. This chapter will provide a concise review of the factors that influence textile-reinforced concrete (TRC), alongside the mechanical properties of AR-glass textiles and foamed concrete. Furthermore, it will discuss the design assumptions that have been adopted, the calculated predictions of TRFC failure, and conclude with a summary.

### 4.2. Reviewing Design Factors of Textile Reinforced Concrete (TRC)

Hegger and Will (2016) have provided guidelines to establish an effective design procedure for TRC. They have proposed that the principal aspect is the impregnation of textile reinforcement, which enhances the stress distribution across the multifilament yarn, resulting in improved activation of inner filaments when compared to non-impregnated yarns. Another factor to consider is that matrix cracking has a minimal influence on the strength of impregnated textiles, while the interaction is

significant in non-impregnated textile strength. Hence, in the case of impregnated textiles, it is theoretically possible to predict the bending strength and ultimate tensile strength of textile reinforced concrete, based on the material characteristics of the composite components.

Furthermore, the impregnation of the textile plays a crucial role in efficiently utilizing the filament's tensile strength in TRC composite. Through tensile and bending tests, it has been observed that the impregnated textile can achieve about 75% of the filament's tensile strength within the TRC composite. In contrast the achievable filament tensile strength of non-impregnated textile reduced to approximately 45% (Raupach et al., 2006; Dilthey et al., 2014).

This leads to a high level of compatibility with the ultimate limit state (ULS) approach. It is used in the prediction of the ultimate bending capacity  $M_u$  for a particular cross-section by predetermining the characteristics of the composite components and applying the equilibrium condition of bending moments and normal forces across the cross-section (Hegger & Will, 2016; Rempel et al., 2015). Additionally, the durability of impregnated textiles is enhanced compared to non-impregnated textiles. The extent of this enhancement appears to be influenced by the thickness of the impregnation layer. The durability improvement is mainly related to the bond enhancement between the textile and the concrete (Raupach et al., 2006; Dilthey et al., 2014).

Moreover, the impregnation of the textiles can be utilized to achieve the fabric stability required for geometric shapes of the structure element that are required, for example straight reinforcement such as for beams and slabs. However, this impregnation also decreases the flexibility of the textile fabrics, which is essential for creating curved shapes. Table 4.1 summarizes a comparison between impregnated and non-impregnated textiles (Hegger & Will, 2016).



*Table 4.1: Comparison between impregnated and non-impregnated textiles (Hegger & Will, 2016)*

Property	Impregnated Textile	Non-Impregnated Textile
Strength Efficiency	High	Medium/ Low
Anchor Length	Short	Medium/ Long
Form Stability	High	Low
Geometric Shapes	Straight shapes (Slabs, Beams)	Curved shapes (Shells)

### 4.3. Material Mechanical Properties

#### 4.3.1. AR-Glass Textile Reinforcement

The mechanical performance of the textile reinforcement is mainly determined by the properties of the textile fabrics, particularly the fibre material, the roving cross-sectional area, the binding style of the warp-knitted fabrics (e.g., tricot, plain stitch bond), and, finally, the fabric impregnation (Hegger & Will, 2016). The AR-glass textile (Mapegrid G220) used in this research was manufactured by MAPEI Group, and the textile technical datasheet is available in Appendix B. It is an impregnated textile with a mesh spacing of 25 mm × 25 mm. The experimental findings presented in Table 4.2 are slightly higher than the specifications provided in the datasheets. Figure 4.1 illustrates the experimental results obtained for AR-glass textile reinforcement.

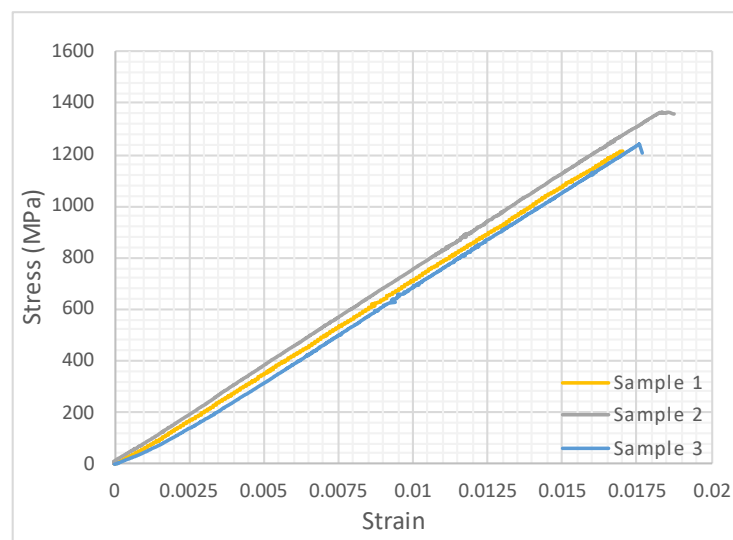


*Figure 4.1: Experimental results for AR-glass textile reinforcement*

Table 4.2: The properties of AR-glass textile reinforcement

AR-Glass Textile Reinforcement	Average Ultimate Tensile Stress (MPa) $F_{uTex}$	Average Tensile Modulus of Elasticity (GPa) $E_{Tex}$	Ultimate Strain $\epsilon_{uTex}$	Yarn Area (mm <sup>2</sup> ) $A_Y$
Manufacturer's datasheet	1079	67	0.0168	0.882
Experimental	1253.8	72.8	0.0175	0.882

#### 4.3.2. Foamed Concrete

Foamed concrete (FC) mix was cast in the university lab to determine and utilize its properties in the predicted design of the textile reinforced foamed concrete (TRFC) beam. So, three 100 x 100 x 100 mm cubes and three cylinders 100 x 200 mm were made to determine compressive strength, modulus of elasticity and ultimate strain at 28 days as illustrated in Table 4.3. Concrete mix preparation and properties have been discussed in more detail in chapter three.

Table 4.3: Foamed concrete mix hardened properties.

Concrete Mix	Compressive Strength (MPa)	Modulus of Elasticity ( $E_{FC}$ ) (GPa)	Ultimate Strain ( $\epsilon_{uFC}$ )
Foamed Concrete	28.1	10.464	0.00394

#### 4.4. Design Assumption

It is well known that a code design for structural concrete elements must meet various requirements, such as serviceability, safety, functionality, and economy. In this section, theoretical calculations will aim to predict potential failures in impregnated AR glass textile reinforced foamed concrete (TRFC), to experimentally achieve three different failure cases, hence, allowing for a comprehensive analysis of the structural behaviour exhibited by this combination. In particular, the load-deflection behaviour and crack propagation will be examined in detail in the next Chapter in cases of low and high reinforcement for tension failures, as well as for compression failure. The three failure cases are detailed as follows:

- Textile reinforced foamed concrete beam failing in tension with low reinforcement under three-point load testing (TRFC-Ten<sub>1</sub>).
- Textile reinforced foamed concrete beam failing in tension with high reinforcement under three-point load testing (TRFC-Ten<sub>2</sub>).
- Textile reinforced foamed concrete beam failing in compression under three-point loads (TRFC-Com).

These calculations are based on prior knowledge of the composite components' characteristics in TRFC beams as shown in Table 4.2 and Table 4.3. For the theoretical derivations, the parabolic rectangular stress block in the Eurocode 2 (EC2) for the ultimate strength design calculations is adopted in this study. The analysis of a cross-section at the ultimate limit state is based on the following assumptions:

- The cross-section of TRFC remains in-plane after loading. This suggests that the strain in reinforcement and concrete are linearly proportional to the perpendicular distance from the neutral axis.
- The tensile strength of the concrete is not taken in account.
- In the compression zone, the stresses are determined from the design stress/strain relationship given in Figure 4.2.
- Foamed concrete and reinforcement textile exhibit a reliable bonding behaviour.

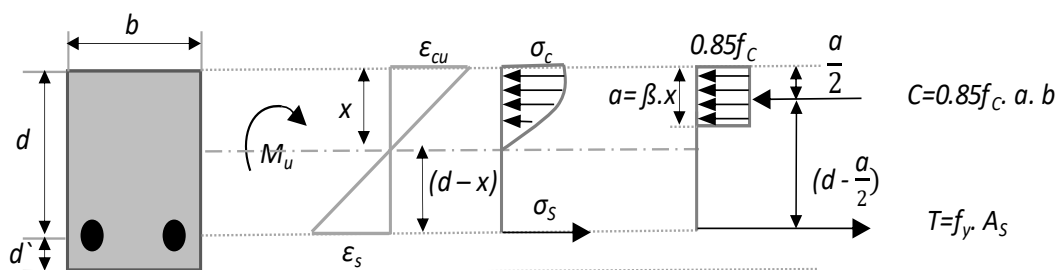


Figure 4.2: Parabolic-rectangular design stress block for the ultimate limit state (EC2)

In Figure 4.2  $d$  is the equivalent effective reinforcement depth;  $\epsilon_{cu}$  is the concrete ultimate strain;  $\epsilon_s$  is the steel strain;  $X$  is the neutral axis depth;  $a$  is the compressive concrete depth;  $\sigma_c$  is the concrete stress;  $\sigma_s$  is the steel stress;  $f_c$  is the ultimate

compressive strength;  $T$  is the steel tension force and  $C$  is the concrete compressive force.

Figure 4.2 demonstrates the replacement of the curved stress block with an equivalent rectangular block of intensity  $0.85 f_c$  and depth ( $a = \beta.X$ ).  $\beta$  is taken to be equal to 0.85 according to the current design compressive strength (28 MPa) (McCormac & Brown, 2014).

Utilizing the Excel analysis tool, Solver, enables the determination of an optimal value that fulfils the equilibrium conditions of forces across the cross-section of the TRFC beam. This approach enables the prediction of the ultimate bending capacity,  $M_u$ , and hence the applied load that would result in failure of the beam by surpassing its ultimate bending capacity  $M_u$ , will be estimated. The input variables and constraint values for Solver undergo continuous adjustments until the appropriate amount of textile cross section and beam dimensions are achieved to satisfy the three failure modes (TRFC-Ten<sub>1</sub>) failure, (TRFC-Ten<sub>2</sub>) failure, (TRFC-Com) failure. To maintain a consistent performance comparison, the beam dimensions are kept same for all cases. The current calculations have not considered any factor of safety, as their purpose is only to predict the outcome of the experimental study. The predictions will be examined against the actual experimental results in chapter Five.

#### 4.5. TRFC Beam Failure in Tension with Low Reinforcement (TRFC-Ten<sub>1</sub>)

##### 4.5.1. Moment Capacity Calculation

The TRFC-Ten<sub>1</sub> beam is intentionally designed to fail in tension to examine its flexural performance with low reinforcement. The textile reinforcement consists of two layers, with four yarns ( $n_\gamma$ ) in each layer. The textile reinforced foamed concrete (TRFC-Ten<sub>1</sub>) stress block is presented in Figure 4.3. The Solver data input is given in Table 4.2, Table 4.3 and Table 4.4.

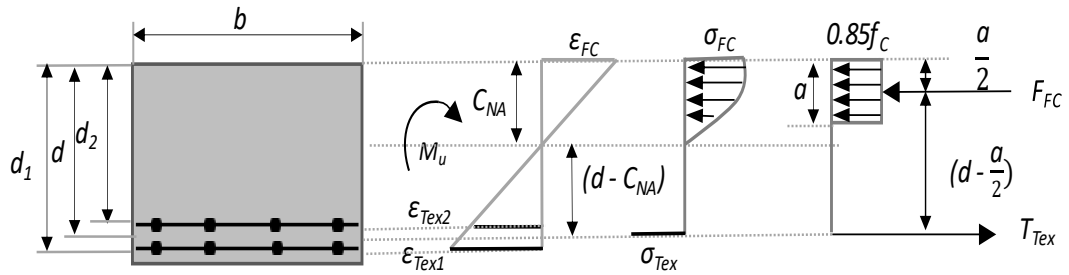


Figure 4.3: Parabolic-rectangular design stress block for the TRFC-Ten1 cross section.

In Figure 4.3  $d$  is the equivalent effective reinforcement depth;  $\varepsilon_{FC}$  is the foamed concrete strain;  $\varepsilon_{Tex1}$  and  $\varepsilon_{Tex2}$  are the textile strain at the 1<sup>st</sup> layer and at the 2<sup>nd</sup> layer respectively;  $C_{NA}$  is the neutral axis depth;  $a$  is the compressive foamed concrete depth;  $\sigma_{FC}$  is the foamed concrete stress;  $\sigma_{Tex}$  is the textile stress;  $f_c$  is the ultimate compressive strength;  $T_{Tex}$  is the textile tension force, and  $F_{FC}$  is the foamed concrete compressive force.

Table 4.4: Input design details used in Solver for TRFC-Ten<sub>1</sub>

Input data	Value
$b$ (mm)	100
$h$ (mm)	55
$d_1$ (mm)	50
$d_2$ (mm)	45
$d$ (mm)	47.5
Area of textile $A_{Tex}$ (mm <sup>2</sup> )	7.06

To calculate the moment capacity ( $M_u$ ) using the Solver tool, the compressive FC depth ( $a$ ) and FC strain ( $\varepsilon_{FC}$ ) are considered as variables. Also, the textile stress at the 1<sup>st</sup> layer ( $\sigma_{Tex1}$ ) is constrained to the value of the ultimate tensile strength ( $\varepsilon_{uTex}$ ). The following equations were utilized in this design:

$$\frac{\varepsilon_{Tex1}}{(d_1 - C_{NA})} = \frac{\varepsilon_{FC}}{C_{NA}} \quad (4.1)$$

$$\frac{\varepsilon_{Tex2}}{(d_2 - C_{NA})} = \frac{\varepsilon_{FC}}{C_{NA}} \quad (4.2)$$

$$\sigma_{Tex1} = E_{Tex} \varepsilon_{Tex1} \quad (4.3)$$

$$\sigma_{Tex2} = E_{Tex} \varepsilon_{Tex2} \quad (4.4)$$

The calculations for the ultimate bending capacity,  $M_u$ , obtained from the Solver, are presented in Table 4.5. The calculated textile stress in the 1<sup>st</sup> layer ( $\sigma_{Tex1}$ ) reaches a

value of 1079 MPa which matches the ultimate tensile strength of the textile before the maximum strength of the formed concrete is reached. This indicates that the failure occurs in tension.

*Table 4.5: TRFC-Ten<sub>1</sub> Solver results*

Output data	Value
$a$ (mm)	3.03
$\sigma_{Tex1}$ (MPa)	1079
$\sigma_{Tex2}$ (MPa)	962.83

The total textile tension force ( $T_{Tex}$ ) is equal to the sum of the textile tension force in the 1<sup>st</sup> layer ( $T_{Tex1}$ ) and the textile tension force in the 2<sup>nd</sup> layer  $T_{Tex2}$ :

$$T_{Tex1} = \sigma_{Tex1} n_Y A_Y \quad (4.5)$$

$$T_{Tex1} = 1079 \times 4 \times 0.882 = 3.8 \text{ kN}$$

$$T_{Tex2} = \sigma_{Tex2} n_Y A_Y \quad (4.6)$$

$$T_{Tex2} = 962.83 \times 4 \times 0.882 = 3.4 \text{ kN}$$

$$T_{Tex} = T_{Tex1} + T_{Tex2} \quad (4.7)$$

$$T_{Tex} = 3.8 + 3.4 = 7.2 \text{ kN}$$

The foamed concrete compressive force ( $F_{FC}$ ) is:

$$F_{FC} = 0.85 a b f_c \quad (4.8)$$

$$F_{FC} = 0.85 \times 3.03 \times 100 \times 28 = 7.2 \text{ kN}$$

By observing the values of  $F_{FC}$  and  $T_{Tex}$ , it is evident that the foamed concrete compressive force and the total textile tension force are equal indicating the fulfilment of the equilibrium condition. Hence the TRFC-Ten<sub>1</sub> predicted ultimate bending capacity ( $M_u$ ) is:

$$M_u = F_{uTex} A_{Tex} \left( d - \frac{a}{2} \right) \quad (4.9)$$

$$M_u = 1079 \times 7.06 \times \left( 47.5 - \frac{3.03}{2} \right) = 0.35 \text{ kN.m}$$

## 4.5.2. Shear and Moment Diagram

Excel was utilized to estimate the applied load that leads to tension failure for the TRFC-Ten<sub>1</sub> beam to verify the beam's shear capacity and avoid shear failure. Table 4.6 and Table 4.7 present TRFC-Ten<sub>1</sub> beam details and calculations respectively. Shear ( $V$ ) and moment ( $M$ ) diagrams for the TRFC-Ten<sub>1</sub> beam are illustrated in Table 4.4. Excel spreadsheets of the theoretical calculations are in Appendix C.

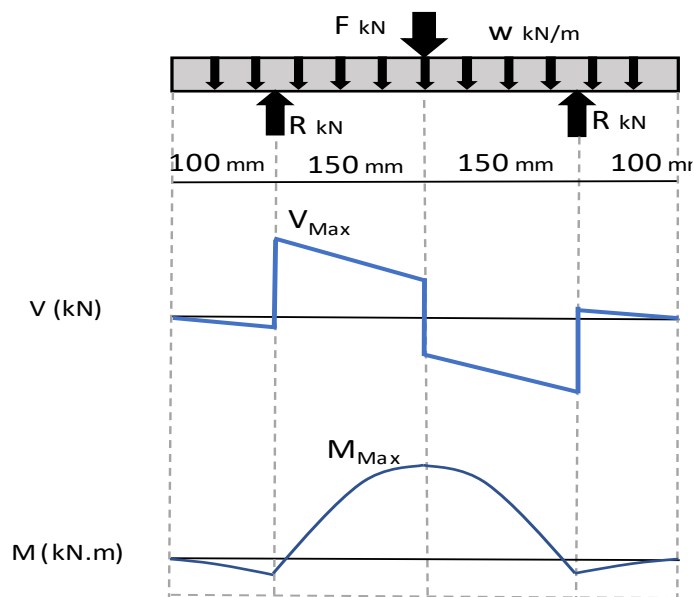


Figure 4.4: Shear ( $V$ ) and moment ( $M$ ) diagram for TRFC-Ten<sub>1</sub> beam.

Table 4.6: TRFC-Ten<sub>1</sub> beam details.

Input data	Value
Density ( $\text{kg}/\text{M}^3$ )	1800
Compressive strength (MPa)	28.1
$b$ (mm)	100
$d$ (mm)	47.5
Beam length (mm)	500

Table 4.7: Shear & Moment results for TRFC-Ten<sub>1</sub>

Output data	Value
Applied load $F$ (kN)	4.7
Max shear force $V_{Max}$ (kN)	2.37
Max moment $M_{Max}$ (kN.m)	0.35

The applied load  $F$  that results in the ultimate moment capacity (0.35 kN.m) is determined to be 4.6 kN. To evaluate the potential for shear failure, the beam shear capacity ( $V_c$ ) is calculated in accordance with (ACI 318, 2011):

$$V_C = 2\lambda b d \sqrt{f_c} \quad (4.10)$$

The coefficient  $\lambda$  for lightweight concrete is defined as 0.85 according to (ACI 318, 2011). Therefore:

$$V_C = 2 \times 0.85 \times 100 \times 47.5 \times \sqrt{28} = 42.73 \text{ kN}$$

Considering that the maximum shear force does not surpass the beam shear capacity ( $V_C$ ), it is evident that no shear failure will occur during the experimental stage.

#### 4.6. TRFC Beam Failure in Tension with High Reinforcement (TRFC-Ten<sub>2</sub>)

##### 4.6.1. Moment Capacity Calculation

TRFC-Ten<sub>2</sub> beam is intentionally designed to fail in tension to examine its flexural performance with high reinforcement. The textile reinforcement consists of two layers, with eight yarns ( $n_Y$ ) in each layer, and the area of the textile ( $A_{Tex}$ ) measures 14.11 mm<sup>2</sup>. Figure 4.5 demonstrates parabolic-rectangular design stress block for the TRFC-Ten<sub>2</sub> cross section.

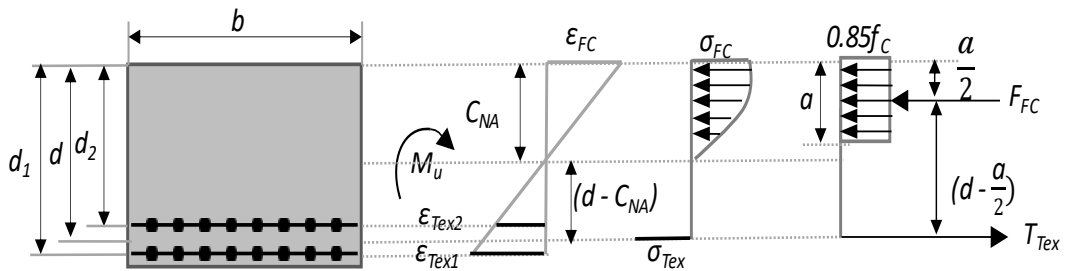


Figure 4.5: Parabolic-rectangular design stress block for the TRFC-Ten<sub>2</sub> cross section.

The moment capacity of the TRFC-Ten<sub>2</sub> beam is calculated using the same method as described in Section 4.5.1. The prediction calculations for the ultimate bending capacity,  $M_u$ , obtained from the Solver, are presented in Table 4.8. It is apparent that the calculated textile stress in the 1<sup>st</sup> layer ( $\sigma_{Tex1}$ ) reaches a value of 1079 MPa which aligns with the ultimate tensile strength of the textile prior to reaching the maximum strength of the foamed concrete. This observation suggests that the failure will occur due to tension.



*Table 4.8: TRFC-Ten<sub>2</sub> Solver results*

Output data	Value
$a$ (mm)	6.03
$\sigma_{Tex1}$ (MPa)	1079
$\sigma_{Tex2}$ (MPa)	953.3
$T_{TEX}$ (kN)	14.35
$F_{FC}$ (kN)	14.35
$M_u$ (kN.m)	0.68

#### 4.6.2. Shear and Moment Diagram

As outlined in Section 4.5.2, the TRFC-Ten<sub>2</sub> beam's shear capacity is calculated to ensure that no shear failure occurs. Shear and Moment results for the TRFC-Ten<sub>2</sub> beam are presented in Table 4.9.

*Table 4.9: Shear & Moment results for TRFC-Ten<sub>2</sub>*

Output data	Value
Applied load $F$ (kN)	9
Max shear force $V_{Max}$ (kN)	4.51
Beam shear capacity ( $V_c$ ) (kN)	42.73
Max moment $M_{Max}$ (kN.m)	0.68

Given that the maximum shear force does not exceed the beam's shear capacity ( $V_c$ ), it is evident that no shear failure will occur during the experimental stage.

#### 4.7. TRFC Beam Failure in Compression (TRFC-Com)

##### 4.7.1. Moment Capacity Calculation

The failure of the TRFC-Com beam is intentionally designed to occur in compression, allowing for an examination of its flexural performance through a three-point flexural test. The textile reinforcement consists of three layers, with eight yarns ( $n_Y$ ) in each layer. The textile reinforced foamed concrete (TRFC-Com) stress block is presented in Figure 4.6. The Solver data input is in Table 4.2, Table 4.3 and Table 4.10.

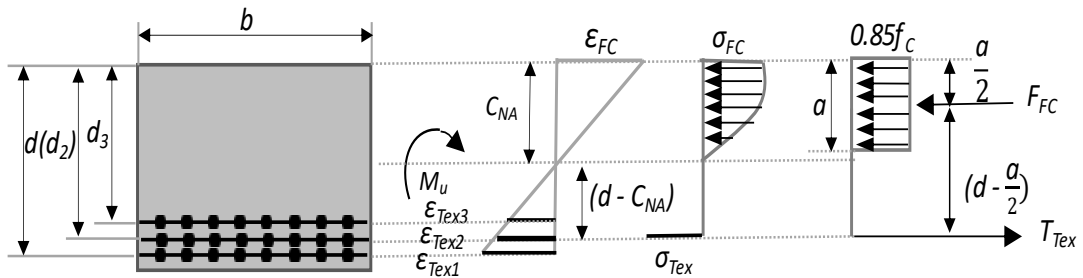


Figure 4.6: Parabolic-rectangular design stress block for the TRFC-Com cross section.

Table 4.10: The input design details in the Solver for TRFC-Com

Input data	Value
$b$ (mm)	100
$h$ (mm)	55
$d_1$ (mm)	50
$d_2$ or $d$ (mm)	45
$d_3$ (mm)	40
Area of textile $A_{Tex}$ (mm <sup>2</sup> )	21.17

The moment capacity ( $M_u$ ) of the TRFC-Com beam is determined using a similar method as described in Section 4.5.1. However, the Solver variables utilized are FC compressive depth ( $a$ ) and textile strain  $\epsilon_{Tex1}$ ,  $\epsilon_{Tex2}$  and  $\epsilon_{Tex3}$ . Additionally, the Solver constraint is set to the maximum FC compressive strength (28.1 MPa).

Table 4.11 presents the calculations for the ultimate bending capacity,  $M_u$ , obtained from the Solver. The calculated foamed concrete compressive strength reaches a value of 28 MPa which matches the ultimate compressive strength of the foamed concrete before the maximum strength of the textile reinforcement is reached. This indicates that the failure occurs in compression.

Table 4.11: TRFC-Com Solver results

Output data	Value
$a$ (mm)	7.31
FC compressive strength (MPa)	27.99
$\sigma_{Tex1}$ (MPa)	864.97
$\sigma_{Tex2}$ (MPa)	877.3
$\sigma_{Tex3}$ (MPa)	734.97
$T_{Tex}$ (kN)	17.4
$F_{FC}$ (kN)	17.4
$M_u$ (kN.m)	0.72

#### 4.7.2. Shear and Moment Diagram

As described in Section 4.5.2, the TRFC-Com beam's shear capacity is calculated to ensure that no shear failure occurs. Shear and Moment results for the TRFC-Com beam are given in Table 4.12.

*Table 4.12: Shear & Moment results for TRFC-com*

Output data	Value
Applied load $F$ (kN)	9.6
Max shear force $V_{Max}$ (kN)	4.81
Beam shear capacity $V_C$ (kN)	40.48
Max moment $M_{Max}$ (kN.m)	0.72

Considering that the maximum shear force does not surpass the beam shear capacity ( $V_C$ ), it is evident that no shear failure will occur during the experimental stage.

#### 4.8. Summary

- The textile impregnation is the key factor to predict the bending strength and ultimate tensile strength of textile reinforced concrete (TRC), based on the prior known material characteristics of the composite components. Additionally, the impregnated textile exhibits notable enhancement in the durability, stability, and bonding behaviour of TRC.
- The hardened properties of the textile reinforcement and foamed concrete mix were experimentally determined in the university lab. Hence, these findings are used in the design calculation of the textile reinforced foamed concrete (TRFC).
- To establish a design calculation guideline, the prior known properties of the TRFC composite and the parabolic-rectangular design stress block by Eurocode 2 for the ultimate limit state were incorporated.
- Theoretical calculations of the potential failures of the impregnated AR glass textile reinforced foamed concrete (TRFC) were carried out to experimentally achieve three different failures, low and high reinforcement for tension failure cases, as well as a compression failure case. The aim is to experimentally examine and analyse the structural behaviour exhibited by these combinations in the laboratory.
- The calculated predictions for the three types of failure in TRFC beams, with dimensions of 55 mm in height, 100 mm in width, and 500 mm in length, are presented in Table 4.13.

*Table 4.13: The calculated predictions for the four types of failures in TRFC beams*

Sample Name	Textile Area (mm <sup>2</sup> )	Ultimate Load (kN)	Ultimate Moment (kN.m)	Maximum Shear Force Applied (kN)	Shear Capacity (kN)	Loading Type	Failure Type
TRFC-Ten <sub>1</sub>	7.06	4.6	0.35	2.37	42.73	3 Points	Tension
TRFC-Ten <sub>2</sub>	14.11	9	0.68	4.52	42.73	3 Points	Tension
TRFC-Com	21.17	9.6	0.72	4.81	40.48	3 Points	Compression

## Chapter 5 Flexural and Pull-out Tests Behaviour of Textile Reinforcement Foamed Concrete

### 5.1. Introduction

Textile-reinforced concrete (TRC) composite consists of a cement-based matrix (fine-grained concrete, commonly known as mortar) reinforced with textile fabric. Extensive exploration of the characteristics of TRC composites can be found in the research literature, encompassing aspects such as textile materials and geometric shapes, properties of the cement-based matrix, interfacial bonds, and the flexural performance of the TRC composite.

This chapter describes an experimental program comprising flexural and pull-out tests carried out on AR fibre textile-reinforced concrete. The flexural test involved the evaluation of four beam samples, each representing a specific variant of textile reinforced concrete. These variants include textile-reinforced foamed concrete (TRFC), textile-reinforced foamed concrete with short fibre (TRFCS), textile-reinforced concrete (TRC) utilized as a control sample, and textile-reinforced concrete with short fibre (TRCS) also employed as a control sample.

### 5.2. Materials Used

While Chapter Three provides an overview of certain materials, this section delves further into the list of materials employed in the experimental procedures outlined in this chapter as shown Figure 5.1.

#### 5.2.1. Short Fibre

The short fibres used in this study are of the AR-glass type, characterized by a length of 12 mm and a diameter of 20  $\mu\text{m}$ . With a density of 2.68 g/cm<sup>3</sup>, these fibres exhibit a tensile strength ranging between 1000 and 1700 MPa. Additionally, the Young's modulus is reported at 72.0 GPa. The AR-glass short fibres are selected for their

mechanical properties, contributing to enhanced structural integrity and performance in the foamed concrete.

### 5.2.2. Fly Ash

The specific fly ash variant employed was (CEMEX 450-N), falling under the N fineness category and B loss on ignition category. This fly ash, sourced from CEMEX Innovation Holding Ltd in the United Kingdom, adheres to the stringent requirements outlined in BS EN 206-1 Concrete – Part 1: 1995. For a detailed insight into the chemical composition, refer to Table 5.1. The analysis of fly ash, silica fume, and limestone was conducted in the university laboratory by Alma'aitah and Ghiassi (2002).

Fly ash exhibits distinctive physical characteristics in its particulate form. Manifesting as fine particles, the maximum particle size  $45\mu\text{m}$ . In its wet state, the pH level of fly ash registers between 9 and 10, contributing to its alkaline nature. The density of fly ash falls within the range of 800 to  $1000\text{ kg/m}^3$ .

### 5.2.3. Silica Fume

Elkem Microsilica Grade 920E is the chosen silica fume. Supplied by Elkem Materials, this product conforms to BS EN 13263-1 (2009). For detailed insights into its chemical composition, please refer to Table 5.1. It has a greyish colour and a melting point ranging between 1550 and 1570 degrees Celsius. The specific gravity of silica fume falls within the range of 2.2 to 2.3, and its bulk density fluctuates between 200 and  $700\text{ kg/m}^3$ . Additionally, the mean particle size is approximately  $0.15\ \mu\text{m}$ .

### 5.2.4. Superplasticiser

Sika Visco Crete-20 RM (GB) is a liquid admixture meticulously produced to fulfil a dual role within concrete mixes, acting both as a water reducer and a plasticizer. Compliant with the stringent standards outlined in BS EN 934-2. This product

attributes to enhance workability while simultaneously reducing water content, thereby elevating the efficiency and performance of concrete mixes.

### 5.2.5. Limestone

As per the provided data sheet, the limestone employed in the study is a high-purity calcium carbonate powder sourced from Longcliff. The limestone appearance is characterized by an off-white, fine powder texture. With a calcium carbonate content of 98.25% and a specific gravity of 2.65. The sizes range from  $3\mu\text{m}$  to  $300\mu\text{m}$ . For chemical composition, refer to Table 5.1.

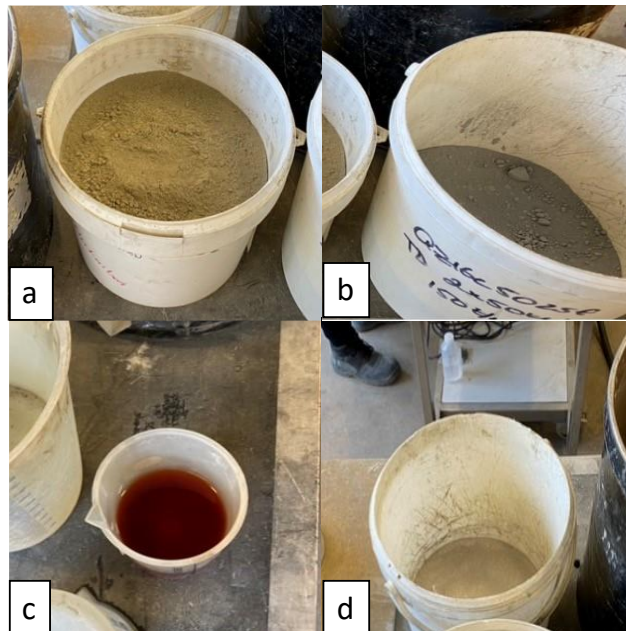


Figure 5.1: Used materials: (a). fly ash (b). silica fume (c). superplasticizer (d). limestone

Table 5.1: Chemical composition of fly ash, silica fume, and limestone (Alma'aitah & Ghiassi, 2022)

Chemical Composition	Fly Ash (%)	Silica Fume (%)	Limestone (%)
Cl-	0.01	0.3	-
SO <sub>3</sub>	0.65	2	-
CaO	4.63	1	-
SiO <sub>2</sub> , Al <sub>2</sub> O <sub>3</sub> , Fe <sub>2</sub> O <sub>3</sub>	82.55	-	-
Na <sub>2</sub> O	2.52	-	-
MgO	1.85	-	-
PO <sub>4</sub> <sup>3-</sup>	0.39	-	-
SiO <sub>2</sub>	-	85	-
Si	-	0.4	-
CaCO <sub>3</sub>	-	-	98.25
Loss on ignition	-	-	1.75
Others	7.4	11.3	-

### 5.3. Flexural Test

Three-point bending tests were conducted to assess the flexural strength of TRFC, TRFCS, TRC, and TRCS samples under three failure cases: two tension cases (Ten<sub>1</sub> and Ten<sub>2</sub> with low and high reinforcement, respectively) and one compression case (Com), allowing for a comprehensive comparison and selection of the most suitable mix for specific engineering applications. Digital Image Correlation (DIC) was initially employed to measure displacements and track crack propagation. However, a video gauge was utilized for the subsequent samples due to a DIC camera malfunction during the experiment. This section covers various topics, including mix components and their properties, test specimens and preparations, measurement tools, and results and analysis.

#### 5.3.1. Mixes Components and Their Properties

Four different concrete mixes were prepared with a targeted compressive strength of 28 MPa at 28 days. These included foamed concrete mix (FC), foamed concrete with short fibre mix (FCS), fine-grained concrete mix (C) sourced from relevant literature (Alma'aitah & Ghiassi, 2022), and fine-grained concrete with short fibre mix (CS)



obtained as a ready mix. The components for FC and FCS mixes are detailed in Table 5.2, while those for the C mix are outlined in Table 5.3.

The CS mix, a ready mix (Planitop HDM Maxi), comprises two integral components: a component A powder is high-strength cement-based mortar infused with short glass fibres (constituting 3% of the binder volume), selected aggregates, and component B consists of special admixtures and synthetic polymers in a water dispersion, following a formula developed in the MAPEI Research Laboratories, depicted in Figure 5.2. Planitop HDM Maxi adheres to the standards set by EN 1504-9. This ready mix, when paired with mesh from the Mapegrid G 220, serves as a structural "reinforced" concrete.

Table 5.2: Components for FC and FCS mixes

Mix Name	Cement (Kg/m <sup>3</sup> )	Sand (Kg/m <sup>3</sup> )	Water (L)	Foam (L)	AR-glass Short Fiber (%) *
FC	620.7	931.03	248.28	203.35	-
FCS	620.7	931.03	248.28	203.35	3

\*By the binder volume



Figure 5.2: Ready mix (Planitop HDM Maxi) - Component A and Component B

Table 5.3: Components for C mix (Alma'aitah & Ghiassi, 2022)

Mix Name	Cement (Kg/m <sup>3</sup> )	Sand (Kg/m <sup>3</sup> )	Fly Ash (Kg/m <sup>3</sup> )	Silica Fume (Kg/m <sup>3</sup> )	Limestone (Kg/m <sup>3</sup> )	Water (L)	Superplasticiser (L)
C	273	910	546	45.5	45.5	273	8.19

To assess the compressive strength, three 100 × 100 × 100 mm cubes were cast for each mix, adhering to the guidelines outlined in BS EN-12390-3: 2019. Table 5.4 presents the mean compressive strength, mean hardening density after 28 days, along with their respective standard deviations (S. D), and the mixes' workability. Following the concrete casting process, all specimens were moulded and covered with a plastic sheet for 24 hours. Subsequently, the specimens were demoulded and subjected to a 28-day curing process within a water tank situated in the laboratory environment, as elucidated in Figure 5.3.

Table 5.4: Compressive strength, densities, and workability of the mixes

Concrete Mix	Mean Comp Strength (MPa)	S. D	Mean Density (kg/m <sup>3</sup> )	S. D	Workability (mm)
Foamed concrete (FC)	28.7	0.5	1794	7.2	315
Foamed concrete + Short fibre (FCS)	29.1	0.8	1837	8	305
Fine-grained concrete (C)	29.5	0.5	2101	19.5	355
Fine-grained concrete + Short fibre (CS)	28.2	0.6	2006	13.8	310



Figure 5.3: Preparing and determining the sample's properties.

In this research, the AR-glass textile (Mapegrid G220) employed was produced by MAPEI Group. This textile is impregnated, with a mesh spacing of 25 mm × 25 mm see Figure 5.4. The experimental results are given in Table 5.5.

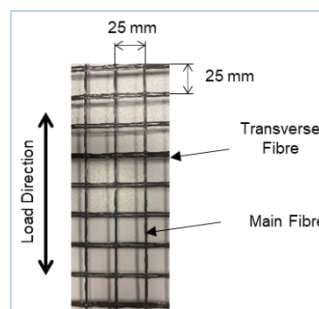


Figure 5.4: The load direction of the AR-glass textile

Table 5.5: AR-glass textile experimental results

Reinforcement	Ultimate Tensile Strength (MPa)	Tensile Modulus of Elasticity (GPa)	Ultimate Strain
AR-Glass Textile	1092	70	0.0172

### 5.3.2. Test Specimens and Preparations

Three-point bending tests were conducted on simply supported beams, each measuring 55 mm in depth, 100 mm in width, and 500 mm in length, as theoretically calculated in Chapter Four, illustrated in Figure 5.5. The bending test was conducted by using a Zwick Universal test machine, under displacement control at a crosshead rate of 1 mm/min. The beams used in the tests included textile reinforced foamed concrete (TRFC), textile reinforced foamed concrete with short fibre (TRFCS), textile reinforced concrete with short fibre (TRCS), and textile reinforced concrete (TRC).

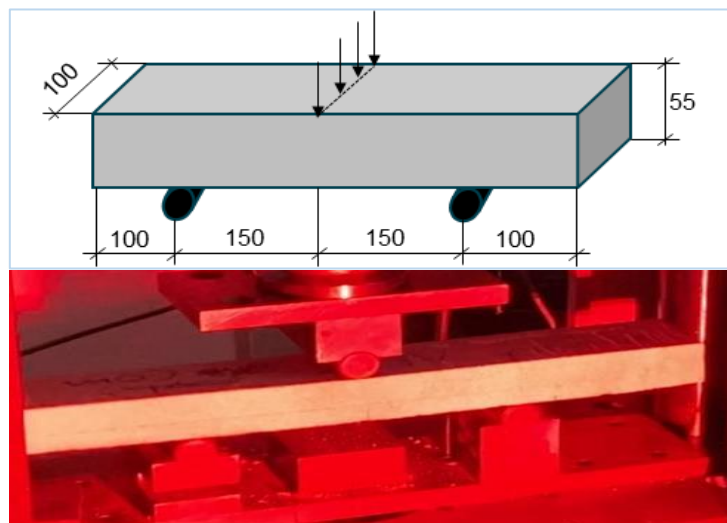


Figure 5.5: Three-point bending tests (dimensions in mm)

To prepare the beams as shown in Figure 5.6, plywood forms were fabricated with removable sides. This allowed for the insertion of textile layers between the sides of the form, maintaining a 5 mm spacing between the layers. The textile layers were cut to size and placed in the bottom of one of the forms. The other form was placed on top of the textile layers, and the sides of the form were screwed or hinged together. Before fitting the textile layers, all internal surfaces were cleaned, and oil brushed. A total of 12 beam samples were cast, consisting of four mix types. Each mix type had

three different reinforcement ratios calculated theoretically in Chapter Four. These ratios were generated to represent three specific failure mechanisms: low and high reinforcement for tension failure cases ( $Ten_1$  and  $Ten_2$ , respectively), and compression failure cases (Com) for each beam type. Following casting, the beams were covered with a plastic sheet for 24 hours and then stored and cured in water tanks in the laboratory environment for 28 days, as shown in Figure 5.7.

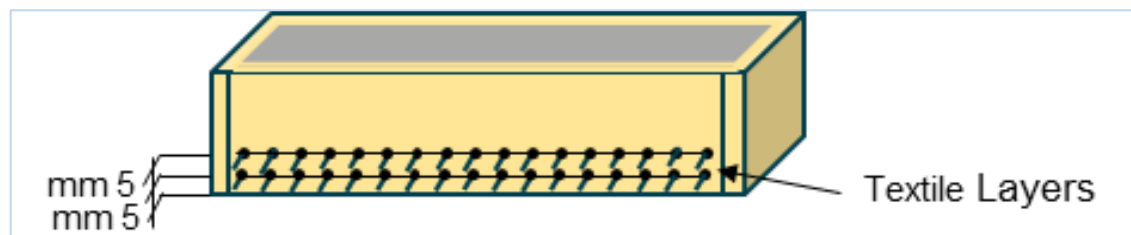


Figure 5.6: Textile layers insertion in the Plywood forms sides



Figure 5.7: Samples casting and curing.

During the bending tests, Digital Image Correlation (DIC) was initially employed to measure displacements and cracks. However, due to the DIC camera malfunctioning throughout the experiment, not all samples were measured by it. Instead, a video gauge was used for the remaining samples, as detailed in Table 5.6.

Table 5.6: Sample details

Sample Name	Reinforcement Ratio	Failure Case	Measurement Tool
TRFC-Ten <sub>1</sub>	0.0017	Tension	Video Gauge
TRFC-Ten <sub>2</sub>	0.0033	Tension	DIC
TRFC-Com	0.0053	Compression	DIC
TRFCS-Ten <sub>1</sub>	0.0017	Tension	DIC
TRFCS-Ten <sub>2</sub>	0.0033	Tension	Video Gauge
TRFCS-Com	0.0053	Compression	DIC
TRCS-Ten <sub>1</sub>	0.0017	Tension	DIC
TRCS-Ten <sub>2</sub>	0.0033	Tension	DIC
TRCS-Com	0.0053	Compression	DIC
TRC-Ten <sub>1</sub>	0.0017	Tension	Video Gauge
TRC-Ten <sub>2</sub>	0.0033	Tension	Video Gauge
TRC-Com	0.0053	Compression	Video Gauge

### 5.3.3. Measurement Tool

#### 5.3.3.1. Digital Image Correlation (DIC)

Digital Image Correlation (DIC) serves as a non-destructive and optical measurement tool. DIC is designed to measure displacements. Furthermore, it has proven effective in analysing and quantifying crack propagation and crack width in objects. The DIC method has the potential to provide a simple, accurate, and cheap option compared to conventional measurement methods. These benefits have led many researchers to adopt the DIC approach in their studies according to the UK's National Physical Laboratory (NPL) (McCormick & Lord, 2010).

The digital correlation technique relies on comparing selected images, including a reference image (taken before loading) and deformed images (captured after loading). A charge-coupled device (CCD) camera is used to capture images of the sample surface. The surface requires a random distribution of the grey levels, often achieved by spraying small black spots of paint onto a white background (Destrebecq et al., 2011).

For analysis, these images are digitised and recorded in a computer to monitor the displacement and deformation using a correlation algorithm. The correlation algorithm is based on monitoring the intensity of the pixel at  $(x,y)$  in the reference image and the pixel at  $(x+\Delta x, y+\Delta y)$  in the deformed image during movement as shown in Figure 5.8. Full-field deformation or displacement data can be generated by repeating this procedure on many subset images (Wang et al., 2009). In the present study, a region of Interest (ROI) corresponds to a rectangle-shaped area,  $280 \times 55$  mm. Its location at midspan enables for monitoring of the potential affected area, as illustrated in Figure 5.9.

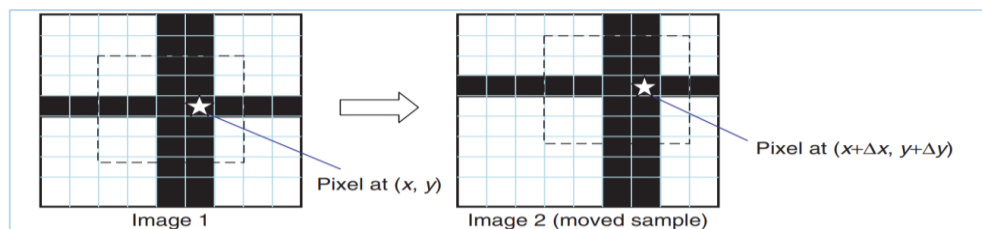


Figure 5.8: Image frames taken before and after deformation (Wang et al., 2009)

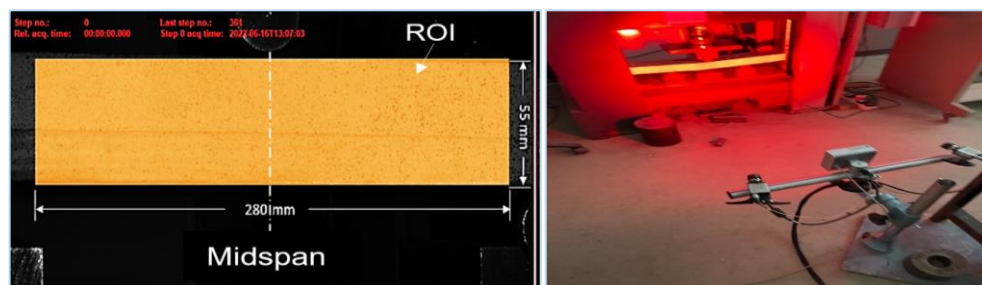


Figure 5.9: Region of Interest (ROI) located at midspan for DIC monitoring.

### 5.3.3.2. Video Gauge

A video gauge is a non-contact measurement tool. The concept of the Video Gauge is to match patterns by normalised correlation algorithms. In other words, a target is detected within a video frame, and then a measurement point is assigned to that target. The Video Gauge can measure and monitor the deflection of the tested samples in real-time. Additionally, no sample preparation is required (Potter & Setchell, 2006). Figure 5.10 illustrates a three-point bending test using a Video Gauge.



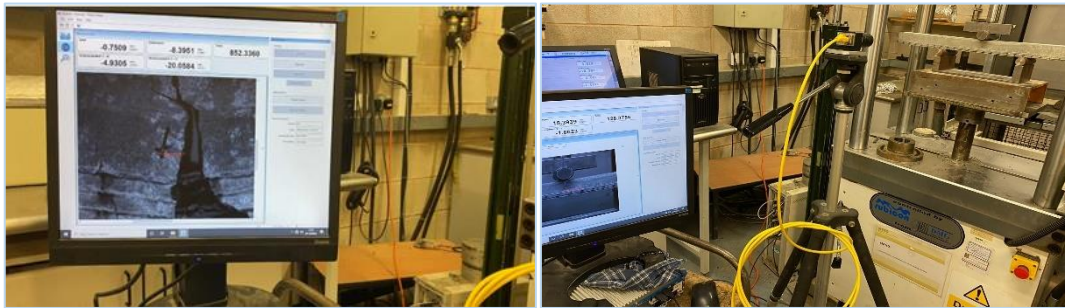


Figure 5.10: Three-point bending test using a Video Gauge

### 5.3.4. Results and Analysis

Load deflection analysis is an essential method used in structural engineering to assess the mechanical behaviour of a beam subjected to bending loads. The analysis in this section is based on failure case comparison, concrete mix comparison, ultimate flexural strength, and crack propagation behaviour.

#### 5.3.4.1. Failure Case Comparison

The load-deflection curves in Figure 5.11 reveal consistent stiffness behaviour among the three failure cases—two tension cases ( $Ten_1$  and  $Ten_2$  with low and high reinforcement, respectively) and one compression case (Com)—across each concrete mix in the initial linear elastic region. Beyond the elastic limit, a noticeable non-linear response emerges in the Com beams, indicating superior ductility and enhanced energy absorption as illustrated in Figure 5.12. The energy absorption refers to the area below the load vs. deflection curve until failure. For instance, the absorbed energy for TRFCS-Com rises notably by 302.1% and 631.7% compared to samples TRFCS- $Ten_2$  and TRFCS- $Ten_1$ , respectively. This enhanced performance is attributed to the significant reinforcement in the Com beams, which strengthens them against bending forces, leading to an increased load capacity.

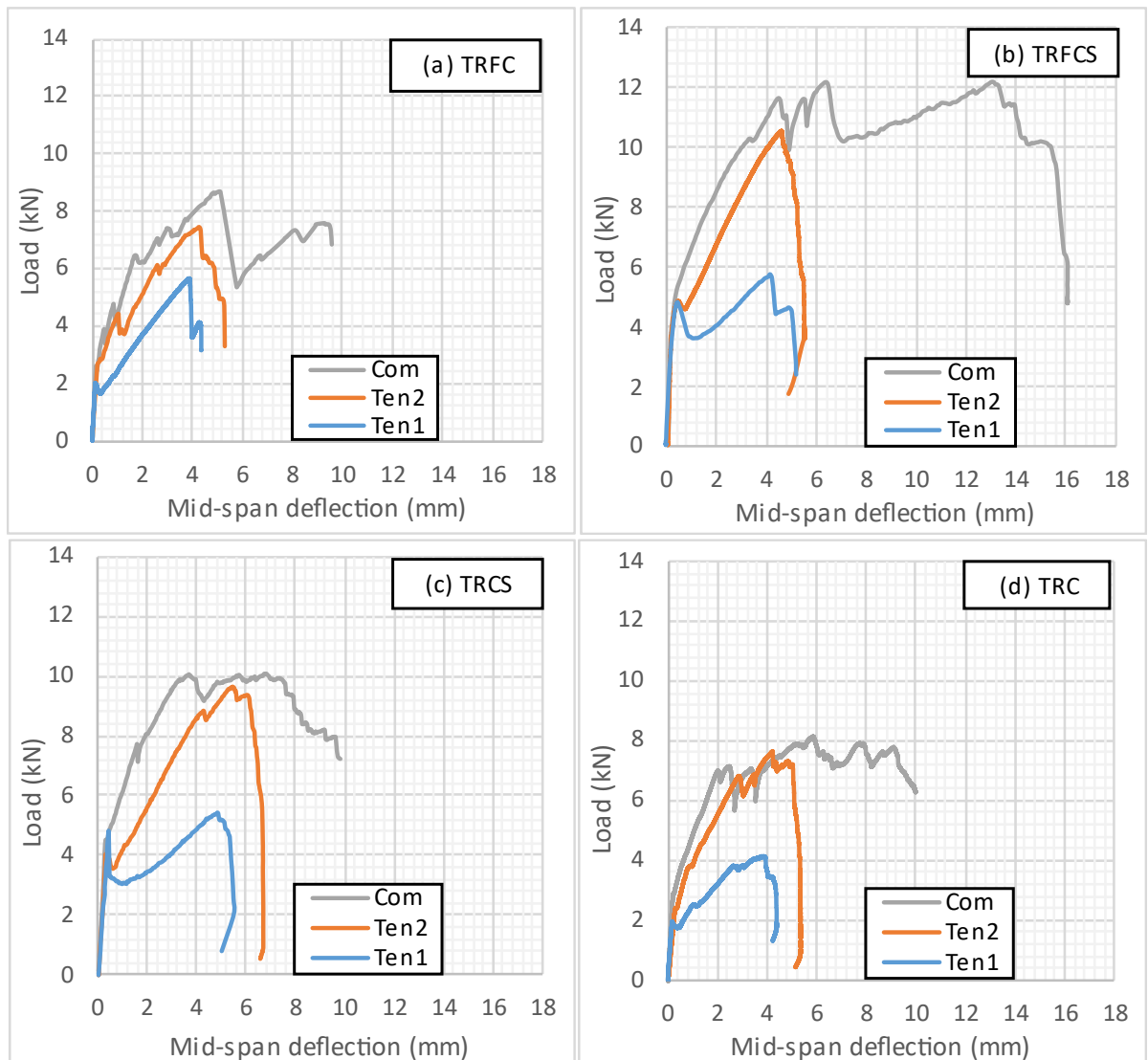


Figure 5.11: Comparison of failure cases in flexural load-deflection curves for (a) TRFC, (b) TRFCS, (c) TRCS, and (d) TRC of samples

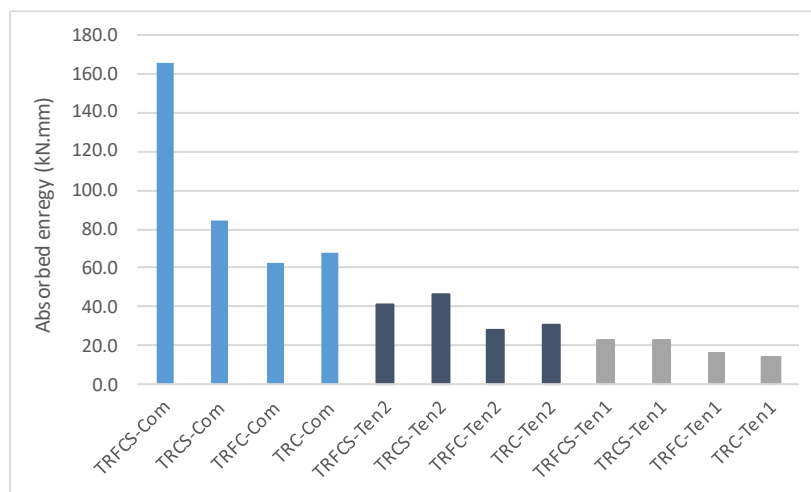


Figure 5.12: Comparison of energy absorption among TRFC, TRFCS, TRCS, and TRC samples under three failure cases: Com, Ten<sub>2</sub>, and Ten<sub>1</sub>

### 5.3.4.2. Concrete Mixes Comparison

In the elastic region, the response of TRFCS (Textile reinforced foamed concrete with short glass fibres) and TRCS (Textile reinforced concrete with short fibre) demonstrate a stiffer performance compared to TRC (Textile reinforced concrete) and TRFC (Textile reinforced foamed concrete), as shown in Figure 5.13. This heightened stiffness and enhanced crack resistance in TRFCS and TRCS can be attributed to the presence of short glass fibres, distinguishing them from TRC and TRFC. Notably, TRFCS and TRCS exhibit a load ranging from 4 kN to 4.8 kN, indicating their superior resistance to deformation under applied loads, reaching the point at which the samples start to deform plastically. In contrast, TRC and TRFC exhibit a lower load range of 2 kN to 3 kN. Furthermore, sample stiffness is calculated using Equation (5.1) (Sudhakar & Muthusubramanian, 2024) and results are given in Table 5.7, highlighting the stiffer performance of TRFCS and TRCS samples compared to TRFC and TRC samples.

$$k = \frac{V_y}{\Delta_y} \quad 5.1)$$

where  $k$  is the stiffness index;  $V_y$  is the yield load; and  $\Delta_y$  is the yield deflection.

Table 5.7: Stiffness of TRFCS, TRCS, TRFC, and TRC samples

Sample Name	Stiffness Index ( $k$ ) (kN/mm)
TRFCS-Com	24.3
TRCS-Com	20.1
TRFC-Com	15.0
TRC-Com	15.9
TRFCS-Ten <sub>2</sub>	21.7
TRCS-Ten <sub>2</sub>	18.2
TRFC-Ten <sub>2</sub>	13.2
TRC-Ten <sub>2</sub>	11.9
TRFCS-Ten <sub>1</sub>	19.8
TRCS-Ten <sub>1</sub>	17.1
TRFC-Ten <sub>1</sub>	13.6
TRC-Ten <sub>1</sub>	12.8

The ductility factor ( $\mu$ ) represents a member's ability to undergo deformation beyond the elastic limit while sustaining a reasonable load-carrying capability until complete failure. It is calculated for the samples using Equation (5.2) (Kwan et al., 2002):

$$\mu = \frac{\Delta_{max}}{\Delta_y} \quad (5.2)$$

where  $\mu$  is the ductility factor;  $\Delta_{max}$  is the maximum deflection at ultimate load; and  $\Delta_y$  is the yield deflection.

As illustrated in Figure 5.13 and Table 5.8, samples failing under compression (Com) demonstrate the highest capacity for plastic deformation. Specifically, the ductility factors measured at 3.6 and 3.5 for the TRFCS-Com and TRCS-Com samples, respectively, surpass those of the TRFC-Com and TRC-Com samples, which exhibit lower ductility values of 2.6 and 2.4, respectively. This significant difference underscores the superior ductility and deformability of the TRFCS-Com and TRCS-Com beams compared to the other tested samples. Clearly, the inclusion of short fibres plays a pivotal role in enhancing the toughness of these samples.

For samples failing under tension  $Ten_2$  and  $Ten_1$  a similar ductility factor range of (1.5 to 1.7) and (1.1 to 1.3) respectively was measured. This similarity is expected because the failure occurs in tension and all the samples share an identical reinforcement.

However, it is worth noting that in the tension failure case ( $Ten_2$ ), both the TRFCS and TRCS samples exhibit a higher load capacity when compared to the TRFC and TRC samples, even though all specimens share an identical amount of reinforcement, as illustrated in Figure 5.13 (b). This intriguing difference may be attributed to the incorporation of short fibres (3% of the binder volume), which enhances the bond between the textile reinforcement and the concrete matrix. Consequently, this improvement facilitates a more efficient transfer of stresses between the reinforcement and the concrete matrix.

In essence, short fibres serve as bridging elements within the concrete matrix. As cracks begin to form and propagate, these fibres act to distribute stress more

uniformly across the concrete, thereby impeding crack propagation and enhancing the absorbed energy of the sample. This is supported by research conducted by Bing et al. (2012), which underscores the enhancement in flexural strength and overall toughness achieved by incorporating short fibres into foamed concrete. Another factor is the inclusion of short fibres, which led to a slight increase in the compressive strength of the TRFCS sample compared to the TRFC sample. Specifically, the compressive strength of the TRFCS sample was measured at 29.1 MPa, while that of the TRFC sample was 28.7 MPa.

*Table 5.8: Ductility factor of TRFCS, TRCS, TRFC, and TRC samples*

Sample Name	Ductility Factor ( $\mu$ )
TRFCS-Com	3.6
TRCS-Com	3.5
TRFC-Com	2.6
TRC-Com	2.4
TRFCS-Ten <sub>2</sub>	1.5
TRCS-Ten <sub>2</sub>	1.7
TRFC-Ten <sub>2</sub>	1.5
TRC-Ten <sub>2</sub>	1.7
TRFCS-Ten <sub>1</sub>	1.1
TRCS-Ten <sub>1</sub>	1.3
TRFC-Ten <sub>1</sub>	1.2
TRC-Ten <sub>1</sub>	1.3

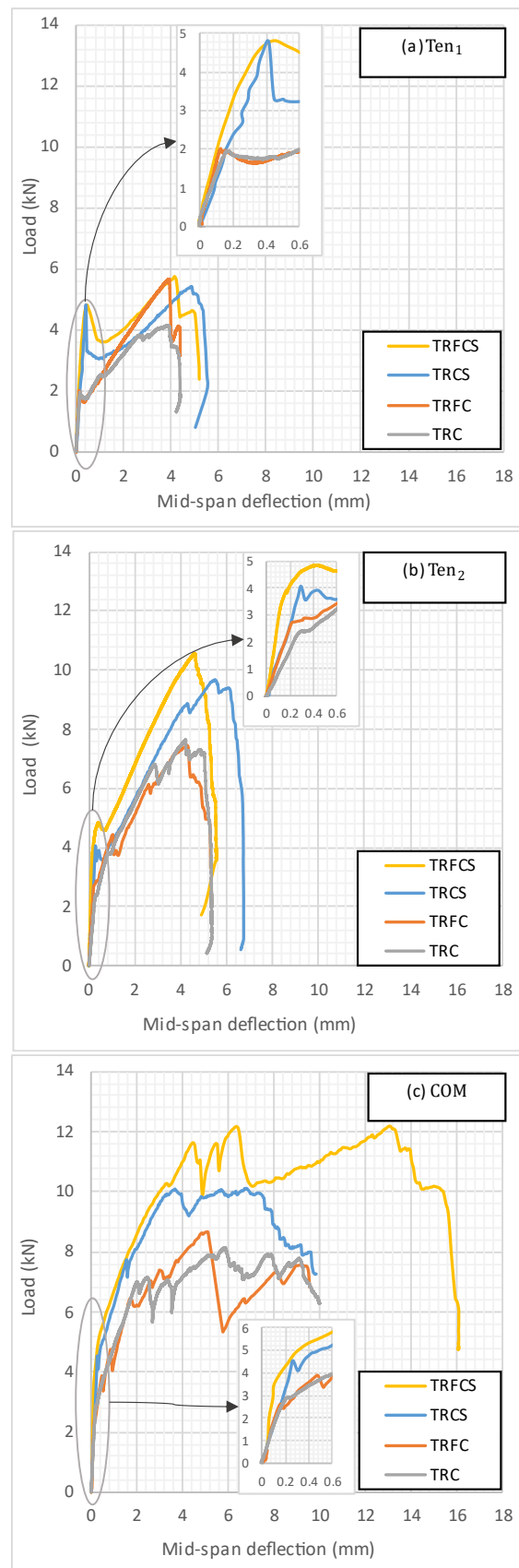


Figure 5.13: Comparison of concrete mixes in flexural load-deflection curves for (a) Ten<sub>1</sub>, (b) Ten<sub>2</sub>, and (c) Com

### 5.3.4.3. Ultimate Flexural Strength and Flexural Strain

Ultimate flexural stress and flexural strain of all samples are determined using Equations (5.3) and (5.4) (ASTM D790, 2010). Through a comparison of the research findings with previously published studies of textile reinforced concrete with concrete compressive strength of around 30 MPa, the potential arises to assess the mechanical behaviour and performance of the research specimens' results. All results are plotted in Figure 5.14 and literature references are given in Table 5.9.

Among the outcomes, the textile-reinforced foamed concrete with short fibres under compression failure (TRFCF-Com) prominently exhibits superior resilience against flexural loads and remarkable ductility in comparison to the other results.

*Table 5.9: Literature review references of the Ultimate flexural strength of the TRC*

Name	Short Fibers	Reference
Literature 1	(PVA, Glass and PP)	(Alma'aitah & Ghiassi, 2022)
Literature 2	-	(Halvaei M. et al, 2020)
Literature 3	-	(Alrshoudi, 2021)

$$\sigma_f = \frac{3PL}{2bd^2} \quad (5.3)$$

where  $\sigma_f$  is flexural stress at max load at mid-point (MPa);  $P$  is the load at a given point on the load-deflection curve (N);  $L$  is the supported span (mm),  $b$  is the width of beam tested (mm), and  $d$  is the depth of beam tested (mm).

$$\varepsilon_f = \frac{6Dd}{L^2} \quad (5.4)$$

where  $\varepsilon_f$  is the strain at failure (mm/mm);  $D$  is the maximum deflection of the centre of the beam (mm);  $L$  is the supported span (mm), and  $d$  is the depth (mm).

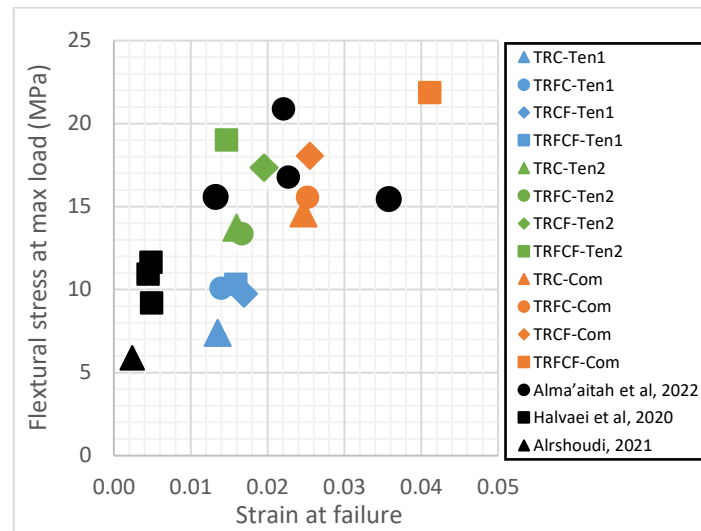


Figure 5.14: Comparison of the ultimate flexural strength and flexural strain at failure between the research samples and selected literature

#### 5.3.4.4. Crack Propagation and Failure Modes

Digital Image Correlation (DIC) was utilized to examine and quantify crack propagation, crack width, and failure patterns to understand the behaviour of the tested beams. Vertical flexural cracks emerged in the central part of the bottom tension zone for all beams, extending towards the compression zone until reaching a failure state.

Crack initiation in the TRFC-Com beam occurred when the applied load reached 2.59 kN. However, in the TRFCS-Com beam, the first cracking load was found to be 4.35 kN, indicating that the TRFC-Com beam requires only approximately 60% of the load compared to the TRFCS-Com beam to initiate cracking.

At the point of failure, TRFCS-Ten<sub>1</sub>, TRCS-Ten<sub>1</sub>, TRCS-Ten<sub>2</sub>, and TRFC-Ten<sub>2</sub> beams exhibited a reduced crack count and wider crack widths compared to TRFCS-Com, TRCS-Com, and TRFC-Com beams. For instance, the former beams displayed crack widths ranging from 2.5 mm to 3 mm, while the maximum crack width for the latter beams was limited to 1.2 mm.

This pattern of multiple cracks characterized by narrow widths can be attributed to the effective stress redistribution capability of TRFCS-Com, TRCS-Com, and TRFC-Com

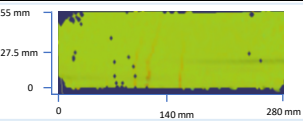
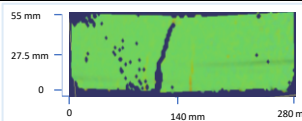
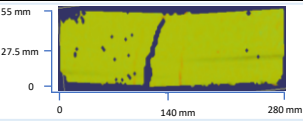
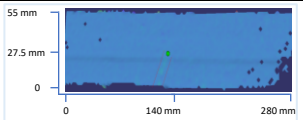
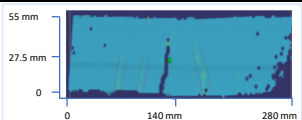
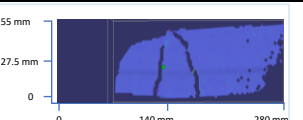
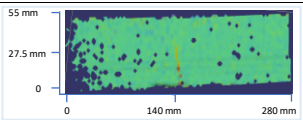
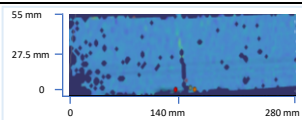
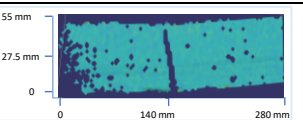
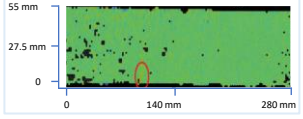
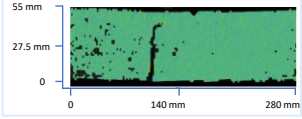
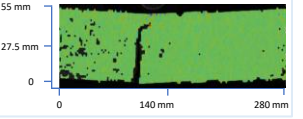
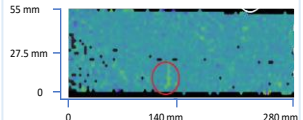
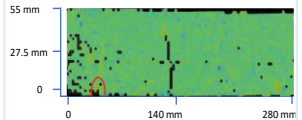
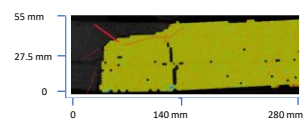
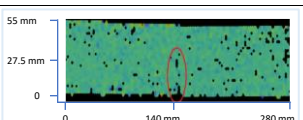
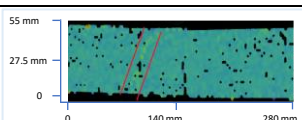
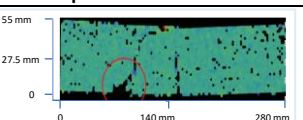
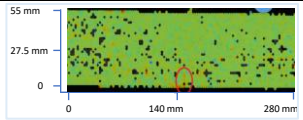
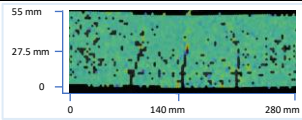
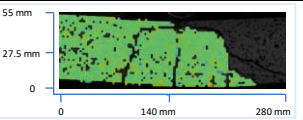


beams. This behaviour is likely due to these beams having a greater number of textile reinforcement layers compared to the others. By increasing the number of textile layers, the failure point of the textile reinforcement is effectively raised, allowing the increased layers to distribute the load more evenly and absorb more energy. This resulted in concrete crushing failure in Com samples along with shear cracks, before reaching a critical failure point in the textile, consequently preventing tensile failure. In contrast, (Ten) samples, with fewer textile reinforcement layers, reached the failure point in the textile first, as shown in Figure 5.15. DIC images illustrating these failure modes are provided in Table 5.10.



Figure 5.15: Comparison between compression failure and tension failure.

Table 5.10: DIC images depict load at crack initiation, ultimate load, and failure

Beam Name	Load at Crack Initiation	Ultimate Load	Load at Failure
(TRFCS-Ten <sub>1</sub> )	 <p>4.82 (kN)</p>	 <p>5.75 (kN)</p>	 <p>5.55 (kN) Tension Failure</p>
(TRFCS-Com)	 <p>4.35 (kN)</p>	 <p>12.15 (kN)</p>	 <p>11.42 (kN) Compression Failure</p>
(TRCS-Ten <sub>1</sub> )	 <p>4.78 (kN)</p>	 <p>5.4 (kN)</p>	 <p>5.2 (kN) Tension Failure</p>
(TRCS-Ten <sub>2</sub> )	 <p>4.06 (kN)</p>	 <p>9.68 (kN)</p>	 <p>9.4 (kN) Tension Failure</p>
(TRCS-Com)	 <p>4.54 (kN)</p>	 <p>10.05 (kN)</p>	 <p>8.8 (kN) Compression Failure</p>
(TRFC-Ten <sub>2</sub> )	 <p>2.74 (kN)</p>	 <p>7.45 (kN)</p>	 <p>6.45 (kN) Tension Failure</p>
(TRFC-Com)	 <p>2.59 (kN)</p>	 <p>8.65 (kN)</p>	 <p>7.57 (kN) Compression Failure</p>

#### 5.3.4.5. Comparison of Experimental and Theoretical Data for TRFC Beams

The comparison between theoretical predictions and experimental maximum bending moments serves to evaluate the agreement and reliability of the results. This comparison is conducted on textile reinforced foamed concrete (TRFC) beams across the failure cases Ten<sub>1</sub>, Ten<sub>2</sub>, and Com. The experimental maximum moment was determined using the formula for the maximum bending moment of a simply supported beam with a point load at mid-span. The results are detailed in Table 5.11.

Table 5.11: Comparison between max experimental and theoretical moment for the TRFC

Failure Case	Experimental Max Moment (kN.m)	Theoretical Max Moment (kN.m)
TRFC-Ten <sub>1</sub>	0.38	0.35
TRFC-Ten <sub>2</sub>	0.59	0.68
TRFC-Com	0.68	0.72

From a visual inspection, it is evident that there is a higher degree of agreement between the experimental and theoretical results for TRFC-Ten<sub>1</sub> and TRFC-Com cases compared to TRFC-Ten<sub>2</sub>, as depicted in Figure 5.16. The percentage variation for TRFC-Ten<sub>1</sub>, TRFC-Ten<sub>2</sub>, and TRFC-Com is calculated as 7.14%, 12.78%, and 6.25%, respectively.

The relatively higher discrepancy in agreement for the TRFC-Ten<sub>2</sub> beam compared to TRFC-Ten<sub>1</sub> may be attributed to the elevated load levels experienced by the former, potentially inducing premature debonding between the textile reinforcement and the foamed concrete matrix.

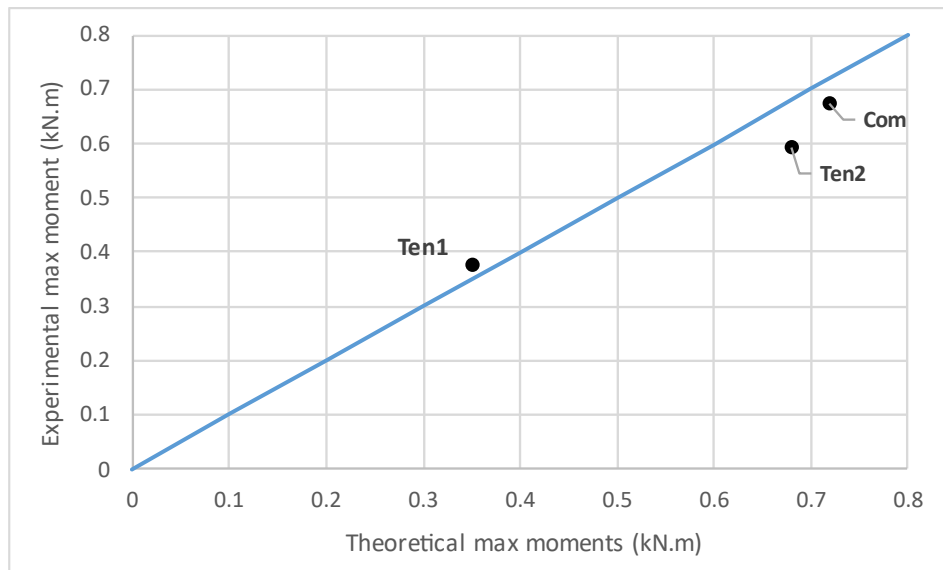


Figure 5.16: Comparison between max moment theoretical and experimental results for TRFC beam.

#### 5.4. Pull-out Test

The characteristics of textile-reinforced concrete (TRC) composites significantly depend on the bond between the textile and the matrix. This bond behaviour influences the entire performance of the composite, governing its strength, toughness, and ductility (Banholzer et al., 2006). Generally, a strong bond often results in a reinforcement fracture with high strength but limited ductility and relatively brittle characteristics. Conversely, a weaker bond tends to cause fibre pullout, resulting in a more ductile composite with reduced strength (Peled, 2016).

Barhum & Mechtcherine (2013), in their study, examined the bonding performance of a single yarn interconnected by transverse fibres, as depicted in Figure 5.17. Ghiassi et al., 2016, suggested that, while a single-sided pull-out test setup might be straightforward, a more comprehensive investigation into the pull-out behaviour of fabrics embedded in mortar and the influence of transverse fibres on bond performance is essential for the development of accurate constitutive models. The current pull-out test extends this prior research to establish a more realistic constitutive model. It involves a thorough exploration of the bonding behaviour of three AR-glass yarns interconnected by transverse fibres along the entire length of the concrete specimens.

Key points of this study include:

- Embedding the textile material along the length of the concrete specimens.
- Employing three textile yarns interconnected by transverse fibres.
- Using similar grips on the specimens to ensure uniformity in slippage if it occurs.

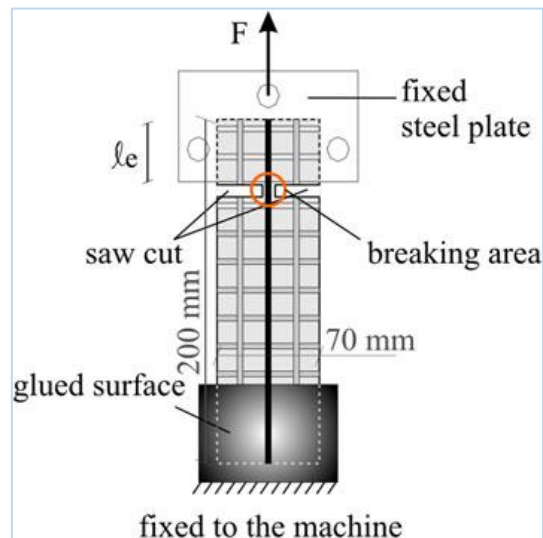


Figure 5.17: Schematic view of specimen geometry and setup used in yarn pullout tests (Barhum & Mechtcherine, 2013)

#### 5.4.1. Test Specimens and Preparations

These tests were performed to investigate the bonding behaviour of the fully embedded textile reinforcement in concrete specimens. The testing procedures were carried out using a Zwick Universal test machine with a maximum load capacity of 200 kN, operating under displacement control conditions at a rate of 1 mm/minute. Load measurements were acquired through the test machine's load cell, while displacements were monitored using two LVDTs positioned on either side of the specimens. The specimens were prepared by embedding three AR-glass yarns interconnected by transverse fibres into concrete mixes. The total length of the textile material was 500 mm, with 400 mm of it being embedded within the concrete. The concrete specimens themselves had dimensions of 400 mm in length, 50 mm in width, and 10 mm in depth. The experimental setup is shown in Figure 5.18.

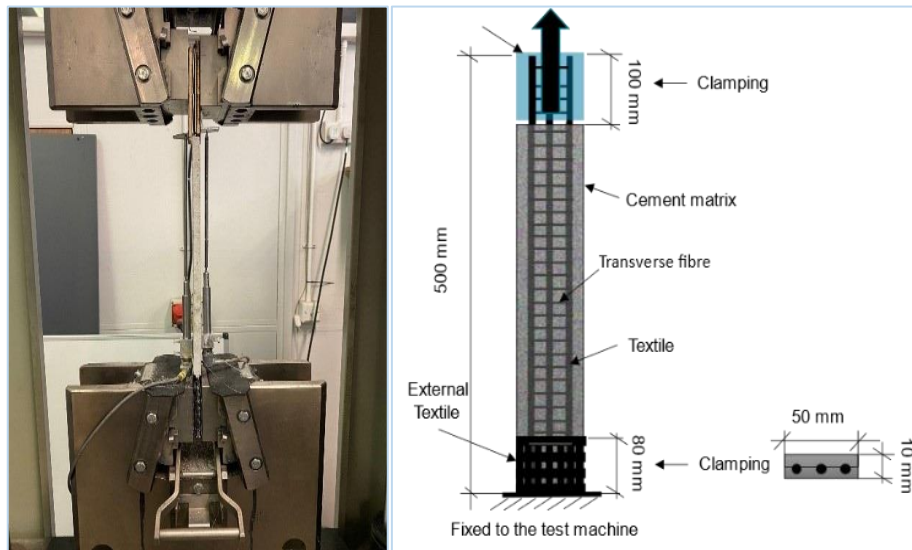


Figure 5.18: Pull-out test setup.

The textile embedding started with the spreading of about 5 mm of concrete on the bottom of the mould. Then the textile reinforcement was laid on this fresh concrete layer and then gently, pressed in and smoothed. After that, the other concrete layer was placed on the textile reinforcement. All specimens were demoulded at a concrete age of two days and then stored in a water tank until reaching an age of 28 days as shown in Figure 5.19.

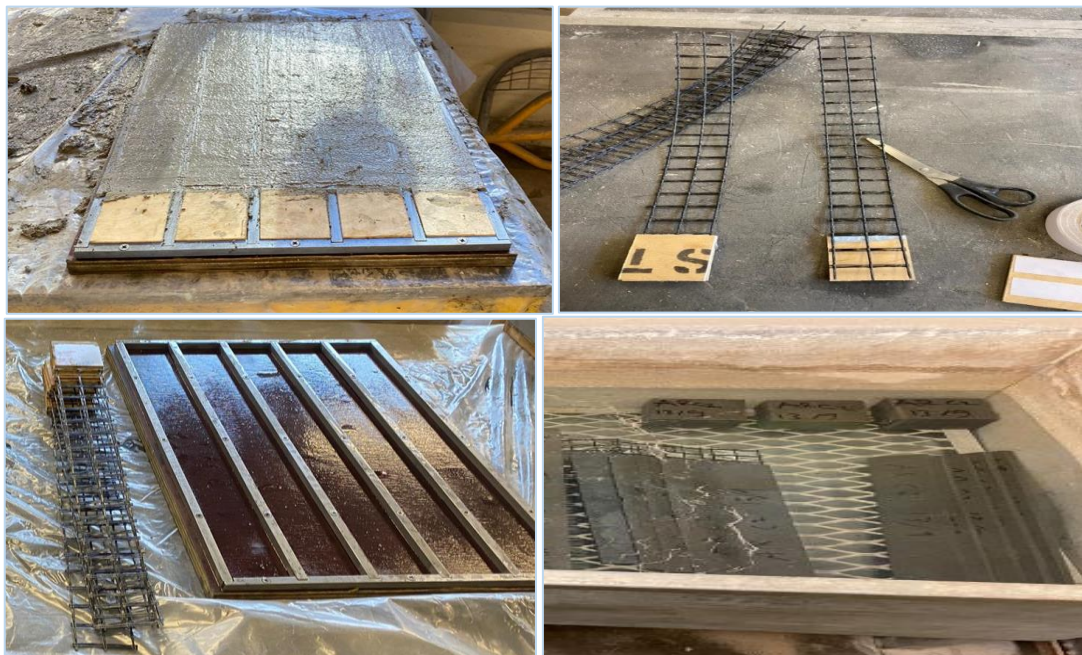


Figure 5.19: Samples preparation, casting, and curing for pull-out test

To ensure a secure grip for pulling the dry textile, steel plates were affixed from the top using epoxy (Sikadure 52) as illustrated in Figure 5.21. Additionally, the lower part of the concrete specimens was externally enveloped with an extra layer of textile by using epoxy to prevent concrete failure and cracking in this region as shown in Figure 5.20. The test specimens are textile reinforced foamed concrete with short fibres (TRFCS) and textile reinforced concrete with short fibres (TRCS). For each combination, three specimens were prepared and subjected to testing, resulting in a total of 6 specimens.



Figure 5.20: Steel plates securely anchored and reinforced with additional textile layers at the other end of the samples



Figure 5.21: Epoxy (Sikadure 52)



#### 5.4.2. Result and Analysis

The graph in Figure 5.22 illustrates the pull-out force and corresponding displacement for TRFCS and TRCS specimens. The pull-out force-displacement curves exhibit fluctuations due to the presence of three yarns in the textile reinforcement for each sample. The ultimate load measurements of the samples are similar, with the TRCS sample exhibiting an ultimate load of 1.98 kN and the TRFCS sample reaching 1.89 kN. However, the TRCS sample demonstrates slightly stiffer behaviour compared to the TRFCS sample. It is also noteworthy that after the initial peak for the TRCS sample, there is a marked decline in the load. Both TRCS and TRFCS samples display similar displacement values, which is understandable because both failures occurred in the textiles of both samples.

In the present study, samples exhibited textile rupture during the pull-out test. This differs from prior research conducted by Barhum & Mechtcherine (2013), Ghiassi et al. (2016), and Alma'aitah & Ghiassi (2022), where the textiles did not reach rupture stages. This occurrence in the current research can be attributed to the embedded length of the textile, which is 400 mm and aligns with the entire length of the specimens. Consequently, the pull-out test assumed characteristics like a tensile test, posing challenges in monitoring the slight displacement of the textile within the concrete using LVDTs.

To address these challenges, it is recommended to employ a tool capable of recording micro movements, such as digital image correlation (DIC). Also, DIC enhances visualization and understanding of crack propagation curve fluctuations. Additionally, conducting the pull-out test with a reduced embedded length is advised to mitigate these complexities in future experiments.

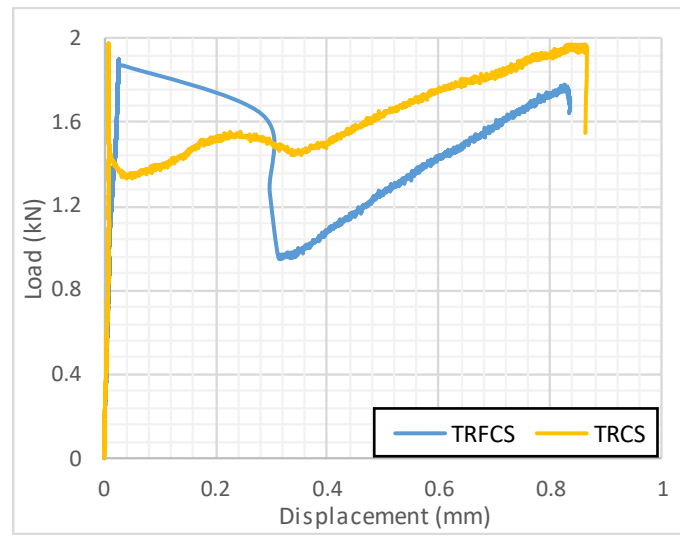


Figure 5.22: Pull-out – Displacement results for TRFCS and TRCS specimens

### 5.5. Summary

- Three-point bending tests of TRFC, TRFCS, TRC, and TRCS samples under two tension cases ( $Ten_1$  and  $Ten_2$  with low and high reinforcement, respectively) and one compression case (Com) have been conducted. Using DIC and video gauge enabled comprehensive comparison for optimal engineering applications.
- TRFCS (Textile-reinforced foamed concrete with short glass fibres) and TRCS (Textile-reinforced concrete with short fibre) exhibit stiffer responses than TRC (Textile-reinforced concrete) and TRFC (Textile-reinforced foamed concrete).
- TRFCS beams under the compression failure exhibit the greatest non-linear response, signifying superior ductility, energy absorption, and load capacity.
- Short fibres enhance the toughness of the TRFCS beams during the plastic phase of the compression failure case.
- TRFC samples under the compression failure beam require only 60% of the load to initiate cracking compared to TRFCS under the compression failure beam, highlighting its lower resilience and ductility.
- TRFCS- $Ten_1$ , TRCS- $Ten_1$ , TRCS- $Ten_2$ , and TRFC- $Ten_2$  beams (under tension failure), at the point of failure, demonstrate fewer cracks and wider crack widths (ranging from 2.5 mm to 3 mm) compared to TRFCS-Com, TRCS-Com, and TRFC-Com beams (under compression failure), which exhibit a maximum crack width of 1.2 mm.
- There is a notable agreement between the experimental and theoretical results, particularly evident in the case of TRFC- $Ten_1$  and TRFC-Com. However, a relatively larger discrepancy is observed for TRFC- $Ten_2$ , which could be attributed to premature debonding occurring between the textile reinforcement and the foamed concrete matrix.
- All specimens underwent textile rupture during pull-out testing. The current pull-out test extends prior research by exploring the bonding behaviour of three AR-glass yarns interconnected by transverse fibres along the entire

length of TRFCS and TRCS samples, aiming to achieve a better understanding of the material behaviour. However, the test encountered the challenge of fluctuating curves in results due to the use of more than one textile.

- The recommendation for the pull-out test suggests utilizing a tool such as digital image correlation (DIC) to capture micro movements. This method allows for a thorough assessment of the test results and facilitates accurate investigation.
- Given the high structural performance observed in the textile reinforced foamed concrete with textile under compression failure (TRFCS-Com) among the tested samples, it is recommended to conduct an experiment involving large-scale beams and slabs using the TRFCS-Com sample. This experimentation should aim to compare its performance directly with that of conventional reinforced concrete.

## Chapter 6 TRFC Life-Cycle Assessment (LCA)

### 6.1. Introduction

Concrete stands as the predominant construction material globally, boasting unparalleled usage. The average annual consumption of concrete per person is approximately 1 tonne, rivalling only water in its scale of use. Given its widespread usage, even modest decreases in greenhouse gas emissions per tonne of produced concrete can yield a notable global influence (Flower & Sanjayan, 2007).

Life cycle assessment (LCA) is conducted to collect data aimed at improving the environmental performance of concrete mixes, including foamed concrete mixes and conventional concrete mixes. By comparing different mixes, LCA empowers decision-makers to identify and mitigate the environmental impacts of concrete mixes. This process contributes to sustainable development in concrete mixes, providing insights for designers, developers, and researchers.

The study follows ISO 14040:2006 and ISO 14044:2006 standards, encompassing four stages: goal and scope, life cycle inventory analysis (LCI), life cycle impact assessment (LCIA), and life cycle interpretation. The goal phase involves articulating the study's purpose, identifying application areas, and specifying the audience. The scope clarifies the chosen product system, defines the functional unit, and outlines system boundaries. The LCI stage quantifies inputs and outputs, while LCIA assesses negative consequences. The interpretation stage analyses outcomes, identifies contributors, and provides recommendations.

A detailed LCA is conducted for various concrete mixes, including foamed concrete with short fibre (FCS), fine-grained concrete (C), foamed concrete with fly ash (FCFA), and conventional concrete (CC). Embodied carbon and energy factors are analysed, revealing environmental impacts. The findings indicate that the FCS mix exhibits the highest embodied CO<sub>2</sub>, primarily attributed to its elevated cement content. Furthermore, the LCA comparison extends to one-way slabs, comparing textile-reinforced foamed concrete (TRFCS) with conventional reinforced concrete (CRC).

Embodied carbon and energy factors highlight the environmental impact, with TRFCS showing higher embodied CO<sub>2</sub> due to elevated cement content. This underscores the imperative for sustainable alternatives to partially substitute cement.

Finally, cost assessments for concrete mixes and slabs reveal that FCS and FCFA mixes are more economical than C mix. TRFCS and CRC slabs exhibit comparable costs, emphasizing the importance of considering both environmental impact and costs in decision-making.

## 6.2. What is LCA?

Life cycle assessment (LCA) is a comprehensive evaluation process that analyses the environmental impact of a product throughout its entire life cycle. This assessment considers the environmental effects associated with both the production and use of the product, providing a holistic perspective on its overall sustainability. By studying the life cycle of a product, LCA allows for the identification and assessment of environmental impacts at various stages, presenting opportunities to address and mitigate these impacts. Ultimately, life cycle assessment serves as a valuable tool in promoting environmentally conscious decision-making and sustainable product development (Robin et al., 1996).

## 6.3. The Purpose and Significance of Implementing LCA

The purpose of conducting a life cycle assessment (LCA) is to collect data to improve the environmental performance of a product. By comparing environmental impacts across various scenarios or different products, the LCA serves as a tool to identify the effect of a product on the environment. This information empowers designers, developers, and managers to make informed decisions for product improvement. Consequently, the LCA contributes to more sustainable and eco-friendly alternative products or within product development and management (ISO 14040:2006).

#### 6.4. Implementing LCA: Methodology and Process

The life cycle assessment (LCA) methodology employed in this research is in accordance with ISO 14040:2006 and ISO 14044:2006 standards. The Life Cycle Assessment (LCA) consists of four stages, as illustrated in Figure 6.1:

- Goal and scope stage,
- Life cycle inventory analysis stage (LCI),
- Life cycle impact assessment stage (LCIA),
- Life cycle interpretation stage.

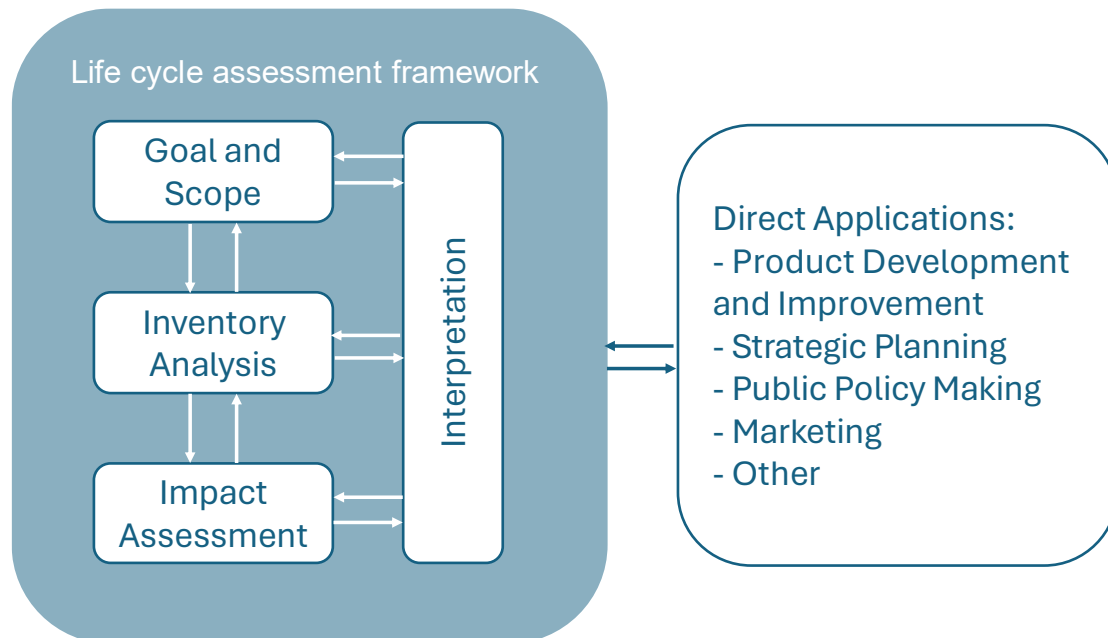


Figure 6.1: Stages of LCA implementation (ISO 14040: 2006)

##### 6.4.1. Goal and Scope

In the goal phase, the primary aim is to clearly express the purpose of the life cycle assessment (LCA) study, providing a detailed response to the essential question of why the study is being conducted. Additionally, this phase involves explicitly defining the application areas of the life cycle assessment. Finally, it entails identifying the potential audience, which encompasses a diverse group including product designers, developers, managers, stakeholders, policymakers, and consumers.

In explaining the scope of the life cycle assessment (LCA) study, describe the chosen product system. Clarify the functional unit that will be used in the LCA. Finally, define the system boundaries of the life cycle stages, and specify whether it encompasses a full LCA, such as cradle-to-grave, or focuses on a specific stage, like cradle-to-gate, as adopted in this research. This chosen scope includes processes, production, manufacturing, and fabrication to be ready to use. The cradle-to-gate approach was selected primarily due to the absence of reliable sources detailing the entire life cycle of textile reinforced foamed concrete, encompassing, use, end-of-life, and recycling stages. For instance, while databases like ICE cover conventional reinforced concrete elements comprehensively cradle-to-grave, they lack sufficient data on the unique properties and life cycle of textile reinforced foamed concrete.

#### 6.4.2. Life Cycle Inventory Analysis Phase (LCI)

Life cycle inventory analysis (LCI) includes the collection and calculation of data to systematically quantify the inputs and outputs of materials and energy linked to a product or system under study.

#### 6.4.3. Life Cycle Impact Assessment Phase (LCIA)

The life cycle impact assessment (LCIA) entails the examination of the negative consequences resulting from a system's inputs and outputs on human health, plant and animal life, and the potential availability of natural resources (Carević et al., 2023). The assessment of LCIA impact involves the transformation of data from the Life Cycle Inventory (LCI) into indicators that measure the environmental impact. Carbon dioxide (CO<sub>2</sub>), methane (CH<sub>4</sub>), and nitrous oxide (N<sub>2</sub>O) are the primary contributors to global warming among greenhouse gases. For this assessment, CO<sub>2</sub> was selected as the indicator for global warming potential due to its higher concentration when compared to CH<sub>4</sub> and N<sub>2</sub>O (DECC, 2015).



#### 6.4.4. Life Cycle Interpretation

The outcomes of both life cycle inventory analysis and life cycle impact assessments are analysed in this stage. Furthermore, significant contributors to the environmental impact of the product system are pinpointed. Conclusions are then derived from these analyses, accompanied by recommendations about the environmental aspects of the product. These recommendations may address potential areas for enhancement or essential environmental information that could be communicated to consumers, contingent on the specific goals of the LCA study. Life cycle interpretation comprises three vital components: the identification of key issues, an evaluation of these issues, and the formulation of conclusions coupled with recommendations.

#### 6.5. Comparative Life Cycle Assessment (LCA) Analysis for Different Concrete Mixes

##### 6.5.1. Goal and Scope, System Boundary and Functional

Within this section, a life cycle assessment (LCA) is undertaken to quantitatively evaluate the environmental effects of the concrete components utilized in this research, compared against conventional counterparts that have the same strength. The analytical boundary encompasses the Cradle-to-Gate phase of the product life cycle, observing the environmental consequences spanning from raw material extraction to the culmination of concrete manufacturing.

The objective of this assessment is to advance the proposition for the integration of foamed concrete within the construction field, thereby attenuating greenhouse gas emissions. Foamed concrete, distinguished by its lightweight properties and exceptional thermal and sound isolation capabilities, is suggested as an ecologically sound alternative. The chosen functional unit is derived from the quantity of materials required by kilogramme and Litre to produce one cubic meter of concrete mix. The concrete mixtures are listed in Table 6.1.

*Table 6.1: Main components of concrete mixes with same compressive strength*

Mix Name	Main Components	Reference
FCS Mix	Foamed concrete with short fibre	Developed mix in this research
C Mix	Fine-grained concrete	(Alma'aitah & Ghiassi, 2022)
FCFA Mix	Foamed concrete with fly ash	(Hashemmoniri & Fatemi, 2023b)
CC Mix	Conventional concrete	(McCormac & Brown, 2014)

### 6.5.2. Life Cycle Inventory Analysis (LCI)

The life cycle inventory (LCI) analysis encompasses data collection and calculation procedures to quantify the inputs required for producing one cubic metre of concrete mix throughout the Cradle-to-Gate phase. Table 6.2 provides a comprehensive breakdown of input quantities for the raw materials involved in producing 1 m<sup>3</sup> of concrete.

*Table 6.2: Materials required to produce one cubic meter of concrete mix.*

Materials	Unit	FCS Mix	C Mix	FCFA Mix	CC Mix
Cement	kg	620.4	273	342	350
Fly Ash	kg	-	546	200	-
Limestone	kg	-	46	-	-
Sand	kg	931	910	900	700
Coarse Aggregate	kg	-	-	-	1400
Water	L	249	273	250	179
Foam	kg	0.3	-	0.34	-
Short Fibre Glass	kg	15	-	-	-
Superplasticiser	L	-	8.19	-	-

### 6.5.3. Life Cycle Impact Assessment (LCIA)

The life cycle impact assessment (LCIA) involves assessing the adverse outcomes arising from the inputs and outputs of a system on human health, plant life, animal life, and the prospective accessibility of natural resources (Carević et al., 2023). The evaluation of LCIA impact involves converting data from the Life Cycle Inventory (LCI) into indicators that gauge the environmental impact (ISO 14040, 2006). The system boundaries for life cycle impact assessment (LCIA) regarding the materials extend from cradle to gate.

The embodied carbon factors, measured in kgCO<sub>2</sub>/kg units, for the materials utilized in concrete mixes, are provided in Table 6.3. It is noteworthy that cement exhibits the highest impact factor, with a value of 0.912 kgCO<sub>2</sub>/kg.

*Table 6.3: Embodied carbon factors for the materials utilized in concrete mixes.*

Materials	Embodied Carbon Factor kgCO <sub>2</sub> /kg	Reference
Cement	0.912	ICE*
Fly Ash	0.004	ICE*
Limestone	0.02	ICE*
Aggregate	0.007	ICE*
Water	0.0004	ICE*
Foam	0.53	(Jhatial et al., 2022)
Short Fibre Glass	0.16	(D. Zhang et al., 2020)
Superplasticiser	1.88	ICE*

ICE\*: The institution of Structural engineering (The structural carbon tool)

The LCIA analysis incorporates the impact of embodied energy, defined as the total non-renewable energy consumed in the production of materials derived from raw resources. Expressed in megajoules (MJ) per unit weight (kg or tonne), area (m<sup>2</sup>), or volume (m<sup>3</sup>) (Cabeza et al., 2013). In this study, the energy consumption impact of the materials within concrete is addressed by aggregating the energy consumption of individual components in the concrete mixes. The embodied energy consumption factors are detailed in Table 6.4.

*Table 6.4: Embodied energy consumption factor*

Materials	Embodied Energy Factor (MJ/kg)	Reference
Cement	4.9	(Thevarajah et al., 2020)
Fly Ash	0	Waste
Limestone	3.04	(Zhu et al., 2021)
Aggregate	0.08	(Thevarajah et al., 2020)
Water	1.2	(Yu & Leung, 2017)
Foam	14.2	(Thevarajah et al., 2020)
Short Fibre Glass	13	(D. Zhang et al., 2020)
Superplasticiser	35	(Yu & Leung, 2017)

#### 6.5.4. Interpretation of Results

The analysis of the life cycle assessment (LCA) for producing 1m<sup>3</sup> of concrete mix, considering four different mixes FCS mix, C mix, FCFA mix, and CC mix will be conducted in this section. The environmental impact evaluation extends from cradle to gate. The findings of the analysis are presented in two sections: the estimated embodied CO<sub>2</sub>, measured in kgCO<sub>2</sub> per 1m<sup>3</sup>, and the energy consumption, expressed in MJ per 1m<sup>3</sup>.

The cumulative embodied carbon for the four concrete mixes is depicted in Figure 6.2. The chart unmistakably illustrates that the foamed concrete with short fibre (FCS) mix exhibits the highest estimated embodied CO<sub>2</sub> among the mixes, registering at 575.2 kgCO<sub>2</sub>/m<sup>3</sup>. This is attributed to its elevated cement content, which carries the highest impact factor on the environment (0.912 KgCO<sub>2</sub>/Kg).

In the case of foamed concrete with fly ash (FCFA), where fly ash constitutes approximately 40% of the cementitious material weight in the mix, the embodied CO<sub>2</sub> decreases notably to 319.8 kgCO<sub>2</sub>/m<sup>3</sup>. Additionally, the fine-grained concrete (C) mix displays the least adverse environmental impact, primarily due to its lower cement content and a higher proportion of fly ash. An illustrative CO<sub>2</sub> calculation for the FCF mix is provided below.

- Cement CO<sub>2</sub> embodied =  $0.912 \frac{\text{kgCO}_2}{\text{kg}} \times 620.4 \frac{\text{kg}}{\text{m}^3} = 565.8 \frac{\text{kgCO}_2}{\text{m}^3}$
- Sand CO<sub>2</sub> embodied =  $0.007 \frac{\text{kgCO}_2}{\text{kg}} \times 931 \frac{\text{kg}}{\text{m}^3} = 6.5 \frac{\text{kgCO}_2}{\text{m}^3}$
- Water CO<sub>2</sub> embodied =  $0.0008 \frac{\text{kgCO}_2}{\text{kg}} \times 248 \frac{\text{kg}}{\text{m}^3} = 0.2 \frac{\text{kgCO}_2}{\text{m}^3}$
- Foam CO<sub>2</sub> embodied =  $0.53 \frac{\text{kgCO}_2}{\text{kg}} \times 0.28 \frac{\text{kg}}{\text{m}^3} = 0.2 \frac{\text{kgCO}_2}{\text{m}^3}$
- Short fibre glass CO<sub>2</sub> embodied =  $0.16 \frac{\text{kgCO}_2}{\text{kg}} \times 15.5 \frac{\text{kg}}{\text{m}^3} = 2.5 \frac{\text{kgCO}_2}{\text{m}^3}$

The total FCS CO<sub>2</sub> embodied =  $575.2 \frac{\text{kgCO}_2}{\text{m}^3}$

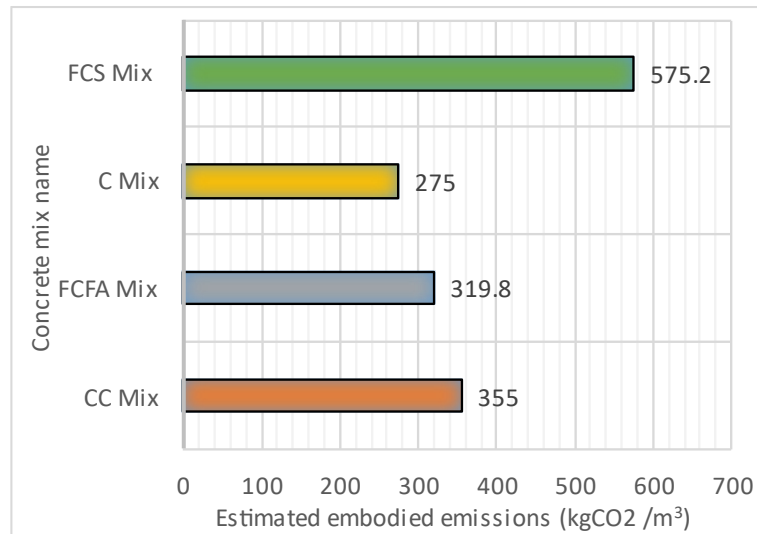


Figure 6.2: Embodied carbon for 1 m<sup>3</sup> concrete mixes

The results of the embodied energy analysis for four concrete mixes are illustrated in Figure 6.3. The FCS mix exhibits the highest embodied energy value, measuring 3616 MJ/m<sup>3</sup>. This elevated value is attributed to its higher cement content compared to the other three concrete mixes C mix, FCFA mix, and CC mix. This highlights the positive impact of substituting cement with more environmentally friendly materials, such as fly ash. An illustrative embodied energy calculation for the FCF mix is provided below.

- Cement embodied energy =  $4.9 \frac{\text{MJ}}{\text{kg}} \times 620.4 \frac{\text{kg}}{\text{m}^3} = 3039.9 \frac{\text{MJ}}{\text{m}^3}$
- Sand embodied energy =  $0.08 \frac{\text{MJ}}{\text{kg}} \times 931 \frac{\text{kg}}{\text{m}^3} = 74.5 \frac{\text{MJ}}{\text{m}^3}$
- Water embodied energy =  $1.2 \frac{\text{MJ}}{\text{kg}} \times 248 \frac{\text{kg}}{\text{m}^3} = 297 \frac{\text{MJ}}{\text{m}^3}$
- Foam embodied energy =  $14.2 \frac{\text{MJ}}{\text{kg}} \times 0.28 \frac{\text{kg}}{\text{m}^3} = 3.9 \frac{\text{MJ}}{\text{m}^3}$
- Short fibre glass embodied energy =  $13 \frac{\text{MJ}}{\text{kg}} \times 15.5 \frac{\text{kg}}{\text{m}^3} = 201 \frac{\text{MJ}}{\text{m}^3}$

The total FCS embodied energy =  $3616 \frac{\text{MJ}}{\text{m}^3}$

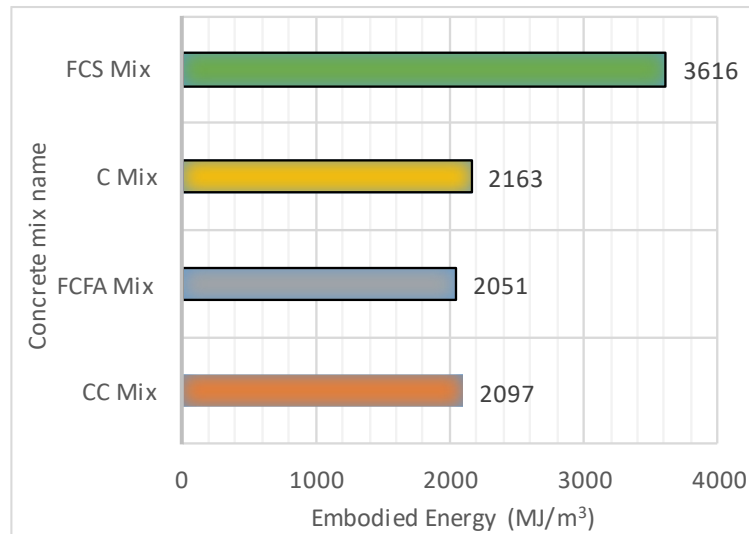


Figure 6.3: Embodied energy for 1 m<sup>3</sup> concrete mixes

In summary, when analysing the estimated embodied CO<sub>2</sub> and embodied energy per 1m<sup>3</sup> of concrete mix, the foamed concrete with a short fibre mix displays a less favourable performance compared to conventional concrete mixes. It is noteworthy, however, that the lightweight nature of foamed concrete contributes to a reduction in the dead load within buildings. This, in turn, leads to the expectation of smaller structural elements, thereby improving both the embodied CO<sub>2</sub> and embodied energy. Another noteworthy consideration is the use of textiles as reinforcement with foamed concrete as opposed to steel reinforcement with conventional concrete, which necessitates less concrete cover. As a reasonable extension, the next section will present a life cycle assessment (LCA) comparison between a one-way conventionally reinforced solid slab (CRC) and a one-way textile reinforced foamed concrete with a short fibre (TRFCS) slab, aiming to establish a more realistic model.

#### 6.6. Comparative Life Cycle Assessment (LCA) of One-Way (CRC) Slab and One-Way TRFCS Slab

A life cycle analysis (LCA) will be conducted to compare a one-way conventionally reinforced solid (CRC) slab with a one-way AR glass fibre textile reinforced foamed concrete (TRFCS) slab. The analysis will encompass the Cradle to Gate phase. The assumptions guiding this comparison include:

- The TRFCS slab is a theoretical design based on the specifications outlined in Chapter Four.
- The conventionally reinforced solid (CRC) slab is sourced from existing literature.
- Both slabs share the same area, but their depths differ as per their respective designs.
- Both slabs are designed to carry the same ultimate bending moment ( $M_u$ ), set at 24 kN.m in this scenario.

In the comparison, a design example of a simply supported one-way reinforced solid slab for interior building use is quoted from the design textbook (McCormac & Brown, 2014). The design entails a slab with dimensions of 3 m in width, 9 m in length, and 0.16 m in depth. The main reinforcement comprises 12  $\phi$  bars at 250 mm spacing, transverse reinforcement includes 10  $\phi$  bars at 250 mm spacing, and the ultimate bending moment ( $M_u$ ) is specified as 24 kN.m.

Using the Excel analysis tool, Solver, and based on Section 4.7 in Chapter Four, the ultimate bending moment ( $M_u$ ) for the one-way TRFCS-Com slab is theoretically designed, also set at 24 kN.m. The TRFCS slab's dimensions include a width of 3 m, a length of 9 m, and a depth of 0.15 m. The reinforcement consists of three layers of AR fibre textile with a mesh spacing of 25 mm  $\times$  25 mm.

#### 6.6.1. Goal and Scope, System Boundary and Functional Units

This life cycle assessment (LCA) study aims to evaluate and compare the environmental impact of one-way AR fibre textile-reinforced foamed concrete slab (TRFCS) with that of one-way conventional concrete solid slab (CRC). The study will specifically focus on the environmental contributions of the Cradle-to-Gate phase of the product life cycle, extending from the extraction of raw materials to the completion of concrete slabs production. The study's primary target audience encompasses researchers, architects, and engineers involved in construction projects, equipping them with insights into the ecological footprint of different concrete types.

The volume of concrete slabs was quantified using cubic meters (m<sup>3</sup>) as the functional unit.

### 6.6.2. Life Cycle Inventory Analysis (LCI)

The life cycle inventory (LCI) analysis involves collecting data and employing calculation procedures to quantify the inputs and outputs associated with the construction of both the one-way slab with textile-reinforced foamed concrete (TRFCS) and the one-way slab with conventional reinforced concrete (CRC). This analysis spans the Cradle-to-Gate phase. Table 6.5 offers a detailed breakdown of input quantities for the raw materials necessary in producing 4.05 m<sup>3</sup> of the TRFCS slab while Table 6.6 provides a comprehensive breakdown for 4.32 m<sup>3</sup> of the CRC slab.

*Table 6.5: Materials required to produce 4.05 m<sup>3</sup> of the TRFCS slab.*

Materials	Unit	TRFCS slab
Cement	kg	2511
Sand	kg	3770.7
Water	L	1006.5
Foam	kg	1.1
Short Fibre Glass	kg	63.9
AR Fibre Glass Textile	kg	20.3

*Table 6.6: Materials required to produce 4.32 m<sup>3</sup> of the CRC slab.*

Materials	Unit	CRC Slab
Cement	kg	1512
Sand	kg	3024
Coarse Aggregate	kg	6048
Water	L	773.3
Steel Reinforcement	kg	162.4

### 6.6.3. Life Cycle Impact Assessment (LCIA)

The definition of life cycle impact assessment (LCIA) is provided in Section 6.3.3. The system boundaries for LCIA, concerning materials, encompasses from cradle to gate. The factors under consideration are the embodied carbon factor (measured in kgCO<sub>2</sub>/m<sup>3</sup>) and the embodied energy factor (measured in MJ/m<sup>3</sup>) for both the TRFCS



slab and the CRC slab. Details of the embodied carbon and energy factors can be found in Table 6.7.

*Table 6.7: Embodied carbon and energy factors for the concrete slabs*

Slab Name	Embodied Energy Factor (KgCO <sub>2</sub> /m <sup>3</sup> )	Energy Intensity (MJ/m <sup>3</sup> )
TRFCS	615	3838
CRC	436	3676

#### 6.6.4. Interpretation of Results

This section is dedicated to the examination of outcomes from the life cycle assessment (LCA) to produce a 4.05 m<sup>3</sup> TRFCS slab and a 4.32 m<sup>3</sup> CRC slab. The results of this analysis are categorized into two main sections: estimated embodied CO<sub>2</sub> and energy consumption. Embodied CO<sub>2</sub> is quantified in kilograms (kgCO<sub>2</sub>), presenting insights into the carbon footprint associated with production. Simultaneously, energy consumption is expressed in megajoules (MJ), providing a comprehensive measure of the energy intensity involved in the manufacturing process.

Figure 6.4 illustrates the embodied carbon for both the TRFCS slab and the CRC slab. Notably, the TRFCS slab demonstrates a higher embodied CO<sub>2</sub>, registering at 2489.7 kgCO<sub>2</sub>, compared to the CRC slab, which shows a lower value of 1883.5 kgCO<sub>2</sub>. The primary contributor to this disparity is the elevated cement content in the TRFCS slab, totalling 2511 kg, in contrast to the CRC slab's more modest 1512 kg.

The noticeable contrast in embodied CO<sub>2</sub> between the TRFCS and CRC slabs is a direct outcome of the differing compositions, specifically the substantial variance in cement quantity.

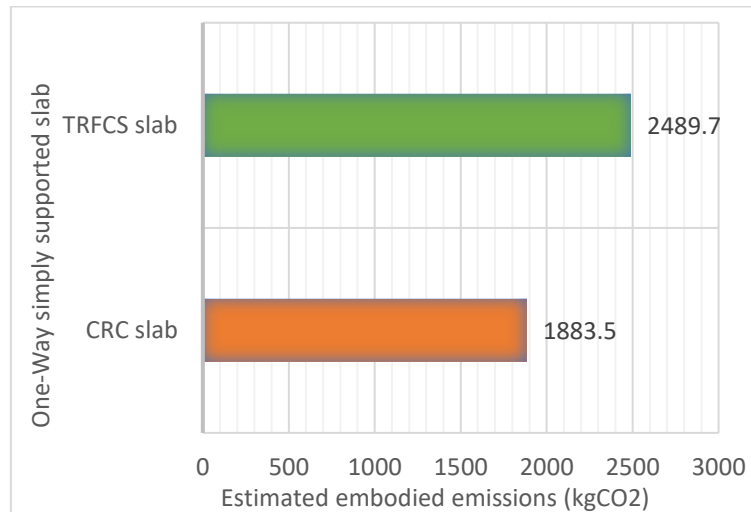


Figure 6.4: Embodied carbon for the TRFCS slab and the CRC slab

The outcomes of the embodied energy analysis for both the TRFCS slab and the CRC slab are visually represented in Figure 6.5. Despite the TRFCS slab exhibiting a higher cement content compared to the CRC slab, an interesting balance emerges when considering the higher embodied energy of the steel reinforcement in the CRC slab, resulting in an overall similarity in the embodied energy analysis for both slabs.

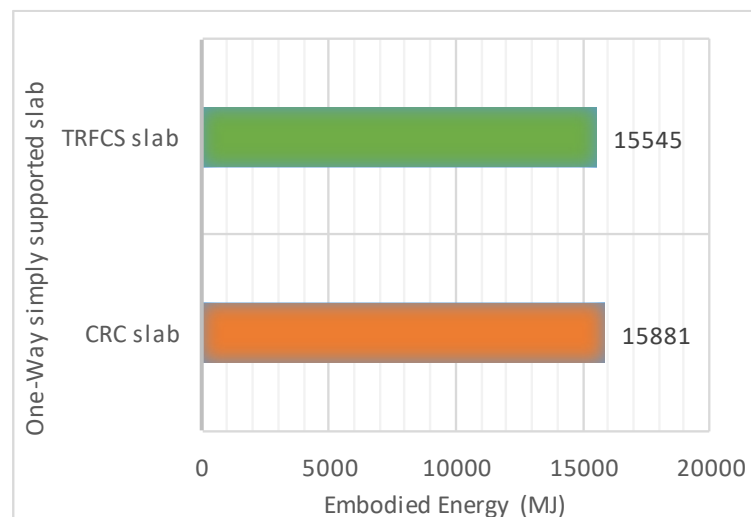


Figure 6.5: Embodied energy for the TRFCS slab and the CRC slab

In summary, the pronounced adverse effects of cement usage emphasize the potential positive impact of adopting more sustainable practices, such as substituting cement with environmentally friendly alternatives like fly ash. By reducing dependence on materials with high environmental impact, there exists an opportunity to mitigate the overall carbon footprint associated with TRFCS slab production. This strategy towards

greener alternatives aligns with broader sustainability goals and fosters environmentally conscious decision-making within the construction industry.

### 6.7. Cost Assessment

The total cost evaluation of concrete mixes, encompassing FCS mix, C mix, FCFA mix, and CC mix, is presented in Figure 6.6. Additionally, Figure 6.7 displays the cost of 4.05 m<sup>3</sup> TRFCS slab and 4.32 m<sup>3</sup> CRC slab. The boundary system extends from the cradle to the gate phase, allowing for a comprehensive assessment and comparison of various options by considering upfront expenditures. The FCS mix and FCFA mix, priced at £323 and £244 per 1 m<sup>3</sup>, respectively, prove to be more economical than the C mix, which costs £382 per 1 m<sup>3</sup>. This cost advantage is because of the presence of cost-effective foam materials. This results in the production of potentially cost-efficient concrete mixes. Similarly, the TRFCS slab and CRC slab exhibit comparable costs.

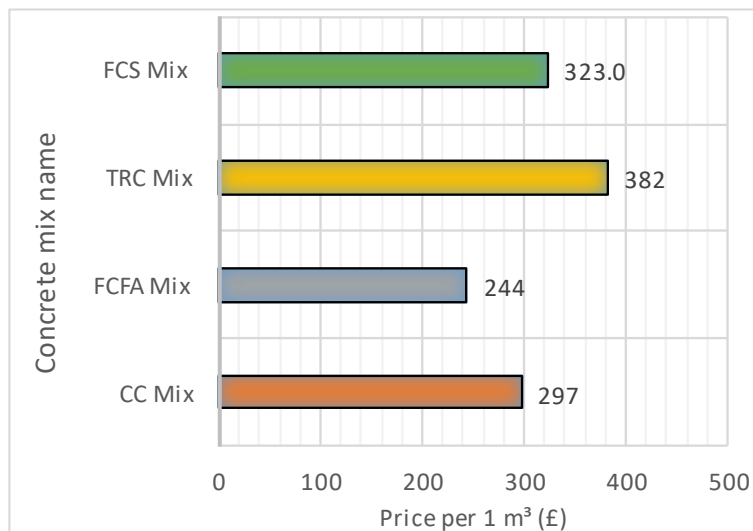


Figure 6.6: Cost of 1 m<sup>3</sup> concrete mixes, FCS mix, C mix, FCFA mix, and CC mix.

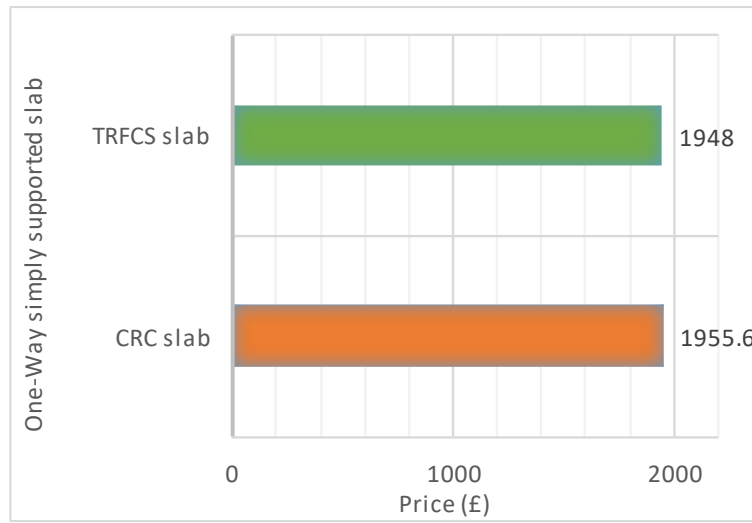


Figure 6.7: Cost of  $4.05 \text{ m}^3$  TRFCS slab and  $4.32 \text{ m}^3$  CRC slab

### 6.8. Summary

- The study follows ISO 14040:2006 and ISO 14044:2006 standards, involving four stages: goal and scope, life cycle inventory analysis (LCI), life cycle impact assessment (LCIA), and life cycle interpretation.
- A comprehensive LCA has been conducted for diverse concrete mixes, including FCS mix, C mix, FCFA mix, and CC mix, analysing embodied carbon and energy factors to unveil environmental impacts.
- Findings reveal that the FCS mix stands out with the highest embodied CO<sub>2</sub>, primarily due to its elevated cement content.
- The LCA comparison has been expanded to one-way slabs, textile-reinforced foamed concrete (TRFCS) against conventional concrete (CRC), highlighting embodied carbon and embodied energy.
- Results show that TRFCS exhibits higher embodied CO<sub>2</sub>, emphasizing the need for sustainable alternatives to partially replace cement.
- Cost assessments indicate that FCS and FCFA mixes are more economical than C mix.
- TRFCS and CRC slabs show comparable costs, highlighting the significance of weighing both environmental impact and costs in decision-making.
- Due to the lack of reliable sources comprehensively detailing the entire life cycle of textile reinforced foamed concrete, there is a pressing need for further research and data collection to better understand its environmental impacts and the sustainability implications throughout its entire life cycle.

## Chapter 7 Conclusion and Recommendations

### 7.1. Conclusions

- This study provides a comprehensive guide to optimizing foamed concrete mixes, covering materials, mix design, and testing. FC-5, with a targeted density of  $1800 \text{ kg/m}^3$  and a water-to-cement ratio of 0.4, demonstrates competitive strength-to-density ratios. Testing highlights the balance between workability, compressive strength (28.1 MPa), and density ( $1782 \text{ kg/m}^3$ ). FC-5 also displays a modulus of elasticity of 10.464 GPa and an ultimate strain of 0.00394, with a flexural strength of 1.93 MPa. However, toner inclusion increases FC compressive strength while also increasing density by approximately 20% compared to controls, leading to a negative impact on the lightweight properties of FC.
- Drawing from experimental data of the foamed concrete mix (FC-5) and Eurocode 2 guidelines, a design calculation guideline is formulated for textile reinforced foamed concrete (TRFC). Theoretical calculations anticipate potential failures of impregnated AR glass textile reinforced foamed concrete (TRFC), addressing low ( $Ten_1$ ) and high ( $Ten_2$ ) reinforcement scenarios for tension and compression (Com) failure cases. The TRFC beams were standardized with dimensions of 55 mm (height), 100 mm (width), and 500 mm (length).
- Three-point bending tests were carried out to assess the flexural behaviour of four simply supported beam samples, including textile-reinforced foamed concrete (TRFC), textile-reinforced foamed concrete with short fibre (TRFCS), textile-reinforced concrete (TRC), and textile-reinforced concrete with short fibre (TRCS), under three failure cases  $Ten_1$ ,  $Ten_2$ , and Com. Digital Image Correlation (DIC) is employed to measure displacements and track crack propagation.
- The experimental and theoretical results show significant agreement, specifically, the variation for TRFC- $Ten_1$ , TRFC- $Ten_2$ , and TRFC-Com is calculated as 7.14%, 12.78%, and 6.25%, respectively.

## Conclusions and Recommendations

- Short fibres enhance the elastic limit of the TRFCS samples require 40% more load to initiate cracking compared to TRFC samples, exhibiting its higher resilience and ductility.
- Compression failure sample cases (Com) exhibit more cracks and narrower crack widths at the point of failure which exhibit a maximum crack width of 1.2 mm, compared to sample under tension failure (Ten<sub>1</sub> and Ten<sub>2</sub>) demonstrate fewer cracks and wider crack widths (ranging from 2.5 mm to 3 mm).
- The TRFCS-Com sample exhibits the highest non-linear response among all samples, indicating its exceptional ductility. It demonstrates an energy absorption capacity of 165 kN·mm, which significantly surpasses the second highest energy absorption value of 84 kN·mm observed in the TRCS-Com sample.
- In the LCA comparison of one-way slabs, textile-reinforced foamed concrete (TRFCS) is evaluated against conventional reinforced concrete (CRC), both having identical dimensions of 3 m in width, 9 m in length, and 0.16 m in depth. Additionally, both CRC and TRFCS slabs have the same ultimate bending moment ( $M_u$ ), specified as 24 kN.m.
- The TRFCS slab exhibits a higher embodied CO<sub>2</sub> of 2490 kgCO<sub>2</sub> compared to the CRC slab's 1884 kgCO<sub>2</sub>, primarily due to its increased cement content. However, substituting a portion of the cement with 40% fly ash in the concrete mix has led to a significant reduction in embodied CO<sub>2</sub>, to approximately half of its original value.
- Both TRFCS and CRC slabs display similar results in the embodied energy analysis, with each having an embodied energy of 15700 MJ.
- TRCS and TRFCS specimens underwent textile rupture during pull-out testing. This may be due to the high embedded length of the textile, which is 400 mm. Consequently, the pull-out test assumed characteristics like a tensile test, posing challenges in monitoring the slight displacement of the textile within the concrete using LVDTs.

## Conclusions and Recommendations

### 7.2. Recommendations

- Further research is needed to establish foamed concrete code designs and develop standardized methods for foam concrete design.
- Microstructure studies are essential for a deeper understanding of the effects of different short fibres, silica, and toner on the fresh and hardened properties of foamed concrete, including bubble stability, density, compressive strength, and thermal and acoustic properties.
- The effects of various mixing, transporting, and pumping methods on the stability of the foam in foamed concrete mixes should be thoroughly investigated. These methods play a crucial role in ensuring the production of large quantities of foamed concrete that meet design standards. Understanding the impact of each method on foam stability is essential for optimizing the quality and consistency of the final product.
- Investigation into the bond behaviour of different textile reinforcements and foamed concrete with varying densities is recommended.
- Further comprehension of structural element performance across various failure scenarios of reinforced textile foamed concrete requires further investigation.
- Given the superior structural performance exhibited by the textile reinforced foamed concrete with textile under compression failure (TRFCS-Com) among the tested samples, coupled with its outstanding thermal and sound insulation capabilities, it is recommended to undertake a large-scale experiment utilizing TRFCS-Com slabs. This initiative aims to explore its potential application in reinforced concrete slabs, thereby further validating its feasibility and efficacy in practical construction scenarios.
- Due to the limited understanding of the extended performance of textile reinforced foamed concrete, it is recommended to delve deeper into its long-term behaviour, specifically focusing on deflection caused by creep and shrinkage. This is crucial for ensuring its reliability and competitiveness as an alternative to conventional reinforced concrete elements.



## Conclusions and Recommendations

- The recommendation for the pull-out test suggests utilizing a tool such as digital image correlation (DIC) to capture micro movements. This method allows for a thorough assessment of the test results and facilitates accurate investigation. Additionally, conducting the pull-out test with a reduced embedded length (less than 400 mm) is advised to mitigate these complexities in future experiments.

### 7.3. Limitation

- During the experiments, Digital Image Correlation (DIC) encountered technical issues leading to the loss of some samples, necessitating their reproduction and the use of video gauges instead. Additionally, the COVID-19 pandemic disrupted lab access, imposing limitations on the experiment's duration.

## References

- ACI 213R-03 Committee. (2003). Guide for structural lightweight aggregate concrete: report of ACI committee 213. *International Journal of Cement Composites and Lightweight Concrete*.
- ACI 523.2R-96 Committee. (1997). Guide for Precast Cellular Concrete Floor, Roof, and Wall Units. *Concrete*, 2–6.
- ACI 523.3R-14 Committee. (2014). Guide for Cellular Concretes above 50 lb/ft<sup>3</sup> (800 kg/m<sup>3</sup>). *Technical Documents*, 3, 17.
- Alkurdi\*, N. M., Mohammad, F. A., & Klalib, H. A. (2021). Mechanical properties and direct tensile strength of waste toner foamed concrete. *Journal of Advanced Civil Engineering Practice and Research 2550-1933 © Ababil Publishers*, 11:10-20,(February).
- Alma'aitah, M., & Ghiassi, B. (2022). Development of cost-effective low carbon hybrid textile reinforced concrete for structural or repair applications. *Construction and Building Materials*, 341(April), 127858. <https://doi.org/10.1016/j.conbuildmat.2022.127858>
- Alma'aitah, M., Ghiassi, B., & Dalalbashi, A. (2021). Durability of Textile Reinforced Concrete: Existing Knowledge and Current Gaps. *Applied Sciences 2021*, Vol. 11, Page 2771, 11(6), 2771. <https://doi.org/10.3390/APP11062771>
- Alrshoudi, F. (2021). *Textile-Reinforced Concrete Versus Steel-Reinforced Concrete*.
- Amran, M. (2020). Influence of structural parameters on the properties of fibred-foamed concrete. *Innovative Infrastructure Solutions*, 5(1), 16. <https://doi.org/10.1007/s41062-020-0262-8>
- Amran, M., Alyousef, R., Alabduljabbar, H., Khudhair, M. H. R., Hejazi, F., Alaskar, A., Alrshoudi, F., & Siddika, A. (2020). Performance properties of structural fibred-foamed concrete. *Results in Engineering*, 5(August 2019), 100092. <https://doi.org/10.1016/j.rineng.2019.100092>

- Amran, M., Lee, Y., Vatin, N., Ngian, S., Yee, Y., & Murali, G. (2020). Design efficiency, characteristics, and utilization of reinforced foamed concrete: A review. *Crystals*, *10*(10), 1–35. <https://doi.org/10.3390/cryst10100948>
- Amran, Y. H. M., Farzadnia, N., & Ali, A. A. A. (2015). Properties and applications of foamed concrete; A review. *Construction and Building Materials*, *101*, 990–1005. <https://doi.org/10.1016/j.conbuildmat.2015.10.112>
- ASTM C330. (2009). Standard Specification for Lightweight Aggregates for Structural Concrete. *ASTM International*, *552*(18), 4. <https://doi.org/10.1520/C0330>
- ASTM D790. (2010). *Standard Test Methods for Flexural Properties of Unreinforced and Reinforced Plastics and Electrical Insulating Materials (Standard No. ASTM D790)* ASTM International. <https://doi.org/10.1520/D0790-10>.
- Bamonte, P., Caverzan, A., Kalaba, N., & Lamperti Tornaghi, M. (2017). Lightweight concrete containing phase change materials (PCMs): A numerical investigation on the thermal behaviour of cladding panels. *Buildings*, *7*(2), 35. <https://doi.org/10.3390/buildings7020035>
- Banholzer, B., Brockmann, T., & Brameshuber, W. (2006). Material and bonding characteristics for dimensioning and modelling of textile reinforced concrete (TRC) elements. *Materials and Structures/Materiaux et Constructions*, *39*(8), 749–763. <https://doi.org/10.1617/S11527-006-9140-X/METRICS>
- Barhum, R., & Mechtcherine, V. (2013). Influence of short dispersed and short integral glass fibres on the mechanical behaviour of textile-reinforced concrete. *Materials and Structures/Materiaux et Constructions*, *46*(4), 557–572. <https://doi.org/10.1617/s11527-012-9913-3>
- Batool, F., & Bindiganavile, V. (2017). Air-void size distribution of cement based foam and its effect on thermal conductivity. *Construction and Building Materials*, *149*, 17–28. <https://doi.org/10.1016/j.conbuildmat.2017.05.114>

- Bensadoun, F., Verpoest, I., Baets, J., Müssig, J., Graupner, N., Davies, P., Gomina, M., Kervoelen, A., & Baley, C. (2017). Impregnated fibre bundle test for natural fibres used in composites. *Journal of Reinforced Plastics and Composites*, 36(13), 942–957. <https://doi.org/10.1177/0731684417695461>
- Bing, C., Zhen, W., & Ning, L. (2012). Experimental Research on Properties of High-Strength Foamed Concrete. *Journal of Materials in Civil Engineering*, 24(1), 113–118. [https://doi.org/10.1061/\(ASCE\)MT.1943-5533.0000353](https://doi.org/10.1061/(ASCE)MT.1943-5533.0000353)
- Brady, Watts, G. R. A., & Jones, R. (2001). Specification for Foamed Concrete. *TRL Limited*, 78.
- Brameshuber, W., Brockmann, T., Curbach, M., Meyer, C., Vilkner, G., Mobasher, B., Peled, A., Krüger, M., Reinhardt, H. W., & Wastiels, J. (2006). *Textile Reinforced Concrete - State-of-the-Art Report of RILEM TC 201-TRC*. RILEM Publications SARL.
- BS EN-12390-13:2013. (2019). Testing hardened concrete Part 13: Determination of secant modulus of elasticity in compression. *BSI Standards Publication*, 31 July 2019.
- BS EN-12390-3:2019. (2019). Testing hardened concrete. *BRITISH STANDARD*, 38(10).
- BS EN 12350-1:2000. (2000). *Testing fresh concrete Part 1: Sampling* BSI Standards Publication, 2000.
- BS EN 12350-5:2019. (2019). Testing hardened concrete - Part 5: Flexural strength of test specimens. *BSI Standards Publication*, 31 July 2019.
- BS EN 12350-6 (2019). *Testing fresh concrete Part 6 Density*. BSI Standards Publication, 6 June 2019.
- BS EN 12390-7 (2009) *Testing hardened concrete Part 7: Density of hardened concrete* BSI Standards Publication, (2009).
- BS EN 12620:2002. (2004). BRITISH STANDARD: Aggregates for concrete. *BRITISH STANDARD*, 17 August 2004, 12–14.
- BS EN 197-1:2011. (2019). Cement - Part 1: Composition, specifications and conformity

- criteria for common cements. *BSI Standards Publication*, 28 February 2019.
- Cabeza, L. F., Barreneche, C., Miró, L., Morera, J. M., Bartolí, E., & Inés Fernández, A. (2013). Low carbon and low embodied energy materials in buildings: A review. *Renewable and Sustainable Energy Reviews*, 23, 536–542. <https://doi.org/10.1016/j.rser.2013.03.017>
- Carević, I., Naletilić, H., & Štirmer, N. (2023). Life cycle analysis of reinforced concrete floor slab through three different waste management scenarios. *Građevinar*, 75(08.), 765–773. <https://doi.org/10.14256/JCE.3696.2023>
- Chen, H. J., Huang, C. H., & Tang, C. W. (2010). Dynamic properties of lightweight concrete beams made by sedimentary lightweight aggregate. *Journal of Materials in Civil Engineering*, 22(6), 599–606. [https://doi.org/10.1061/\(ASCE\)MT.1943-5533.0000061](https://doi.org/10.1061/(ASCE)MT.1943-5533.0000061)
- Chica, L., & Alzate, A. (2019). Cellular concrete review: New trends for application in construction. *Construction and Building Materials*, 200, 637–647. <https://doi.org/10.1016/j.conbuildmat.2018.12.136>
- Chun, Y., Claisse, P., Naik, T. R., & Ganjian, E. (2007). Sustainable Construction Materials and Technologies. In *International Conference on Sustainable Construction Materials and Technologies, 11–13 June, 2007, Coventry, Uk*.
- Curbach, M., Jesse, J., Hegger, J., Will, N., Aldea, C., & Brameshuber, W. (2006). *STATE OF THE ART REPORT – TEXTILE REINFORCED CONCRETE / APPLICATIONS OF TEXTILE REINFORCED CONCRETE*.
- DATAtab. (2024). *DATAtab: Statistical Software*. Retrieved from <https://datatab.net/>
- DECC. (2015). *2014 UK Greenhouse Gas Emissions, Provisional Statistical release* (Issue March). [https://www.gov.uk/government/uploads/system/uploads/attachment\\_data/file/416810/2014\\_stats\\_release.pdf](https://www.gov.uk/government/uploads/system/uploads/attachment_data/file/416810/2014_stats_release.pdf)
- Dey, V., Zani, G., Colombo, M., Di Prisco, M., & Mobasher, B. (2015). *Flexural impact response of textile-reinforced aerated concrete sandwich panels*.

<https://doi.org/10.1016/j.matdes.2015.07.004>

Dhasindrakrishna, K., Ramakrishnan, S., Pasupathy, K., & Sanjayan, J. (2021). Collapse of fresh foam concrete: Mechanisms and influencing parameters. *Cement and Concrete Composites*, 122(March). <https://doi.org/10.1016/j.cemconcomp.2021.104151>

Dolatabadi, M. K., Janetzko, S., Gries, T., Sander, A., Textiltechnik, I., & Aachen, R. (2010). AN ANALYTICAL INVESTIGATION OF CEMENT PENETRATION WITHIN BUNDLE OF FIBERS. I, 69–78.

El Kadi, M., Kapsalis, P., Van Hemelrijck, D., Wastiels, J., & Tysmans, T. (2020). Influence of loading orientation and knitted versus woven transversal connections in 3D textile reinforced cement (TRC) composites. *Applied Sciences (Switzerland)*, 10(13). <https://doi.org/10.3390/app10134517>

Falliano, D., De Domenico, D., Ricciardi, G., & Gugliandolo, E. (2018). Experimental investigation on the compressive strength of foamed concrete: Effect of curing conditions, cement type, foaming agent and dry density. *Construction and Building Materials*, 165, 735–749. <https://doi.org/10.1016/j.conbuildmat.2017.12.241>

Falliano, D., De Domenico, D., Ricciardi, G., & Gugliandolo, E. (2019). Improving the flexural capacity of extrudable foamed concrete with glass-fiber bi-directional grid reinforcement: An experimental study. *Composite Structures*, 209(October 2018), 45–59. <https://doi.org/10.1016/j.compstruct.2018.10.092>

Ferrara, G., Pepe, M., Dias, R., Filho, T., & Martinelli, E. (2021). *Mechanical Response and Analysis of Cracking Process in Hybrid TRM Composites with Flax Textile and Curauá Fibres*. <https://doi.org/10.3390/polym13050715>

Flower, D. J. M., & Sanjayan, J. G. (2007). Green house gas emissions due to concrete manufacture. *International Journal of Life Cycle Assessment*, 12(5), 282–288. <https://doi.org/10.1065/LCA2007.05.327/METRICS>

Gencil, O., Yavuz Bayraktar, O., Kaplan, G., Benli, A., Martínez-Barrera, G., Brostow, W., Tek,

- M., & Bodur, B. (2021). Characteristics of hemp fibre reinforced foam concretes with fly ash and Taguchi optimization. *Construction and Building Materials*, 294, 123607. <https://doi.org/10.1016/j.conbuildmat.2021.123607>
- Ghiassi, B., Oliveira, D. V., Marques, V., Soares, E., & Maljaee, H. (2016). Multi-level characterization of steel reinforced mortars for strengthening of masonry structures. *Materials and Design*, 110, 903–913. <https://doi.org/10.1016/j.matdes.2016.08.034>
- Gökçe, H. S., Hatungimana, D., & Ramyar, K. (2019). Effect of fly ash and silica fume on hardened properties of foam concrete. *Construction and Building Materials*, 194, 1–11. <https://doi.org/10.1016/j.conbuildmat.2018.11.036>
- Graf, W., Hoffmann, A., Möller, B., Sickert, J. U., & Steinigen, F. (2007). Analysis of textile-reinforced concrete structures under consideration of non-traditional uncertainty models. *Engineering Structures*, 29(12), 3420–3431. <https://doi.org/10.1016/j.engstruct.2007.08.013>
- Gries, T., Raina, M., Quadflieg, T., & Stolyarov, O. (2016). Manufacturing of Textiles for Civil Engineering Applications. *Textile Fibre Composites in Civil Engineering*, 3–24. <https://doi.org/10.1016/B978-1-78242-446-8.00002-1>
- Gries, T., Roye, A., Offermann, P., Engler, T., & Peled, A. (2006). *Textile Reinforced Concrete - State-of-the-Art Report of RILEM TC 201-TRC*. RILEM Publications SARL./Textiles (pp. 11–26).
- Halvaei, M., Jamshidi, M., Latifi, M., & Ejtemaei, M. (2020). Experimental investigation and modelling of flexural properties of carbon textile reinforced concrete. *Construction and Building Materials*, 262. <https://doi.org/10.1016/j.conbuildmat.2020.120877>
- Hartig, J., Häußler-Combe, U., & Schicktanz, K. (2008). Influence of bond properties on the tensile behaviour of Textile Reinforced Concrete. *Cement and Concrete Composites*, 30(10), 898–906. <https://doi.org/10.1016/j.cemconcomp.2008.08.004>
- Hashemmoniri, S., & Fatemi, A. (2023). Optimization of lightweight foamed concrete using fly

- ash based on mechanical properties. *Innovative Infrastructure Solutions*, 8(1), 1–12.  
<https://doi.org/10.1007/s41062-022-01016-2>
- Hegger, J., & Voss, S. (2004). Textile reinforced concrete under biaxial loading. *6th Rilem Symposium on Fibre- Reinforced Concretes (FRC), BEFIB 2004, September*, 1463–1472.
- Hegger, J., & Voss, S. (2008). *Investigations on the bearing behaviour and application potential of textile reinforced concrete*. 30, 2050–2056.  
<https://doi.org/10.1016/j.engstruct.2008.01.006>
- Hegger, J., & Will, N. (2016). Textile-Reinforced Concrete: Design Models. In *Textile Fibre Composites in Civil Engineering* (pp. 189–2047). Woodhead Publishing.  
<https://doi.org/10.1016/B978-1-78242-446-8.00009-4>
- Hegger, J., Will, N., & Curbach, M. (2006). *State of the Art Report – Textile Reinforced Concrete/ Mechanical behaviour of textile reinforced concrete*. 133–185.
- Hilal, A. A., Thom, N. H., & Dawson, A. R. (2014). Pore structure and permeation characteristics of foamed concrete. *Journal of Advanced Concrete Technology*, 12(12), 535–544.  
<https://doi.org/10.3151/jact.12.535>
- Hilal, A. A., Thom, N. H., & Dawson, A. (2015). The Use of Additives to Enhance Properties of Pre- Formed Foamed Concrete. *International Journal of Engineering and Technology*, 7(4), 286–293. <https://doi.org/10.7763/ijet.2015.v7.806>
- Hulimka, J., Krzywoń, R., & Jędrzejewska, A. (2017). Laboratory Tests of Foam Concrete Slabs Reinforced with Composite Grid. *Procedia Engineering*, 193, 337–344.  
<https://doi.org/10.1016/j.proeng.2017.06.222>
- ISO 14040. (2006). *ISO 14040:2006 -Life Cycle Assessment*.  
<https://www.iso.org/standard/38498.html>
- ISO 14044. (2006). ISO 14044 Environmental management-Life cycle assessment-Requirements and guidelines Management environnemental-Analyse du cycle de vie-Exigences et lignes directrices. *The International Organization for Standardization, 2006*,



7.

[https://www.saiglobal.com/PDFTemp/Previews/OSH/iso/updates2006/wk26/ISO\\_14044-2006.PDF](https://www.saiglobal.com/PDFTemp/Previews/OSH/iso/updates2006/wk26/ISO_14044-2006.PDF)

Jhatial, A. A., Goh, W. I., Mastoi, A. K., Traore, A. F., & Oad, M. (2022). Environmental assessment and mechanical properties of Polypropylene fibres reinforced ternary binder foamed concrete. *Environmental Science and Pollution Research*, 29(2), 2985–3007. <https://doi.org/10.1007/S11356-021-15076-X/TABLES/10>

Jones, M. R., & McCarthy, A. (2005). Preliminary views on the potential of foamed concrete as a structural material. *Magazine of Concrete Research*, 57(1), 21–31. <https://doi.org/10.1680/macrc.2005.57.1.21>

Jones, M. R., Ozlutas, K., & Zheng, L. (2016). Stability and instability of foamed concrete. *Magazine of Concrete Research*, 68(11), 542–549. <https://doi.org/10.1680/macrc.15.00097>

Kearsley, E. P., & Wainwright, P. J. (2002). Ash content for optimum strength of foamed concrete. *Cement and Concrete Research*, 32(2), 241–246. [https://doi.org/10.1016/S0008-8846\(01\)00666-4](https://doi.org/10.1016/S0008-8846(01)00666-4)

Kosmatka, S., Kerkhoff, B., & Panarese, W. (2002). *Design and Control Design and Control of*.

Kozłowski, M., & Kadela, M. (2018). Combined Experimental and Numerical Study on Fracture Behaviour of Low-Density Foamed Concrete. *IOP Conference Series: Materials Science and Engineering*, 324(1). <https://doi.org/10.1088/1757-899X/324/1/012031>

Kwan, A., Islam, M., & Pam, H. (2002). Flexural strength and ductility of reinforced concrete beams. *Proceedings of the Institution of Civil Engineers: Structures and Buildings*, 152(4), 361–369. <https://doi.org/10.1680/stbu.2002.152.4.361>

Laukaitis, A., & Fiks, B. (2006). Acoustical properties of aerated autoclaved concrete. *Applied Acoustics*, 67(3), 284–296. <https://doi.org/10.1016/j.apacoust.2005.07.003>

Lee, Y. L., Lim, J. H., Lim, S. K., & Tan, C. S. (2018). Flexural Behaviour of Reinforced Lightweight

- Foamed Mortar Beams and Slabs. *KSCE Journal of Civil Engineering*, 22(8), 2880–2889. <https://doi.org/10.1007/s12205-017-1822-0>
- Li, M., & Li, V. C. (2013). Rheology, fiber dispersion, and robust properties of engineered cementitious composites. *Materials and Structures/Materiaux et Constructions*, 46(3), 405–420. <https://doi.org/10.1617/s11527-012-9909-z>
- Li, M., Tan, H., He, X., Jian, S., Li, G., Zhang, J., Deng, X., & Lin, X. (2023). Enhancement in compressive strength of foamed concrete by ultra-fine slag. *Cement and Concrete Composites*, 138(September 2022). <https://doi.org/10.1016/j.cemconcomp.2023.104954>
- Liu, Z., Zhao, K., Hu, C., & Tang, Y. (2016). Effect of Water-Cement Ratio on Pore Structure and Strength of Foam Concrete. *Advances in Materials Science and Engineering*, 2016. <https://doi.org/10.1155/2016/9520294>
- Lu, J. X. (2023). Recent advances in high strength lightweight concrete: From development strategies to practical applications. *Construction and Building Materials*, 400, 132905. <https://doi.org/10.1016/J.CONBUILDMAT.2023.132905>
- McCormac, J., & Brown, R. (2014). *Design of reinforced concrete* (9th ed.). John Wiley & Sons.
- Mechtcherine, V. (2016). Durability of Structures Made of or Strengthened Using Textile-Reinforced Concrete. *Textile Fibre Composites in Civil Engineering*, 151–168. <https://doi.org/10.1016/B978-1-78242-446-8.00007-0>
- Mechtcherine, V., & Lieboldt, M. (2011). Permeation of water and gases through cracked textile reinforced concrete. *Cement and Concrete Composites*, 33(7), 725–734. <https://doi.org/10.1016/j.cemconcomp.2011.04.001>
- Mobasher, B. (2016). Textile Fiber Composites: Testing and Mechanical Behavior. *Textile Fibre Composites in Civil Engineering*, 101–150. <https://doi.org/10.1016/B978-1-78242-446-8.00006-9>
- Mobasher, B., Brameshuber, W., Brockmann, T., Peled, A., Reinhard, H. W., & Wastiels, J.

- (2009). Textile Reinforced Concrete - State-of-the-Art Report of RILEM TC 201-TRC. RILEM Publications SARL./ Main Production Technologies. In *Metal Based Functionally Graded Materials*. <https://doi.org/10.2174/978160805038310901010006>
- Nambiar, E. K. K., & Ramamurthy, K. (2006). Influence of filler type on the properties of foam concrete. *Cement and Concrete Composites*, 28(5), 475–480. <https://doi.org/10.1016/j.cemconcomp.2005.12.001>
- Nambiar, E. K. K., & Ramamurthy, K. (2007). Air-void characterisation of foam concrete. *Cement and Concrete Research*, 37(2), 221–230. <https://doi.org/10.1016/j.cemconres.2006.10.009>
- Neville, A. . (2010). Concrete Technology second edition. In *Longman Group UK Limited*1987. <https://doi.org/10.6004/jnccn.2015.0201>
- Neville, A. . (2011). *Properties of Concrete, 4th*. London: Pitman Publishing.
- Newman, J., & Owens, P. (2003). Concreting large-volume (mass) pours. In *Advanced Concrete Technology*. <https://doi.org/10.1016/B978-075065686-3/50299-8>
- Pan, Z., Hiromi, F., & Wee, T. (2007). Preparation of high performance foamed concrete from cement, sand and mineral admixtures. *Journal Wuhan University of Technology, Materials Science Edition*, 22(2), 295–298. <https://doi.org/10.1007/s11595-005-2295-4>
- Panesar, D. K. (2013). Cellular concrete properties and the effect of synthetic and protein foaming agents. *Construction and Building Materials*, 44, 575–584. <https://doi.org/10.1016/j.conbuildmat.2013.03.024>
- Papanicolaou, C. G. (2016). Applications of Textile-Reinforced Concrete in the Precast Industry. *Textile Fibre Composites in Civil Engineering*, 227–244. <https://doi.org/10.1016/B978-1-78242-446-8.00011-2>
- Peled, A. (2016). Bonds in Textile-Reinforced Concrete Composites. *Textile Fibre Composites in Civil Engineering*, 63–99. <https://doi.org/10.1016/B978-1-78242-446-8.00005-7>

- Peled, A., Cohen, Z., Pasder, Y., Roye, A., & Gries, T. (2008). Influences of textile characteristics on the tensile properties of warp knitted cement based composites. *Cement and Concrete Composites*, 30(3), 174–183.  
<https://doi.org/10.1016/j.cemconcomp.2007.09.001>
- Pillar, N. M. P., & Repette, W. L. (2015). The effect of fibers on the loss of water by evaporation and shrinkage of concrete. *Revista IBRACON de Estruturas e Materiais*, 8(1), 8–13.  
<https://doi.org/10.1590/s1983-41952015000100003>
- Portal, W. N., Lundgren, K., Wallbaum, H., & Malaga, K. (2015). Sustainable Potential of Textile-Reinforced Concrete. *Journal of Materials in Civil Engineering*, 27(7), 04014207.  
[https://doi.org/10.1061/\(ASCE\)MT.1943-5533.0001160/ASSET/74EC5CB0-5A97-46F2-A91E-83224DBD88D2/ASSETS/IMAGES/LARGE/FIGURE10.JPG](https://doi.org/10.1061/(ASCE)MT.1943-5533.0001160/ASSET/74EC5CB0-5A97-46F2-A91E-83224DBD88D2/ASSETS/IMAGES/LARGE/FIGURE10.JPG)
- Raj, A., Sathyan, D., & Mini, K. M. (2019). Physical and functional characteristics of foam concrete: A review. *Construction and Building Materials*, 221, 787–799.  
<https://doi.org/10.1016/j.conbuildmat.2019.06.052>
- Ramamurthy, K., & Nambiar, K. (2009). A classification of studies on properties of foam concrete. *Cement and Concrete Composites*, 31(6), 388–396.  
<https://doi.org/10.1016/j.cemconcomp.2009.04.006>
- Reinhardt, H.-W., Krüger, M., Brameshuber, W., & B. Banholzer. (2006). State of the Art Report – Textile Reinforced Concrete/Bond. *State-of-the-Art Report of RILEM Technical Committee 201-TRC: Textile Reinforced Concrete*.
- Rempel, S., Kulas, C., & Hegger, J. (2015). *BEARING BEHAVIOR OF IMPREGNATED TEXTILE REINFORCEMENT*.
- Robin, Clarke., Heijungs, R., Huppes, G., & Dutilh, C. E. (1996). *Life Cycle Assessment: What it is and how to do it*. Paris : UNEP, Industry and Environment, 91.
- Schladitz, F., Frenzel, M., Ehlig, D., & Curbach, M. (2012). *Bending load capacity of reinforced concrete slabs strengthened with textile reinforced concrete*.

<https://doi.org/10.1016/j.engstruct.2012.02.029>

Schneider, H. N., & Schätzke, C. (2006). *Textile Reinforced Concrete – Applications and prototypes*. 297–308. <https://doi.org/10.1617/2351580087.029>

Serudin, A. M., Mydin, M. A. O., & Ghani, A. N. A. (2022). Investigating The Load Carrying Capacities of Lightweight Foamed Concrete Strengthen with Fiber Mesh. *International Journal of Integrated Engineering*, 14(4), 360–376. <https://doi.org/10.30880/ijie.2022.14.04.028>

Shankar, A. N., Chopade, S., Srinivas, R., Kumar, N., Eftikhaar, H. K., Sethi, G., & Singh, B. (2023). Physical and mechanical properties of foamed concrete, a literature review. *Materials Today: Proceedings*, 44(4), 936–944. <https://doi.org/10.1016/J.MATPR.2023.10.105>

Sudhakar, A., & Muthusubramanian, B. (2024). Flexural response of textile-reinforced sandwich slab with modified polymeric core. *Structures*, 59(December 2023), 105679. <https://doi.org/10.1016/j.istruc.2023.105679>

Tambe, Y., & Nemade, P. (2022). Physical and mechanical properties of foamed concrete, a literature review. *Songklanakarinn Journal of Science and Technology*, 44(4), 936–944. <https://doi.org/10.1016/j.matpr.2023.10.105>

Tan, J. H., Lim, S. K., Lim, J. H., Tunku, U., Rahman, A., & Lumpur, K. (2011). Flexural Behaviour of Reinforced Lightweight Foamed Concrete Beams. *University Tunku Abdul Rahman, Kuala Lumpur, Malaysia.*, 1, 1–6. <http://www.communityresearch.org.nz/wp-content/uploads/formidable/FLEXURAL-BEHAVIOUR-OF-REINFORCED-LIGHTWEIGHT-FOAMED-CONCRETE-BEAMS-Augustus-Jun-Hui-TAN.pdf>

The Institution of Structural Engineers. (2022). *Reinforced Autoclaved Aerated Concrete (RAAC) Panels Investigation and Assessment*.

Thevarajah, B. ., Jayasinghe, M., Lewangamage, C., & Ibell, T. (2020). Embodied Energy and Carbon Footprint of Two Storied Refuge Space with Lightweight Load Bearing Panels.

- MERCon 2020 - 6th International Multidisciplinary Moratuwa Engineering Research Conference, *Proceedings*, 19–24.  
<https://doi.org/10.1109/MERCON50084.2020.9185324>
- Wijesinghe, K. A. P., Gunasekara, C., Law, D. W., Hidallana-Gamage, H. D., Wanasekara, N., & Wang, L. (2024). Thermal and acoustic performance in textile fibre-reinforced concrete: An analytical review. *Construction and Building Materials*, 412(January), 134879.  
<https://doi.org/10.1016/j.conbuildmat.2024.134879>
- WORLD PUMPS. (2017). Foam concrete provides stable solution at landfill. In *World Pumps* (Vol. 2017, Issue 3, pp. 24–26). Elsevier Ltd. [https://doi.org/10.1016/s0262-1762\(17\)30061-5](https://doi.org/10.1016/s0262-1762(17)30061-5)
- Xu, S., & Li, H. (2007). Bond properties and experimental methods of textile reinforced concrete. *Journal Wuhan University of Technology, Materials Science Edition*, 22(3), 529–532. <https://doi.org/10.1007/s11595-006-3529-9>
- Yang, E. H., Sahmaran, M., Yang, Y., & Li, V. C. (2009). Rheological control in production of engineered cementitious composites. *ACI Materials Journal*, 106(4), 357–366.  
<https://doi.org/10.14359/56656>
- Yousefieh, N., Joshaghani, A., Hajibandeh, E., & Shekarchi, M. (2017). Influence of fibers on drying shrinkage in restrained concrete. *Construction and Building Materials*, 148, 833–845. <https://doi.org/10.1016/j.conbuildmat.2017.05.093>
- Yu, J., & Leung, C. K. Y. (2017). Strength Improvement of Strain-Hardening Cementitious Composites with Ultrahigh-Volume Fly Ash. *Journal of Materials in Civil Engineering*, 29(9), 05017003. [https://doi.org/10.1061/\(ASCE\)MT.1943-5533.0001987/ASSET/7E5A4FA1-7B88-4B56-ABB4-83DA3CE73282/ASSETS/IMAGES/LARGE/FIGURE7.JPG](https://doi.org/10.1061/(ASCE)MT.1943-5533.0001987/ASSET/7E5A4FA1-7B88-4B56-ABB4-83DA3CE73282/ASSETS/IMAGES/LARGE/FIGURE7.JPG)
- Zhang, D., Yu, J., Wu, H., Jaworska, B., Ellis, B. R., & Li, V. C. (2020). Discontinuous micro-fibers as intrinsic reinforcement for ductile Engineered Cementitious Composites (ECC). *Composites Part B: Engineering*, 184, 107741.

## Reference

---

<https://doi.org/10.1016/J.COMPOSITESB.2020.107741>

Zhang, Z., Provis, J. L., Reid, A., & Wang, H. (2015). Mechanical, thermal insulation, thermal resistance and acoustic absorption properties of geopolymer foam concrete. *Cement and Concrete Composites*, 62, 97–105.  
<https://doi.org/10.1016/j.cemconcomp.2015.03.013>

Zheng, L., Sharon, X., Huo, & Yuan, Y. (2008). Strength, Modulus of Elasticity, and Brittleness Index of Rubberized Concrete. *Journal of Materials in Civil Engineering*, 1561(2), 1–2.  
[https://doi.org/10.1061/\(ASCE\)0899-1561\(2008\)20](https://doi.org/10.1061/(ASCE)0899-1561(2008)20)

Zhu, H., Zhang, D., Wang, T., McBain, M., & Li, V. C. (2021). Intrinsic self-stressing and low carbon Engineered Cementitious Composites (ECC) for improved sustainability. *Cement and Concrete Research*, 149, 106580.  
<https://doi.org/10.1016/J.CEMCONRES.2021.106580>

## Appendix A: Foamed Concrete Mix Design

**Mix Design Example (Mix FC-5)**

Target Density	kg/m <sup>3</sup>	1,800.00
Cement	kg/m <sup>3</sup>	620.69
Water / Cement	Ratio	0.40
<b>Water calculation</b>		
water	kg/m <sup>3</sup>	248.28
<b>Sand Calculation</b>		
Sand	kg/m <sup>3</sup>	931.03
C / S (cement/ Sand)	0.67	0.67
<b>Densities</b>		
Specific Gravity of Cement	kg/m <sup>3</sup>	3,150.00
Specific Gravity of Sand	kg/m <sup>3</sup>	2,650.00
Unit weight of water	kg/m <sup>3</sup>	1,000.00
Specific Gravity of Foaming Agent	kg/m <sup>3</sup>	1,050.00
Unit weight of Foam	kg/m <sup>3</sup>	50.00
<b>Components by Volumes in m<sup>3</sup></b>		
Cement	m <sup>3</sup>	0.19704444
water	m <sup>3</sup>	0.248276
Sand	m <sup>3</sup>	0.35133358
<b>Total of Components</b>		<b>0.80</b>
<b>Foam calculation</b>		
Volume required to fill by Foam	m <sup>3</sup>	0.20
<b>Total Volume of components</b>	m <sup>3</sup>	<b>1.00</b>
<b>Foam agent and its water calculation</b>		
Foam volume m <sup>3</sup>	m <sup>3</sup>	0.20
Foam needed	Liter	203.35
Amount of foaming agent	Liter	0.41
Amount of water needed to produce foam	Liter	10.17

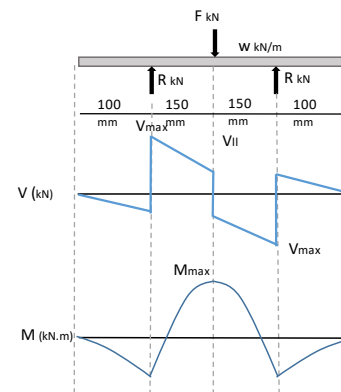


## Appendix B: AR-glass textile (Mapegrid G220) Technical Data

TECHNICAL DATA (typical values)		
PRODUCT IDENTITY		
Type of fibre:	A.R. glass fibre	
Zirconia content (ZrO <sub>2</sub> ) (%):	≥ 16	
Total weight (g/m <sup>2</sup> ):	250	
Mesh size (mm):	21 x 21	
Load-resistant area per unit of width (mm <sup>2</sup> /m):	≥ 35	
FINAL PERFORMANCE		
Performance characteristic	Test method	Product performance
Characteristic tensile strength (MPa):	LG DPCSLP n. 1/2019	≥ 917
Average tensile strength (MPa):	LG DPCSLP n. 1/2019	1079
Average tensile modulus of elasticity (GPa):	LG DPCSLP n. 1/2019	67
Average elongation at failure (%):	LG DPCSLP n. 1/2019	1.68

### Appendix C: Theoretical Calculations of TRFC-Com

Design to fail in compression	
width <b>b</b> (mm)	100
depth <b>d</b> (mm)	45
depth <b>dI</b> (mm)	50
depth <b>dII</b> (mm)	45
depth <b>dIII</b> (mm)	40
FC Compressive Strength <b>f<sub>c</sub></b> (MPa)	28.1
FC Ultimate Strain <b>ε<sub>c</sub></b>	0.004
Number of Textile Layers <b>n<sub>L</sub></b>	3
Number of Yarns in a Textil Layer <b>n<sub>y</sub></b>	8
Area of textile yarn <b>A<sub>y</sub></b> (mm <sup>2</sup> )	0.882
Textile Ultimate Tensile Strength <b>F<sub>u</sub></b> (MPa)	1080
Textile Ultimate Strain <b>ε<sub>u</sub></b>	0.0168
Textile modulus of elasticity <b>E<sub>tex</sub></b> (MPa)	67000
FC modulus of elasticity <b>E<sub>fc</sub></b> (MPa)	10464
Area of textile (mm <sup>2</sup> ) <b>A<sub>tex</sub></b>	21.17
Compressive concrete depth (mm) <b>a</b>	7.32
Neutral axis depth (mm) <b>C<sub>na</sub></b>	8.61
Calculated textile strain at 1st layer <b>ε<sub>tex1</sub></b>	0.012909977
Calculated textile strain at 2nd layer <b>ε<sub>tex2</sub></b>	0.013094046
Calculated textile strain at 3rd layer <b>ε<sub>tex3</sub></b>	0.010969734
<b>ε<sub>con</sub></b>	0.002685398
<b>s<sub>con1</sub></b>	28.09999991
<b>σ<sub>tex1</sub></b> (MPa)	864.9684362
<b>σ<sub>tex2</sub></b> (MPa)	877.3011027
<b>σ<sub>tex3</sub></b> (MPa)	734.9722114
<b>F<sub>tex1</sub></b> (N)	6103.217285
<b>F<sub>tex2</sub></b> (N)	6190.23658
<b>F<sub>tex3</sub></b> (N)	5185.963924
<b>F<sub>tex total</sub></b> (N)	17479.41779
<b>F<sub>concrete</sub></b> (N)	17479.41781
To balance	3.04267E-10
<b>output</b>	
Moment capacity <b>M<sub>u</sub></b> (kN.m)	0.72



Input		Output	
FC density (d) (kg/m <sup>3</sup> )	1800	Reaction (R) (kN)	4.820
compressive concrete <b>F<sub>c</sub></b> (MPa)	28	shear (V) (kN)	-0.008
width (b) (m)	0.1	shear (V <sub>max</sub> ) (kN)	4.812
depth <b>m</b>	0.045	shear (V <sub>II</sub> ) (kN)	4.800
Total Length (L) (m)	0.5		
Self-wight (w) (kN/m)	0.081		
(F) (applied Load) (kN)	9.6		

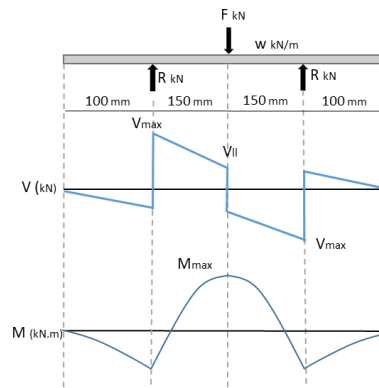
moment (M <sub>max</sub> ) (kN.m)	0.72
-----------------------------------	------

Shear capacity (kN)	40.48
---------------------	-------

Design Case	Moment Capacity (kN.m)	M <sub>max</sub> (kN.m) (due to applied loads)	Shear capacity (kN)	Shear (kN) (due to applied loads)	Notes
Design to fail in Compression (COM)	0.72	0.72	40.48	4.81	Compression Failure

## Appendix C: Theoretical Calculations of the TRFC-Ten2

Design to fail in tension (Ten2)	
Width <b>b</b> (mm)	100
depth <b>dI</b> (mm)	50
depth <b>dII</b> (mm)	45
FC Compressive Strength <b>f<sub>c</sub></b> (MPa)	28
FC Ultimate Strain <b>ε<sub>fc</sub></b>	0.004
Number of Textile Layers <b>n<sub>L</sub></b>	2
Number of Yarns in a Textile Layer <b>n<sub>y</sub></b>	8
Area of textile yarn <b>A<sub>y</sub></b> (mm <sup>2</sup> )	0.882
Textile Ultimate Tensile Strength <b>F<sub>utex</sub></b> (Mpa)	1080
Textile Ultimate Strain <b>ε<sub>utex</sub></b>	0.0168
Textile young's modules <b>E<sub>tex</sub></b>	67000
Area of textile (mm <sup>2</sup> )	
<b>A<sub>tex</sub></b>	14.11
Compressive concrete depth (mm)	
<b>a</b>	6.03
Neutral axis depth (mm)	
<b>C<sub>na</sub></b>	7.09
<b>concrete strain</b>	
<b>ε<sub>con</sub></b>	0.002660216
Calculated textile strain at 1st layer	
<b>ε<sub>tex1</sub></b>	0.016104478
Calculated textile strain at 2nd layer	
<b>ε<sub>tex2</sub></b>	0.014228008
Calculated textile strain at 3rd layer	
<b>ε<sub>tex3</sub></b>	
Calculated textile stress at 1st layer	
<b>σ<sub>tex1</sub> (MPa)</b>	1079
Calculated textile stress at 2nd layer	
<b>σ<sub>tex2</sub> (MPa)</b>	953.2765507
F <sub>tex1</sub> (N)	7613.423999
F <sub>tex2</sub> (N)	6726.319342
F <sub>tex3</sub> (N)	
F <sub>tex total</sub> (N)	14339.74334
F <sub>con</sub> (N)	14339.74244
to balance	8.02691E-07
<b>output</b>	
Moment capacity <b>M<sub>u</sub></b> (kN.m)	0.68
Input	Output
FC density (d) (Kg/m <sup>3</sup> )	Reaction (Q) (kN)
1800	4.521
compressive concrete <b>F<sub>c</sub></b> (MPa)	shear (VI) (kN)
28	-0.009
width (b) (m)	shear (V <sub>max</sub> ) (kN)
0.1	4.513
depth (m)	shear (VII) (kN)
0.0475	4.500
Total Length (L) (m)	
0.5	
Self-wight (w) (kN/m)	<b>moment (M<sub>max</sub>) (kN.m)</b>
0.086	0.68
(F) (applied Load) (kN)	<b>Shear capacity (kN)</b>
9	42.73



Design Case	Moment Capacity Kn.m	Mmax (kN.m) (due to applied loads)	Shear capacity (kN)	Shear (due to applied loads) (kN)	Notes
Design to fail in Tension (Ten2)	0.68	0.68	44.98	4.514	Tension Failur

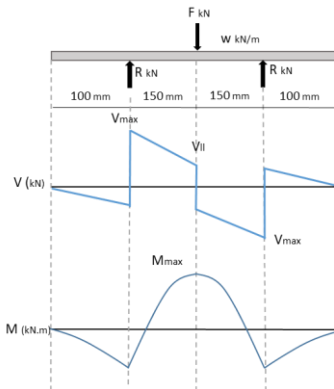
## Appendix C: Theoretical Calculations of the TRFC-Ten1

Design to fail in tension (Ten1)	
Beam width <b>b (mm)</b>	100
Beam depth <b>h (mm)</b>	55
The effective reinforcement depth for 1st layer <b>d1 (mm)</b>	50
The effective reinforcement depth for 2nd layer <b>d2 (mm)</b>	45
The equivalent effective reinforcement depth <b>d (mm)</b>	47.5
FC Compressive strength <b>f<sub>c</sub> (MPa)</b>	28
FC Ultimate strain <b>ε<sub>fc</sub></b>	0.004
Number of textile Layers <b>n<sub>L</sub></b>	2
Number of yarns in a textile Layer <b>n<sub>y</sub></b>	4
Area of textile yarn <b>A<sub>y</sub> (mm<sup>2</sup>)</b>	0.882
Textile ultimate tensile Strength <b>F<sub>utex</sub> (MPa)</b>	1080
Textile ultimate strain <b>ε<sub>utex</sub></b>	0.0168
Textile young's modulus <b>E<sub>tex</sub> (MPa)</b>	67000

Area of textile (mm <sup>2</sup> )	
<b>A<sub>tex</sub></b>	7.06
Compressive concrete depth (mm)	
<b>a</b>	3.03
Neutral axis depth (mm)	
<b>C<sub>na</sub></b>	3.56
Calculated concrete strain	
<b>ε<sub>con</sub></b>	0.001235
Calculated textile strain at 1st layer	
<b>ε<sub>tex1</sub></b>	0.016104
Calculated textile strain at 2nd layer	
<b>ε<sub>tex2</sub></b>	0.014371
Calculated textile stress at 1st layer	
<b>σ<sub>tex1</sub> (MPa)</b>	1079
Calculated textile stress at 2nd layer	
<b>σ<sub>tex2</sub> (MPa)</b>	962.83
Tension force at the 1st layer <b>t<sub>tex1</sub> (N)</b>	3806.71
Tension force at the 2nd layer <b>t<sub>tex2</sub> (N)</b>	3396.85
The total tension force <b>T<sub>tex</sub> (N)</b>	7203.56
Compression force <b>F<sub>c</sub> (N)</b>	7203.56
to balance	9.90463E-08

output	
Moment capacity <b>M<sub>u</sub> (kN.m)</b>	0.35

Input		Output	
FC density (d) (Kg/m <sup>3</sup> )	1800	Reaction (Q) (kN)	2.321
compressive concrete <b>F<sub>c</sub>' (MPa)</b>	28	shear (V <sub>I</sub> ) (kN)	-0.009
width (b) m	0.1	shear (V <sub>max</sub> ) (kN)	2.313
depth m	0.0475	shear (V <sub>II</sub> ) (kN)	2.300
Total Length (L) (m)	0.5		
Self-wight (w) (kN/m)	0.0855	<b>Moment (M<sub>max</sub>) (kN.m)</b>	<b>0.35</b>
(F) (applied Load) (kN)	4.6	<b>Shear capacity kN</b>	42.73



Design Case	Moment Capacity (kN.m)	Mmax (kN.m) (due to applied loads)	Shear capacity (kN)	Shear (due to applied loads) (kN)	Notes
Design to fail in tension (Ten1)	0.35	0.35	4.42	2.370	Tension Failure